ISSN: 2227-6912
E-ISSN: 2790-0479

Azerbaijan Technical University

MACHINE SCIENCE

1
2024

International scientific-technical journal

MACHINE SCIENCE

MAŞINŞÜNASLIQ МАШИНОВЕДЕНИЕ

International scientific-technical journal
Beynəlxalq elmi-texniki jurnal
Международный научно-технический журнал

Number 1
2024

DOI: 10.61413/OSPK4553

Founder: *The Ministry of Education of Azerbaijan Republic*
Təsisçi: *Azərbaycan Respublikası Təhsil Nazirliyi*
Учредитель: *Министерство образования Азербайджанской Республики*

The journal is included into the list confirmed by Higher Attestation Commission of the Azerbaijan Republic of editions for the publication of works of competitors for scientific degrees

Jurnal Azərbaycan Respublikası Ali Atestasiya Komissiyasının təsdiq etdiyi elmi dərəcə iddiaçılarının əsərlərinin çap edildiyi dövri elmi nəşrlərin siyahısına daxil edilmişdir.

Журнал входит в перечень, утвержденных ВАК Азербайджанской Республики, изданий для публикации трудов соискателей ученых степеней

Journal was founded according the order No1861 Ministry of Education of Azerbaijan Republic on the date 25.11.2011. Registration No 3521. Journal is published at least twice a year.

Jurnal Azərbaycan Respublikası Təhsil Nazirliyinin 25.11.2011-ci il tarixli 1861 saylı əmri əsasında təsis edilmişdir. Qeydiyyat No 3521. İldə ən azı iki nömrə nəşr edilir.

Учреждено приказом за №1861 от 25.11.2011 года Министерства образования Азербайджанской Республики. Регистрация № 3521. Ежегодно публикуется два номера.

It has been published since 2001. Published in 2001 - 2011 with a name "Mechanics-machine building"
2001-ci ildən nəşr edilir. 2001 – 2011-ci illərdə "Mexanika-maşınqayırma" adı ilə çap edilmişdir.
Издается с 2001 года. В 2001 – 2011 годах издано под называнием «Механика-машиностроение»

The "MACHINE SCIENCE" journal is supported by Azerbaijan Technical University, which means there are no publication fees for authors.
"MAŞINŞÜNASLIQ" jurnalı Azərbaycan Texniki universiteti tərəfindən dəstəklənir və məqalələrin nəşri üçün müəlliflərdən hər hansı ödəniş tələb olunmur.
Журнал «МАШИНОВЕДЕНИЕ» поддерживается Азербайджанским Техническим Университетом, что означает, что с авторов не взимается плата за публикацию статей.

Editorial address: ***Redaksiyanın ünvanı:*** ***Адрес редакции:***	Baku, AZ1073, H.Javid ave., 25. AztU Tel: (+994 12) 539 12 25 E-mail: msj@aztu.edu.az	© Machine Science, 2024 **ISSN:** 2227-6912 **E-ISSN:** 2790-0479

Contents	3
Yashar MUSAYEV, Carlo LOCCI, Nizami YUSUBOV, Kamran RZAYEV Green hydrogen - fuel of the future.	4-10
Viktor GUZEEV Alexander FILATOV, Alexey MOROZOV, Dmitry ARDASHEV, Anastasia DEGTYAREVA-KASHUTINA Design of parametric hole milling cycles on CNC machines.	11-23
Arif MAMMADOV, Nizami ISMAYILOV, Agil BABAYEV, Mukhtar HUSEYNOV, Ilham ALIYEV Growth dynamics of steel production using innovative technologies (overview).	24-35
Michael PASHKOV, Ilya AVVAKUMOV , Heyran ABBASOVA, Elgun SHABIYEV, Irada ABBASOVA. Analysis of errors occurring during tooth milling operations and technological system factors affecting the accuracy of tooth processing.	36-45
Viktor ARTEMYEV, Natalia MOKROVA, Anar HAJIYEV. Theoretical and practical aspects of the application of the dynamic programming method in optimal control problems.	46-57
Rasim BASHIROV, Fuzuli RASULOV, Ilhama HAMDUL-LAYEVA, Nijat ISMAILOV The influence of defects on the physico-mechanical properties of polymer composite materials and products	58-65
Agasi AGAYEV, Govhar ABBASOVA. Increasing the accuracy of processing parts on CNC lathes.	66-73
Matanat MEHRABOVA, Nizami HUSEYNOV, Vladimir KOCHE MIROVSKY, Aygun KAZIMOVA, Afin NAZAROV, Vusala POLADOVA CdMnSe thin films for solar energy converters.	74-80
PREPARATION OF MANUSCRIPT	81

MACHINE SCIENCE

ISSN: 2227-6912
E-ISSN: 2790-0479

2024, № 1 Pages 4 – 10

GREEN HYDROGEN - FUEL OF THE FUTURE

Yashar MUSAYEV[1,a*], Carlo LOCCI[1,b], Nizami YUSUBOV[2,c], Kamran RZAYEV [2,d]

[1]Siemens Energy AG, Freyeslebenstraße 1, 91058 Erlangen, Germany
[2]Department of Machine Building Technology, Azerbaijan Technical University, Baku, Azerbaijan

E-mail: [a*]*yashar.musayev@siemens-energy.com*, [b]*carlo.locci@siemens-energy.com*, [c]*nizami.yusubov@aztu.edu.az*, [d]*kamran.rzayev@mail.ru*

https://doi.org/10.61413/NVDN2284

Abstract: The critical issue of increase in carbon emissions in the world's atmosphere will have fatal for the stability of the climate. Therefore, increasingly tangible effects of climate change have led the world's economies in recent years to intensify their efforts for a transition away from fossil fuels. An exceptional push for innovation is the development of renewable energy sources. One promising complement to intermittent renewable power generation is the conversion of surplus electricity to energy storing products, like hydrogen. Current industrial supply for hydrogen is derived primarily from a carbon-intensive process based on natural gas (steam reforming). Hydrogen is the lightest and most abundant element in the universe. On Earth, hydrogen is usually present as part of organic compounds such as methane (CH_4), ammonia (NH_3), or water (H_2O) [1, 2]. Siemens Energy is one of the world's leading energy technology companies. An estimated one-sixth of the electricity generated worldwide is based on technologies from Siemens Energy. The portfolio includes conventional and renewable energy technology, such as gas and steam turbines, hybrid power plants operated with green hydrogen, and power generators and transformers. For the development of green energy systems is electrolysis a one of key technology to meet Paris agreement targets. The joint vision of the companies is to advance the technology to produce green hydrogen from innovative PEM (Proton Exchange Membrane, Fig.1) water electrolysis using renewable energy systems. This paper describes how the green hydrogen, produces via electrolysis technology, will play a significant role in satisfying the rising demand of green fuels in the future.

Keywords: *energy transitions, green hydrogen; electrolysis; PEM: Proton Exchange Membrane; MEA: Membrane Electrode Assembly; GDL: Gas-Diffusion-Layer; giga-factory.*

Introduction.

Climate change is widely acknowledged by the largest economies and developing countries as a significant problem that needs to be tackled urgently. A growing number of countries are developing programmes and strategies on greenhouse gas mitigation and decarbonisation roadmaps to overhaul their energy systems and infrastructures within the next decades. Signing states of the Paris agreement are required to cut down emissions by 50% by 2030. The agreement is ratified by the European countries, which engage themselves towards carbon neutrality by 2050. Through a combination of renewables, energy storage, energy efficiency and smart grid technology, a large share of end-use applications will be decarbonised in the coming decades. As more countries foster deep decarbonisation strategies, green hydrogen produced from renewables via water electrolysis is expected to be at the very heart of energy transition as a key piece of the clean energy puzzle. IRENA's 1.5°C scenario projects that hydrogen and derivatives will account for up to 12% of final energy consumption by 2050 [2, 3].

Germany's roadmap towards carbon neutrality puts renewable energies into focus, with wind and solar being the main future energy sources. 80% of gross electricity production must be from renewable by 2030, which is expected to reach 800 TW by the end of the decade [4]. One of the challenges tied to wind and solar renewable resources is the unpredictability which does not optimally follow the energy demand. For this reason, energy storage systems working as an energy buffer are necessary.

Hydrogen is an energy vector. Differently from batteries, hydrogen offers extreme flexibility and can be used in heterogeneous sectors, such as manufacturing, heating, transport and energy. For this reason, Germany plans to install at least 6 GW of hydrogen production capacity by 2030, and an additional 6 GW by 2040 [5]. The Hydrogen Council estimates 232 GW of total electrolysis capacity worldwide, if all the projects announced by manufacturers so far will follow through [6].

Electrolysis is the only way to produce green hydrogen with no CO_2 emissions, but it is still very marginal if compared to hydrogen production from fossil fuels, which represents 96% of hydrogen production nowadays. Mature electrolysis technologies for large scale hydrogen production are two [7]. In alkaline electrolysis, two electrodes operate in potassium hydroxide (KOH). The produced hydrogen and oxygen are separated by a diaphragm. The second one is Proton Exchange Membrane (PEM) electrolysis, in which the catalyst is coated on the membrane (catalyst coated membrane – CCM). In PEM, the protons involved in the catalytic reactions travel efficiently across the membrane. Compared to Alkaline electrolysis, the proton exchange is more efficient for PEM, making this technology more responsive to load fluctuations, hence more suitable for coupling with intermittent technologies such as wind or solar. PEM is however more expensive: the catalytic material for the anode side is Iridium, one of the scarcest materials on earth [8].

Giga Factory: Mass Production of Green Hydrogen via PEM-Technology

PEM electrolysis at industrial scale occurs in a stack made of single cells (Fig. 1): at each side of the membrane, a gas-diffusion-layer (GDL) homogenizes and stabilizes the flow across the membrane and enables the electron flux to the catalytic layers. The core of the cell, defined as membrane electrode assembly (MEA) is then packed between two bipolar plates. Depending on design and hydrogen production requirements, a given number of cells is piled together within two external metal collectors. Such ensemble is defined as stack, whose production ramping up for the Silyzer300® is the main element of this article. A stack for the Silyzer300® is shown in

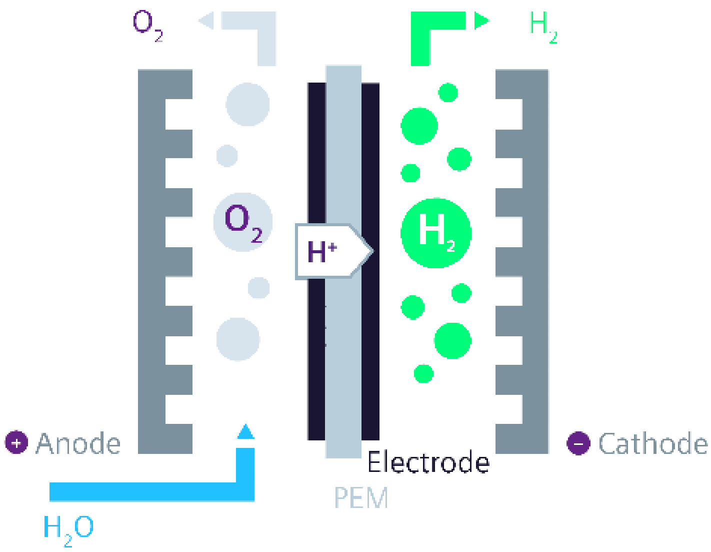

Figure 1. Water Electrolysis process and production of green hydrogen via PEM- Technology

Fig. 2a. In a reference plant configuration, 24 stacks build an array, which is able to produce about 335 Kg/h of hydrogen at full load Fig. 2b. Such production corresponds to 0.55 MW per stack, when the higher heating value of hydrogen is used as a reference.

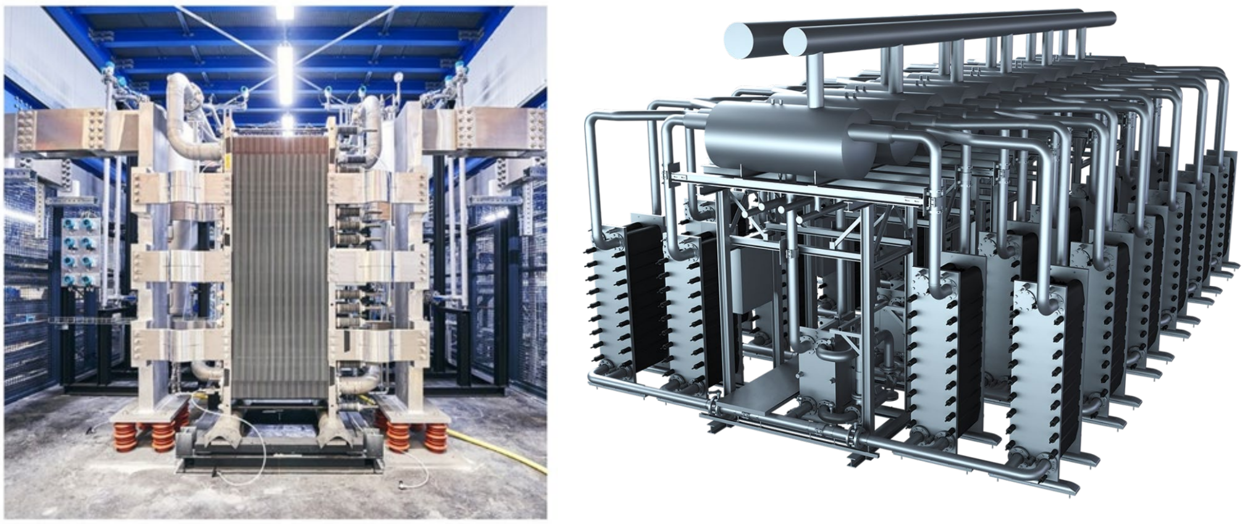

a) b)

Figure 2. Stack (a) & full module array (b) of the Silyzer300® with 24 single module units.

Building a PEM stack for the Silyzer300® is a nearly full automatized process. The way the performance of a module is measured is the polarization curve, which correlates the voltage needed to polarize the cell for a given load of electricity. The stack must be manufactured with a very high level of standardization, from the cells manufacturing up to the module assembly. Slight differences in the process would lead to a modification of the polarization curve, which is an undesired outcome during the quality and testing phase.

Building up a giga-factory for such a highly standardized process, requires then to think thoroughly about the workflow and to find the best optimization between speed of manufacturing and strict control of all the KPIs of the final product.

All the most important elements involved in the cell electrochemical reactions are already involved.

- Coating: the catalytic layers are coated on each side of the membrane, but layering is not done directly on the membrane itself. The first step is to create the layer on carrying foils. This is a very delicate step as imperfect adherence of the catalytic layers might affect the performance of the cell. Here standardization and automation are fundamental and the mechanical and thermal characteristics of the layer are accounted for to regulate the machines;
- Temper: in this step we run a heat treatment to modify and optimize the mechanical characteristics of the coating layer on the foils;
- Cutting machine: up to this phase, the carrying foils are in a roll. In this step, they are cut into sheets of a convenient size for the continuation of the process sequence;
- Sandwich machine: this is the first time the layers enter in contact with the membrane. In a sandwich machine, two foils, one for the anode and one for the cathode side, are attached to the membrane;
- Lamination machine: the sandwich formed in the previous step is then laminated to press the coating onto the membrane;
- Punching machine: the throughput from the lamination machine is cut to obtain the final size corresponding to the active area of the cell. Visual inspection and maneuvering are here

needed, as after this step we finally have the MEA;

- Cell assembly: the cells are now manufactured. This step is fully automated with two robots continuously picking up the cell components and assembling each cell. Each finished cell is then piled one after the other. The need for robots here is fundamental for rapid ramp-up.
- Module pressing: the cells are pressed and screwed. Several screws are used for the operation, which is also fully automated, requiring two additional robots. The modules are finally be tested and shipped to the customer site.

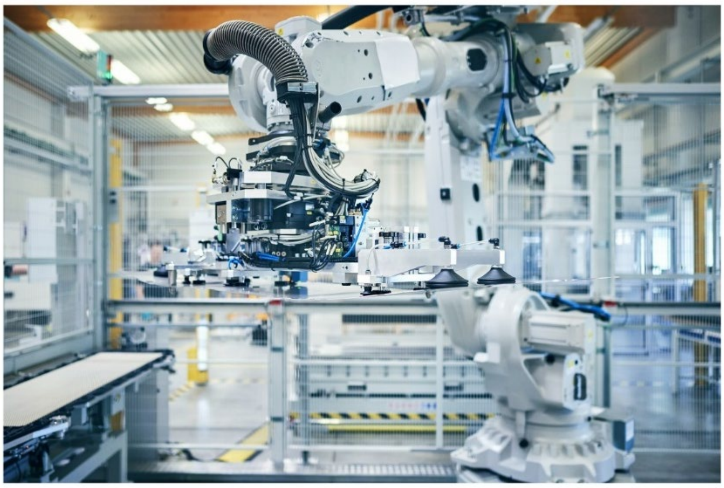

Figure 3. One of the robots involved in the cell manufacturing process

As it can be understood, most of the steps are dedicated to the MEA, and this also had consequence on the way the layout of the giga-factory was architected. Since the target is to produce 3 GW by end of 2025, this is an equivalent of 4 modules per day when the factory will work at full regime.

Such robots need to be continuously monitored to prevent any malfunction and disruption, before any major event occurs. In addition, the machines continuously dialogue together via a cloud network. The coordination of the machine is a fundamental aspect to increase and steer the production efficiency. Only when a given machine is perfectly aligned with the previous step, production times can be highly optimized.

Testing of the modules is fundamental. When the factory will be at full regime, a statistical sample of the modules will be tested. As a reminder, the test consists in running the module at several current loads, and to measure the voltage. The relation between the two provides the polarization curve. The polarization curve is compared to a reference one, which is also reported in the contractual agreements with customers. Any misalignment with the reference polarization curves is a red flag, and the process within the giga-factory needs to be reassessed. To enable fast analysis and process feedback, the giga-factory will continuously store the data from the testing and it will be easier to find discrepancies in the process.

The system coordinating the giga-factory is called manufacturing execution system (MES) which will play a fundamental role during ramping up. From beginning of operations to full regime, the giga-factory will be continuously optimized and the setting up of thousands of parameters will be required. This is the fundamental reason why a central brain is needed, and only a strict monitoring of all the events will allow a satisfactory production. The giga-factory represented a very important investment, from the founding agency up to the industrial actors involved. Hence it is important that its costs will be recovered. It is then highlighted that the giga-factory will also produce potential new products that will be proposed in the market by Siemens Energy. The way the giga-factory was designed was to favor not only automation, but also full flexibility to allow a fast resetting of the machines, dealing with different stack designs and concept. Several possible improvements in future stack designs for PEM manufacturers are discussed, and it is of primary importance for the giga-factory to be able to produce new and more cost competitive stacks. Finally, it can be argued that the giga-factory will be highly demanding in terms of material influx and this might be one of the main challenges for the whole workflow. In the next chapter, such challenges will be detailed and discussed, with potential solutions and perspectives. In particular, poor collaboration within companies might lead to misalignment in the supply chain, potentially delaying further hydrogen market growth and decarbonization targets.

PEM technology will evolve continuously in the next years. New stack designs will appear, new MEAs will be developed and this in very short time ranges. The issue is that recycling techniques optimized for a given stack, might need re-tuning for a different stack, even produced by the same company. If this is true for the MEA for the Iridium recovery process, this is also valid for all the other components, such as GDL, which might not be directly used after refurbishment as incompatible with a new design. Finally, both paths, reduction and recycling have actually to be combined together, posing further challenges to the PEM market for a sustainable supply chain.

Europe puts industrial eco-systems at the center of its economy strategy [9,10]. In total, 14 eco-systems are considered as the main pillar of European transition towards sustainability. Among these 14 eco-systems, “Energy-Renewables” and “Energy-Intensive-Industries” are the main areas in which hydrogen will play a significant role. As a consequence, hydrogen is considered by the European Union as a strategic area among other five. For Europe, strategic areas are industry sectors which need particular attention from European institution due to their strategical importance but also for challenges these areas will face in the future. Raw material supply chain is of concern for PEM technologies. Europe fully acknowledges this challenge and puts the raw material supply chain for hydrogen into focus. In addition, still on a European level, the European Hydrogen Alliance brings European hydrogen actors together, to boost growth and exchange know-how [11,12,13].

It can be argued that without such initiatives, that is government backing up industry, the hydrogen economy could not grow. In [12], it is reported that green hydrogen production has a chicken-egg dilemma. First challenge is the levelized cost of hydrogen, defined as the cost per Kg of hydrogen, accounting for all the costs during production. PEM manufacturers need to invest in R&D to drive cost down, but only if demand grows such investments can happen. However, in order for the demand to grow, the cost of hydrogen must be affordable. As mentioned in the introduction part, 96% of hydrogen nowadays is produced via fossil fuels, with a levelized cost of hydrogen (LCOH) pre-pandemic between USD 0.5 and 1.7 USD [13]. Green hydrogen is nowadays more expensive, with a LCOH between USD 3 and 8. At the moment, it is still uncertain whether the price will reach levels that will trigger enough demand for green hydrogen and for sure, PEM manufacturers will need to rethink and redesign the stacks [14] to increase market attractiveness compared to grey hydrogen. From a technological point of view, immediate measures will be to increase the MEA active area, pressurize the system and finally increase the current density. However, it is also reminded that independently from the measures and the strategies implemented by PEM manufacturers, this always has an effect on long term performance of PEM stacks, also defined as degradation [15], which is a fundamental variable to be taken into account for a sustainable business case. However, the increase in gas prices can still negatively affect the green hydrogen market. In Europe for instance, the merit-order system sets the electricity price as the price coming from the source with the highest marginal costs. Due to high gas prices, this leads Europe, and especially Germany, to high electricity prices, which is a very harsh boundary condition for green hydrogen development as electricity can be considered as the fuel for electrolysis [16].

Another chicken and egg dilemma is how to push companies to invest heavily on hydrogen. We saw above how the giga-factory will need a continuous flux of material to satisfy the ambitious production targets. This means a continuous flux of all the components, from the bipolar plates to the catalytic layers, from the membranes to the external blocks. A disruption of one of these elements would bring to interruption of the factory operations as well as inventory accumulation of idling elements. Such components are built in an eco-system of suppliers and sub-suppliers, which will also need to invest internally to increase their production throughput. In addition, the giga-factory needs reliable and long-term partners. Industrial partnerships will also play a crucial role in this sense, in which big energy players can build joint ventures to enhance specific know-hows. Only with such positive examples, large volume manufacturing will be required more and more.

Conclusion.

Paris agreement represented a strong push for investments into green technologies. Hydrogen is at the center of Europe’s strategy and it is seen as a valid way to store energy from intermittent renewable sources. Only governmental investment and strong commitment to roadmaps will create a favorable environment for the giga-factory to reach its production targets.

PEM electrolysis is a promising technology that holds great potential in the era of sustainable energy production. It can be used to store excess renewable energy, produce high-purity hydrogen for fuel cells, and generate oxygen for various applications. As the demand for renewable energy storage and hydrogen fuel cell technology continues to grow, the use of PEM electrolysis is expected to become more widespread. With further development and investment, PEM electrolysis has the potential to play a critical role in achieving a more sustainable and cleaner.

Acknowledgment

The authors thank the German Federal Ministry of Education and Research (BMBF) for funding part of this work within the H2Giga initiative [17,18].

REFERENCES

[1]. *Innovation trends in electrolysers for hydrogen production*. IRENA, 2022.

[2]. Musayev Y., Klinger A., Dobrenizki L., Schmid G., Yusubov N., Rzayev K. *Green hydrogen as a key technology for the energy of the future* // “Machine-building and Energy: New Concepts and Technologies” International Scientific-practical Conference materials, - Baku, Azerbaijan, AzTU: - 2-3 December, 2021, pp 15-17.

[3]. *Paris Agreement to the United Nations Framework Convention on Climate Change*. T.I.A.S. No. 16-1104. (2015)

[4]. *Regulation (EU)* 2021/1119 of the European Parliament, 2021.

[5]. *Erneuerbare-Energien-Gesetz Deutschlands*, 2023/

[6]. *Hydrogen Action Plan 2021-2025*. Germany National Hydrogen Council, 2021.

[7]. *The future of hydrogen*. IEA Report, 2019.

[8]. *Hydrogen Council, McKinsey & Company, Hydrogen for Net-Zero: A critical cost-competitive*

energy vector, 2021.

[9]. Ryan M. *Recycling and thrifting: the answer to the iridium question in electrolyser growth*, Johnson & Matthey, 2022.

[10]. Xu H., Rasimick B. et al. *DOE Hydrogen and Fuel Cells Program*, Annual Progress Report, 2015.

[11]. *Updating the 2020 New Industrial Strategy*. Communication from the commission of the European parliament, 2020.

[12]. IRENA. *Solving the Chicken and Egg Problem: Auctions for Green Hydrogen*, International Renewable Energy Agency, Abu Dhabi, 2021.

[13]. *Global hydrogen report*, IEA, 2021.

[14]. IRENA. *Green Hydrogen Cost Reduction: Scaling up Electrolysers to Meet the 1.5^{0}C Climate Goal*, International Renewable Energy Agency, Abu Dhab, 2020.

[15]. Papakonstantinou G., Algara-Siller G. et al. *Degradation study of a proton exchange membrane water electrolyzer under dynamic operation conditions*, App Ener, 280, 2020.

[16]. *Green Hydrogen Fuel to Become Competitive Due to War in Ukraine*. Bloomberg New Energy Finance, 2022.

[17]. https://www.wasserstoff-leitprojekte.de/leitprojekte/h2giga. Bundesamt für Bildung und Forschung

[18]. https://www.wasserstoff-leitprojekte.de/leitprojekte/h2mare. Bundesamt für Bildung und Forschung

Received: 15.08.2023
Accepted: 26.01.2024

MACHINE SCIENCE

ISSN: 2227-6912
E-ISSN: 2790-0479

2024 № 1 Pages 11-23

DESIGN OF PARAMETRIC HOLE MILLING CYCLES ON CNC MACHINES

Viktor GUZEEV[1,a], Alexander FILATOV[2,b], Alexey MOROZOV[3,c], Dmitry ARDASHEV[1,d*], Anastasia DEGTYAREVA-KASHUTINA[1,e]

[1]South Ural State University, Chelyabinsk, Russia,
[2]KONAR JSC, Chelyabinsk, Russia,
[3]Vladimir State University named after Alexander and Nikolay Stoletovs, Vladimir, Russia

E-mail: [a]guzeevvi@susu.ru, [b]*fil220387@gmail.com*, [c]ntk_2005@rambler.ru,
[d*]*ardashevdv@susu.ru*, [e]*degtiareva-kashutinaas@susu.ru*

https://doi.org/10.61413/UTPU9024

Abstract: The paper describes the stages of designing a technological cycle, which implements milling the holes with an end mill. We also present the developed CONICALINT software, which generates a G-code with an argument list for calling a technological cycle from the CNC system memory. The developed algorithm for the technological cycle of milling holes with an end mill has a branched structure, since there is a choice between two methods for calculating the internal parameters of the cycle and two milling methods: down cutting or up cutting. The calculation of the internal parameters of the technological cycle consists of calculating the coordinates of the points necessary to construct the helical path of the cutting tool, as well as calculating the value of the maximum permissible value of the helical pitch within a given set of input parameters. The initial data for the calculation are represented by thirteen parameters characterizing the geometry of the cutting tool, the geometry of the desired machined surface, as well as parameters defining the milling method, the calculation method, the cutting mode and the starting points of the cutting tool path. There are eight boundary conditions that determine the acceptable values of the input parameters. Based on these conditions, a system of inequalities is designed with a set of error messages to the user in case of incorrect input of the value of any input parameter. The developed G-code of the technological cycle subroutine for a CNC machine makes it possible to calculate the tool motion, both along helical and conical helical paths, depending on the input parameters. So, you can use it when programming milling of cylindrical and conical holes. The developed CONICALINT software is a visual addition to the developed technological cycle of milling holes that allow you to generate a control G-code with a list of twelve arguments.

Keywords*: parametric milling cycle, G-code, end milling, CNC machine*

Introduction

Currently, in conditions of piece-work and small-batch production, there is a need for a quick changeover of a CNC machine and, accordingly, rapid writing of control programs for part processing [3]. Using cycles for processing typical surfaces built into the CNC system [9], as well as due to the possible lack of other optional tools (Manual Guide i interactive programming software, Conical/Helical Interpolation function, etc.) [6, 8, 12,15], it is not always possible to solve assigned problems when developing control programs without the use of CAM modules, other computer software, or labor-intensive calculations of cutting tool paths [14]. This leads to problems that require theoretical and/or practical solutions. The following main problems have been identified on the topic under analysis. The performance of the process of designing a control program to execute the same operating step on different CNC machines differs. This is due to the presence or absence of desired tools of the system [10,11]. There is no possibility to use the same control program to perform some routine operating steps on different CNC machines [7, 13]. Preparing control programs for processing surfaces of complex profiles is the most labor-intensive process [1, 2, 4, 5].

Thus, the relevance of the topic is associated with the need to develop and implement into the CNC system a technological cycle for milling holes with an end mill, taking into account all the requirements for the geometric parameters of the machined surfaces a rational processing strategy, and cutting modes, and not linked to a specific series and model of this systems.

Stages of technological cycle development

Definition of initial data

The initial parameters of the cutting tool and the required parameters of the machined surface, necessary for calculating the path of the cutting tool within the developed technological cycle for milling holes with an end mill, are visually presented in Figure 1. Table 1 provides a description of these parameters.

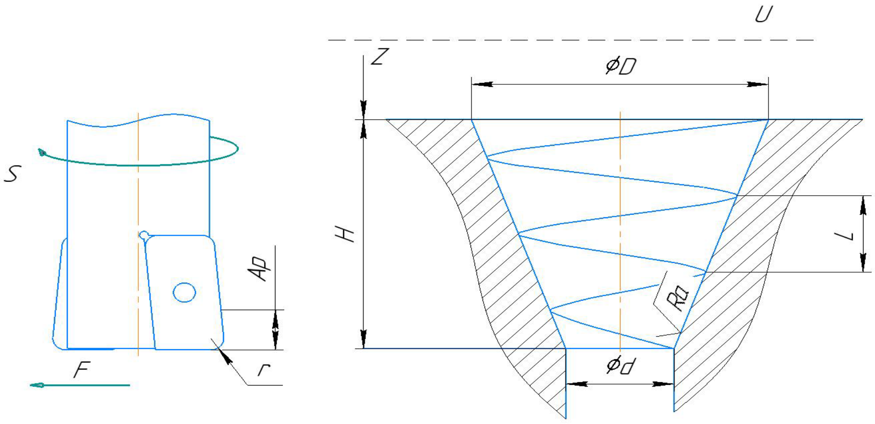

Figure. 1. Initial parameters of the cutting tool and required parameters of the machined surface

Table 1 Description of initial parameters

Parameter	Description
r	End mill wedge radius
H	Required hole depth
D	Initial hole diameter
d	Final hole diameter
Ra	Required roughness of the machined surface
L	Helical pitch value
Z	Z-axis coordinate of the hole origin plane
U	Z-axis coordinate of the clearance plane
S	Spindle rpm
F	Feed
Ap	Maximum axial depth of cut

It is necessary to select the milling method (up or down milling) and specify the calculation method (use the value of the required roughness or a fixed value of the helical pitch to calculate the internal parameters of the technological cycle).

Designation of boundary conditions that determine acceptable values of input parameters

Let us define a set of conditions, the failure of which makes it impossible or incorrect to calculate the tool path within the developed technological cycle, and the CNC machine system generates the corresponding error:

–the value of the initial hole diameter must be greater than the value of the final diameter or equal to it, $D \geq d$;

–the value of the Z-axis coordinate of the clearance plane must be greater than the value of the Z-axis coordinate of the hole origin plane or equal to it, $U \geq Z$;

–the value of the spindle rpm must be positive, $S > 0$;

–the value of the end mill wedge radius must be positive, $r > 0$;

–the value of the required roughness of the machined surface must be positive, $Ra > 0$;

–the value of the initial hole diameter must be positive, $D > 0$;

–the value of the final hole diameter must be positive, $d > 0$;

–the value of the hole depth must be positive, $H > 0$.

Thus, a set of boundary conditions has been determined, the failure of which leads to the operation shutdown of the developed technological cycle, and the CNC machine system issues a corresponding message indicating the incorrectly specified parameter.

Development of a technological cycle algorithm

Let us develop a conditional algorithm for the technological cycle of milling holes with an end mill and depict it in Figure 2. This algorithm has three logical blocks, the decisions on which are made depending on the values of the initial data.

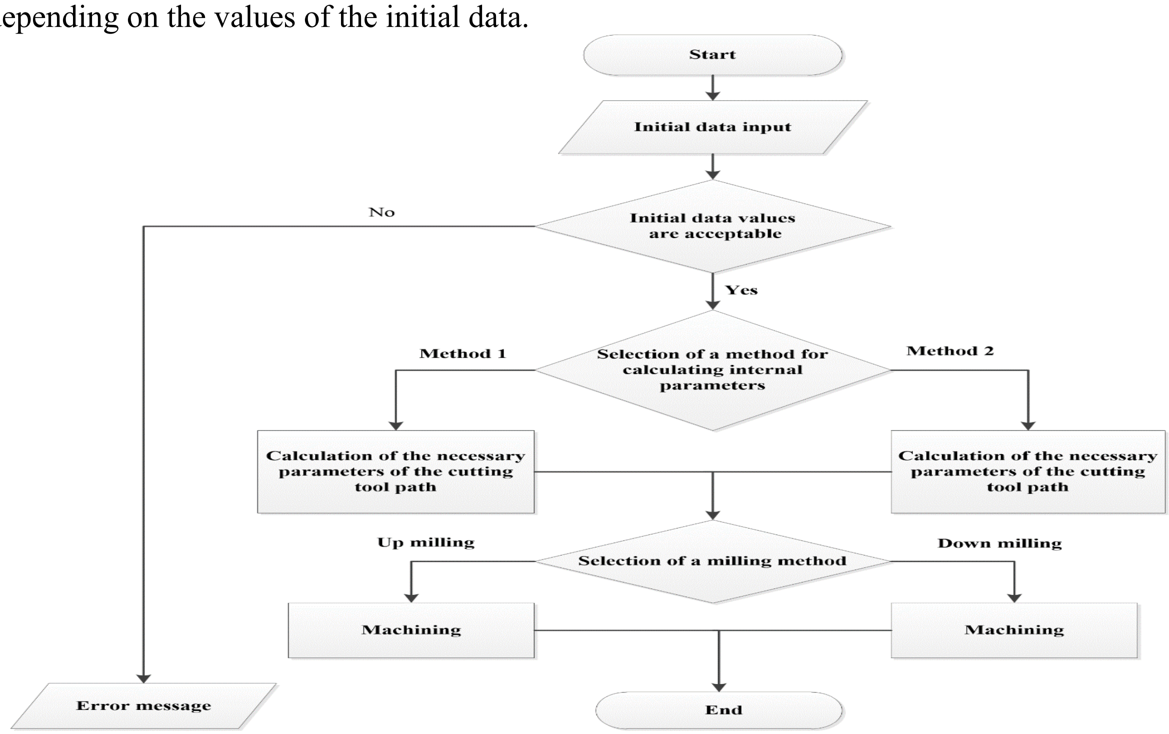

Figure 2. Conditional algorithm for the technological cycle

Calculation of internal parameters of the technological cycle

Using the formula for calculating the deviation of the actual profile of the machined surface from the required one, we recalculate the values of the initial and final diameters of the hole (D_{calc} and d_{calc}, respectively) using formulas (1) and (2):

$$D_{calc} = D + 2 \cdot \left(r - r \cdot \cos(\omega) + r - r \cdot \sin(\omega) \cdot tg(\omega)\right) \tag{1}$$

$$d_{calc} = d + 2 \cdot (r - r \cdot \cos(\omega) + r - r \cdot \sin(\omega) \cdot tg(\omega)) \tag{2}$$

The inclination angle of the machined surface ω is calculated using formula (3). The value of the inclination angle is necessary to calculate the change in the radius of the hole after each full turn of the helical path of the cutting tool, as well as to calculate the maximum permissible value of the helical pitch L, at which the required roughness of the machined surface will be maintained.

$$\omega = arctg\left(\frac{(D_{calc} - d_{calc})/2}{H}\right) \tag{3}$$

For a cylindrical hole, the value of ω will be zero, since the initial and final diameters will have the same value. The value of this angle cannot be negative.

If a path calculation method is chosen that takes into account the required roughness of the machined surface, then we calculate the maximum permissible helical pitch L using formula (4):

$$L = \cos(\omega) \cdot \sqrt{8 \cdot r \cdot Ra} \tag{4}$$

If the calculated value of L is greater than the maximum axial depth of cut Ap, the value of L is taken equal to Ap.

The number K of complete turns of the helical path of the cutting tool is calculated as H/L and rounded to the smallest integer (6). The quotient W of H/L (5) is also necessary to calculate the final coordinate $(X;\ Y;\ Z)$ of the last turn, since if the H/L ratio is not an integer, then the helical motion path will end with an incomplete turn in order to withstand the required hole depth. Therefore,

$$W = \frac{H}{L} \tag{5}$$

$$K = FIX(W) \tag{6}$$

where FIX is the rounding to the smallest integer function used by the CNC system. If the value of W is less than one, then there is no need to calculate the value of the number of complete turns K .

Since the CNC system does not have an arithmetic function for obtaining the remainder of division, we calculate the remainder V from dividing the value of the required hole depth by the number of turns using formula (7):

$$V = H - KL \tag{7}$$

The value V characterizes the depth of the last incomplete turn (if any) in a plane perpendicular to the axis of the rotating cutting tool. Next, the final coordinates of the last incomplete turn (if any) of the path are calculated (Fig. 3).

To do this, we first find the angle β from the X axis in the XY working plane (plane G17 of the CNC system, perpendicular to the axis of the rotating cutting tool), upon reaching which the path of the last incomplete turn (8) will be completed:

$$\beta = 360° \cdot V / L \tag{8}$$

Angle β can take values from 0 to 360, not inclusive. Then, the radius is calculated relative to the center of the hole at which the path of the last full turn ended according to formula (9):

$$I = D/2 - KLtg(\omega) \tag{9}$$

Next, the coordinates $(X; Y; Z)$ are calculated using formulas 10–12:

$$X = \cos(\beta) \cdot \frac{d}{2} \tag{10}$$

$$Y = \sin(\beta) \cdot \frac{d}{2} \tag{11}$$

$$Z = -H \tag{12}$$

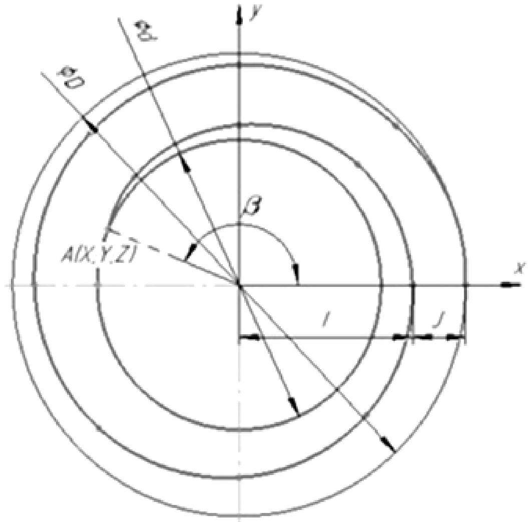

Figure 3. Calculation diagram of the final coordinates of the path

The value by which the radius of the hole changes after each complete turn (13) is calculated last:

$$J = L \cdot tg(\omega) \tag{13}$$

Thus, the missing parameters necessary for the cutting tool path drawing within the framework of the technological cycle being developed for milling conical and cylindrical holes with an end mill are calculated.

Development of a subroutine for a CNC system that implements the technological cycle

When calling a subroutine using G-code, the data (argument values) entered by the programmer is passed to the subroutine. When an argument is defined, the values are assigned to the corresponding local variables. The addresses G, L, N, O, and P cannot be used in arguments. It is also possible to skip addresses that are not required. Local variables corresponding to missing addresses are set to zero.

Table 2 Addresses of arguments and corresponding local variables

Address	Variable number
A	#1
B	#2
C	#3
D	#7
E	#8
F	#9
H	#11

Address	Variable number
I	#4
J	#5
K	#6
M	#13
Q	#17
R	#18
S	#19

Address	Variable number
T	#20
U	#21
V	#22
W	#23
X	#24
Y	#25
Z	#26

Next, we need to assign the available argument addresses used to set the values of the local variables of the cycle being developed to the set of input parameters. We summarize the data in Table 3.

Table 3 Argument addresses used

Parameter	Argument address	Local variable
r	R	#18
ω	C	#3
H	H	#11
D	D	#7
d	E	#8
Ra	A	#1
Z	Z	#26
U	U	#21
S	S	#19
F	F	#9
Ap	Q	#17

Let's develop a subroutine that implements the technological cycle in the educational version of the CIMCO Edit software editor for CNC machines. Having assigned values to the input parameters, we show the result in Figure 4.

```
(ARGUMENT ADDRESSES AND LOCAL VARIABLE NUMBERS)
(#1 - A - RA- REQUIRED VALUE RA );
(#2 - B -    - );
(#3 - C - C - CALCULATION METHOD 1 OR 2);
(#4 - I -    - );
(#5 - J -    - );
(#6 - K -    - );
(#7 - D - D - INITIAL DIAMETER);
(#8 - E - d - FINAL DIAMETR);
(#9 - F - F - FEED);
(#11- H - H - HOLE DEPTH);
(#13-   -    - );
(#17- Q - AP- MAXIMUM CUTTING DEPTH);
(#18- R - r - RADIUS AT THE TOP OF THE CUTTING WEDGE);
(#19- S - S - SPINDLE SPEED);
(#20- T -    - );
(#21- U - U - SAFE PLANE);
(#22- V - V - MILLING METHOD 41 OR 42);
(#23- W -    - );
(#24- X -    - );
(#25- Y -    - );
(#26- Z - Z - BASE PLANE);

(ENTERING VARIABLES)
#1=2       (Ra);
#7=30      (D);
#8=30      (d);
#9=100     (F);
#11=10     (H);
#17=3.     (Ap);
#18=2.4    (r);
#19=1500   (S);
#21=10     (U);
#26=0      (Z);
#3=2       (C);
#22=41     (V);
```

Figure 4. Assigning values to local variables of the cycle

Using the conditional operator "IF" we check the boundary conditions. The result is shown in Figure 5.

```
IF[#7LT#8] TNEN GOTO 3001;
IF[#21LT#26] TNEN GOTO 3002;
IF[#19LE0] TNEN GOTO 3003;
IF[#18LE0] TNEN GOTO 3004;
IF[#1LE0] TNEN GOTO 3005;
IF[#7LE0] TNEN GOTO 3006;
IF[#8LE0] TNEN GOTO 3007;

M99
N3001 #3000=1(THE INITIAL DIAMETER IS SMALLER THAN THE FINAL ON)
N3002 #3000=2(THE SAFE PLANE IS SET INCORRECTLY)
N3003 #3000=3(THE VALUE OF THE SPINDLE SPEED CANNOT BE NEGATIVE OR EQUAL TO 0)
N3004 #3000=4(THE VALUE OF THE RADIUS AT THE VERTE CANNOT BE NEGATIVE OR EQUAL TO 0)
N3005 #3000=5(THE ROUGHNESS VALUE CANNOT BE NEGATIVE OR EQUAL TO 0)
N3006 #3000=6(THE INITIAL DIAMETER CANNOT BE NEGATIVE OR EQUAL TO 0)
N3006 #3000=7(THE FINAL DIAMETER CANNOT BE NEGATIVE OR EQUAL TO 0)
%
```

Figure 5. Checking boundary conditions

Let's introduce additional local variables of the technological cycle and calculate their values using formulas (1–13), depending on the chosen calculation method. The result is shown in Figure 6.

```
(CALCULATION OF VARIABLES);
#101=ATAN[[#7-#8]/[2*#11]]          (SURFACE SLOPE ANGLE);
#115=[#18-[#18*COS[#101]]+[#18-[#18*SIN[#101]]]*TAN[#101]]
                                    (THE AMOUNT OF DEVIATION FROM THE REQUIRED PROFILE);

#7=[#7+[#115*2]]                    (THE VALUE OF THE INITIAL DIAMETER, TAKING INTO ACCOUNT THE DEVIATION);
#8=[#8+[#115*2]]                    (THE VALUE OF THE FINAL DIAMETER, TAKING INTO ACCOUNT THE DEVIATION);

IF[#3EQ2]THEN #103=#1               (CHOOSING A METHOD 2 USING A FIXED SCREW PITCH);
IF[#3EQ2]GOTO1000;

#1=[#1/1000];                       (CONVERSION OF THE VALUE FROM MICRONS TO MM);
#103=[COS[#101]*SQRT[8*#18*#1]]     (CALCULATION OF THE SCREW PITCH VALUE 1);
IF[#103GE#17] THEN #103=#17

N1000;
#104=[#11/#103]                     (CALCULATION OF THE QUOTIENT OF DIVISION W=H/L);
#105=FIX[#104]                      (CALCULATION OF THE NUMBER OF COMPLETE TURNS K);
#108=[[#7/2]-[#105*#103*TAN[#101]]] (RADIUS OF COMPLETION OF THE LAST COMPLETE TURN I);
#112=[#103*TAN[#101]]               (CHANGING THE RADIUS IN ONE TURN J);
#33=1                               (COUNTER);
#106=[#11-[#105*#103]]              (THE REMAINDER OF THE DIVISION V=H-KL);
#107=[360*[#106/#103]]              (BETA ANGLE);

(CALCULATION OF THE FINAL COORDINATES OF THE TRAJECTORY);
#109=[COS[#107]*[#8/2]]             (THE FINAL X COORDINATE OF THE LAST COMPLETE TURN);
#110=[SIN[#107]*[#8/2]]             (THE FINAL y COORDINATE OF THE LAST COMPLETE TURN);
```

Figure 6. Calculating values of local variables of the cycle

Next, using variables and conditional transition operators “IF” and “WHILE” and choosing the method of up or down milling, we describe the tool path using calculated local variables. Figure 7 shows the result.

```
(CUTTING);
S[#19] M3;
G0 G90 Z#21;
G1 G94 Z[#26] F[#9];
G1 G91 G[#114] X[#7/2] Y0;
WHILE [#33LE#105] DO1;
        G[#113] G64 G91 X-[#112] I-[#7/2] Z-[#103];
        #33=#33+1;
        #7=#7-[#112*2];
END1;
IF[#106EQ0] GOTO 2000;
G[#113] X-[#8/2-#109] Y[#110] Z-[#106] I-[#108] J0;
N2000;
G[#113] I-[#109] J-[#110];
G1 G40 X-[#109] Y-[#110];
G0 G90 Z#21;
M5;
M99;
```

Figure 7. Tool path calculation

Thus, a subprogram for the CNC system has been developed that implements the technological cycle of milling holes using an end mill.

Visual modeling of the implementation of the developed technological cycle

Using the path drawing module built into the CIMCO Edit control program editor, we perform a visual simulation of the execution of the developed G-code cycle for milling holes with an end mill. To do this, we need to assign values to the input parameters. Table 4 presents the set of values.

Table 4 Assigned values of variables

Parameter	Local variable	Value
r	#18	0.8
φ_2	#3	1
H	#11	20
D	#7	50
d	#8	50
Ra	#1	1.6
Z	#26	0
U	#21	10
S	#19	1500
M	#13	3
F	#9	0.3
Ap	#17	2

Since the values of the initial and final diameters are equal, the tool path, respectively, should be helical and not have a slope. Figure 8 shows the operating result of the cycle.

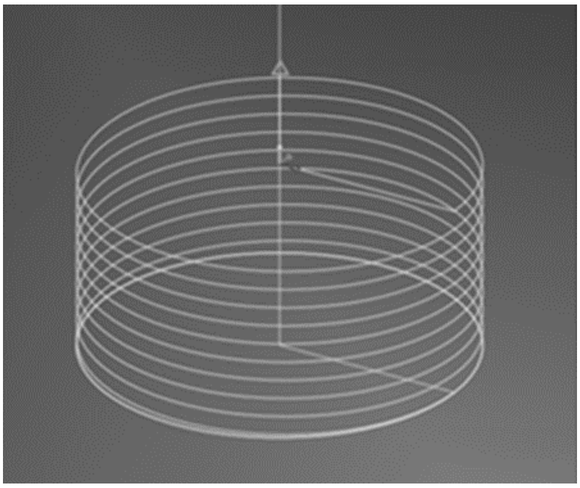

Figure 8. The operating result of the cycle with specified parameters

Next, we change the value of the local variable #8, which is responsible for the final diameter of the hole. We set its value equal to 10. With this value, the slope of the hole should be 45 °. We perform the cycle and present the drawing of the resulting path (Fig. 9).

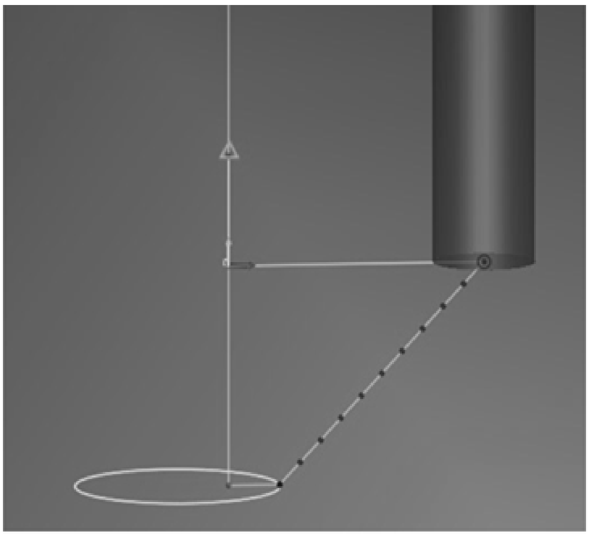

Figure 9. The operating result of the cycle with specified parameters

Figure 9 shows that the CIMCO Edit editor of the control programs does not have an algorithm for drawing a conical helical path, but, nevertheless, it displays the end point of the path that completes each of the turns.

Description of the developed CONICALINT software

Figure 10 presents the developed CONIICALINT software for the Windows operating system. The application is an instrument of graphic visualization for entering the input parameters and generating a G-code control with a set of arguments of the developed technological cycle. This application was designed on the Windows Forms platform in the Microsoft Visual Studio development environment. The application program code is written in the C# programming language.

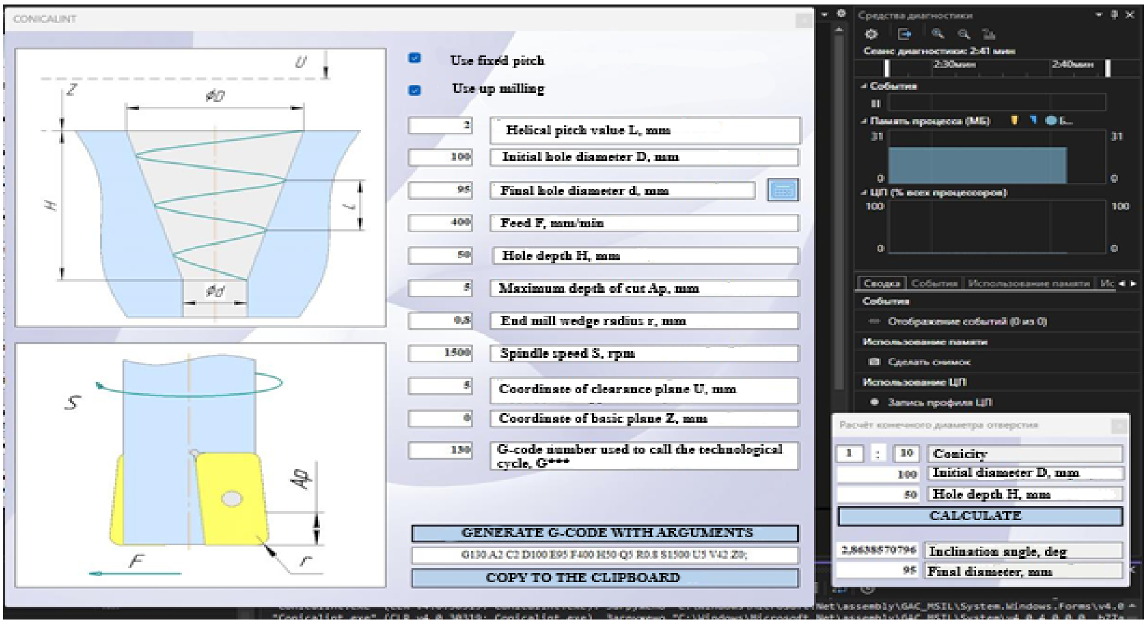

Figure 10. Developed CONICALINT software

This application has the following principle of operation:

1. The user introduces the values of 11 variables, the description of which is given in the “Definition of the initial data” paragraph of this work. If the final diameter of the hole is unknown, and the cone is known, then when the button depicted in Figure 11 is pressed, the calculator window (Fig. 12) is opened to calculate the final diameter of the hole.

Figure 11. Calculator window opening button

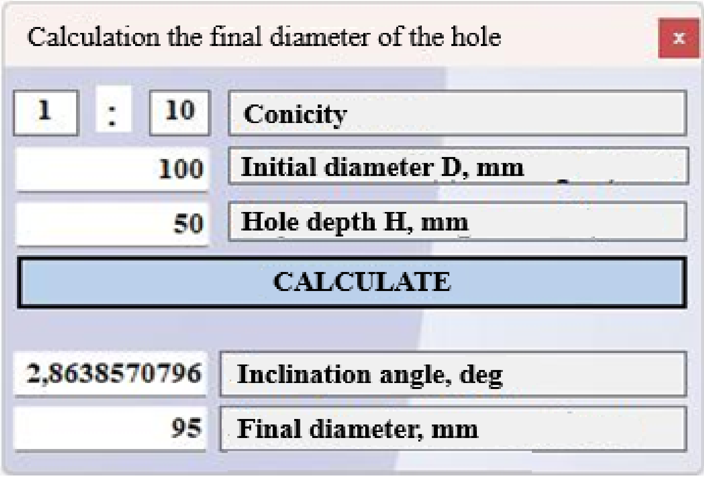

Figure 12. Calculator window

2.The user needs to indicate which of the two methods of calculating the cutting tool path is used. By default, the path calculation method is selected based on the value of the required roughness. If it is necessary to use the methodology that uses a fixed helical pitch to calculate the path, then the user needs to set the corresponding flag shown in Figure 13. It is also possible to choose a milling method in the developed technological cycle. By default, the method of down milling was chosen. We can switch to up milling by setting the corresponding flag (Fig. 13).

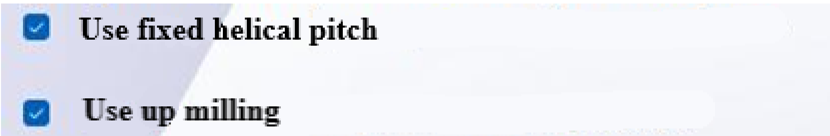

Figure 13. Selecting the path calculation method

3.When clicking the “Generate G-code with arguments” button, the application checks the boundary conditions (see point 2) and the formats of the entered numbers. If an incorrect value for any parameter is entered, the corresponding error message is displayed to the user. The example is shown in Figure 14.

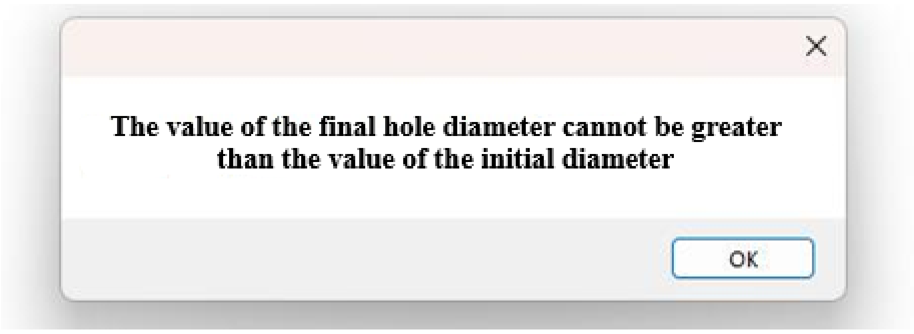

Figure 14. Error message displayed

4.If all entered values pass the check, then the application generates a control G-code with a set of arguments (Fig. 15), through which the developed technological cycle will be called for execution from the memory of the CNC system. Also, for convenience, there is a button for copying the control G-code to the clipboard.

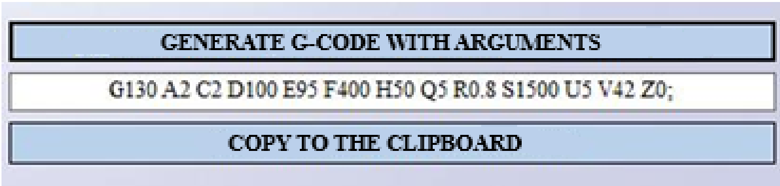

Figure 15. Generated G-code with the set of arguments

The use of CONICALINT software minimizes the risk of making an error when entering incorrect values of input parameters even at the stage of designing the control program using the developed technological cycle.

Design of control programs using the developed technological cycle

To verify the operability of the developed technological cycle for milling holes, let us design a set of control programs for executing a group of operating steps for milling conical and cylindrical holes when machining the “Plate” part, the CAD model of which in an isometric view is presented in Figure 16.

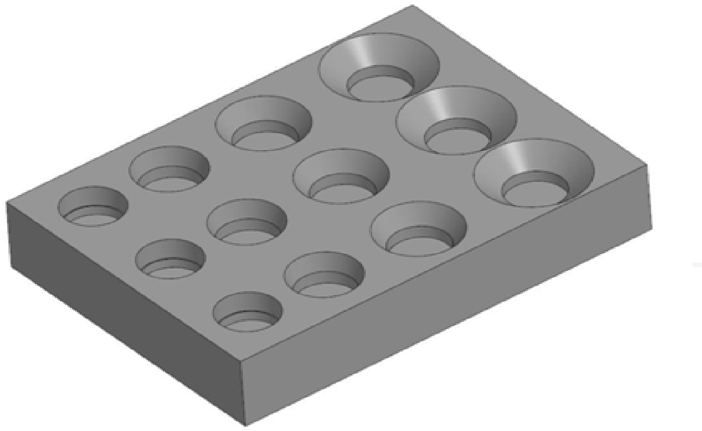

Figure 16. CAD model of the “Plate” part

Using the developed CONICALINT software and the calculator built into it, we generate a G-code with a set of arguments for making each of the twelve holes. The first row of twelve holes must be made with a roughness Ra of 6.3, the second row with a roughness Ra of 3.2, and the third with a constant helical pitch L =0.75 mm. We summarize the data in Table 4.

Table 4 Generated G-codes

Hole number	Generated G-code
1	G130 A6.3 C1 D26 E26 F1280 H11 Q3 R0.8 S3200 U5 V41 Z0;
2	G130 A6.3 C1 D30 E24.105 F1280 H11 Q3 R0.8 S3200 U5 V41 Z0;
3	G130 A6.3 C1 D36 E23.298 F1280 H11 Q3 R0.8 S3200 U5 V41 Z0;
4	G130 A6.3 C1 D45 E41 F1280 H11 Q3 R0.8 S3200 U5 V41 Z0;
5	G130 A3.2 C1 D26 E26 F1280 H11 Q3 R0.8 S3200 U5 V41 Z0;
6	G130 A3,2 C1 D30 E24.105 F1280 H11 Q3 R0.8 S3200 U5 V41 Z0;
7	G130 A3.2 C1 D36 E23.298 F1280 H11 Q3 R0.8 S3200 U5 V41 Z0;
8	G130 A3.2 C1 D45 E41 F1280 H11 Q3 R0.8 S3200 U5 V41 Z0;
9	G130 A0.75 C2 D26 E26 F1280 H11 Q3 R0.8 S3200 U5 V41 Z0;
10	G130 A0.75 C2 D30 E24.105 F1280 H11 Q3 R0.8 S3200 U5 V41 Z0;
11	G130 A0.75 C2 D36 E23.298 F1280 H11 Q3 R0.8 S3200 U5 V41 Z0;
12	G130 A0.75 C2 D45 E41 F1280 H11 Q3 R0.8 S3200 U5 V41 Z0;

Next, we design twelve control programs using the data from Table 4. An example of the text of a control program for milling the first hole using the developed technological cycle is shown in

```
%
O0001(TEST);
;
T1 M6(FREZA D16);
G43 H1 D1;
G54;
G90 G64 G80 G40 G95 G17 G69;
G0 X-22.5  Y-23.5
G0 Z100 M8;
;
G130 A6.3 C1 D26 E26 F1280 H11 Q3 R0.8 S3200 U5 V41 Z0;
;
G0 G153 Z0 M9 M5;
G0 G153 X0 Y0;
M30
%
```

Figure 17. Control program for milling the first hole

In the designed control programs, along with some G-code arguments for calling the developed technological cycle, the coordinates of the center of each hole in the XY working plane are also different.

Results:

1. The initial data is represented by thirteen parameters characterizing the geometry of the cutting tool, the geometry of the required machined surface, as well as parameters that determine the milling method, calculation method, cutting mode and starting points of the cutting tool path.

2. Eight boundary conditions are identified that determine the permissible values of the input parameters. Based on these conditions, a system of inequalities was designed with a set of error messages to the user in case of incorrect input of the value of any of the input parameters.

3. The developed algorithm for the technological cycle of milling holes with an end mill has a branched structure, since there is a choice between two methods for calculating the internal parameters of the cycle and two milling methods: down or up cutting.

4. Calculation of the internal parameters of the technological cycle consists of calculating the coordinates of the points necessary to construct the helical path of the cutting tool and calculating the value of the maximum permissible value of the helical pitch within a given set of input parameters.

5. The developed G-code of the technological cycle subroutine for a CNC machine makes it possible to calculate the tool motion, both along helical and conical helical paths, depending on the input parameters, which allows it to be used when programming milling of cylindrical and conical holes.

6. It is impossible to visually simulate the conical helical path of a cutting tool using the CIMCO Edit control program editor, which leads to the need to verify the operability of the technological cycle directly on a CNC machine.

7. The developed CONICALINT software is a visual addition to the developed technological cycle for milling holes, allowing the generation of a control G-code with a set of twelve arguments.

8. Based on the developed technological cycle for milling holes, 12 control programs with different sets of input parameters were designed. According to these control programs, a group of operating steps was carried out and quality control of the processed surfaces was performed, which showed the compliance of the results of mechanical processing with the initial requirements.

REFERENCES

[1] Ambrosimov S.K., Veprentsev O.Yu., Kosenkov M.A., and Bolshakov A.N. *The study of the parameters of the cut layer during screw milling with a spiral trajectory.* Fundamental and applied problems of technology and technology, 2011, No. 6-3, p

[2] Fleck M.B. *Building the trajectories of forming motions during processing on CNC machines.* Rostov N/D, DSTU, 2006, 184 p.

[3] Golubev A.A., Panov A.V. *A systematic approach to reducing the labor intensity of preparatory operations for CNC machines in pilot production conditions.* Young scientist, 2019, No. 50 (288), pp. 97–101.

[4] Kozlov A.M., Malyutin G.E. *Improving the efficiency of finishing volumetric 3D milling on CNC machines.* Scientific technologies in mechanical engineering, 2014, No. 6, pp. 39–43.

[5] Manurekina K.D., Zhdanova Yu.E. *Production and manufacture of stamping equipment.* Young scientist, 2017, No. 21 (155), pp. 133–136. URL: https://moluch.ru/archive/155/43723 /.

[6] Martinov G.M., Nezhmetdinov R.A., Kozak N.V., and Pushkov R.L. *Applied solutions in the field of control of electrical automation of PCNC class CNC machines.* Industrial automated control systems and controllers, 2011, No. 4, pp. 48–53.

[7] Martinova L.I., Fokin N.N. *An approach to creating a unified programming system for CNC turning and milling machines in interactive mode.* Automation in Industry, No. 5, 2019, pp. 14–17.

[8] Martinova L.I., Kozak N.V., Nezhmetdinov R.A., Pushkov R.L., and Obukhov A.I. *The Russian multi-functional CNC system AxiOMA control: Practical aspects of application.* Automation and Remote Control, 2015, Volume 76, Issue 1, pp.179–186.

[9] Martinova L.I., Martinov G.M. *Prospects for CNC Machine Tools.* Russian Engineering Research, 2019, vol. 39, pp. 1080–1083. DOI: 10.3103/S1068798X19120153

[10] Martinova L.I., Tsai S.Yu. *Development of constant turning cycles.* VESTNIK MSTU "STANKIN", 2021, No. 4 (59), pp.8–11

[11] Nezhmetdinov R.A., Nikishechkin P.A., Pushkov R.L. *Control of automatic tool change on multi-purpose machining centers using unified software solutions.* Industrial automated control systems and controllers, 2016, No. 6, pp. 19–24.

[12] Pushkov R.L., Evstafieva S.V., Rybnikov S.V. *Practical aspects of implementing user access level management in the Axioma Control CNC system.* Materials of the XI All-Russian Scientific and Practical Conference, Orenburg, LLC "University" Publishing Company, 2014, pp. 85–89.

[13] Pushkov R.L., Evstafieva S.V., Sokolov S.V., Abdullaev R.A., Nikishechkin P.A., Kuliev A.U., and Sorokoumov A.E. *Practical aspects of constructing a multi-terminal man-machine interface on the example of the CNC Axiom Control system.* Automation in industry, 2013, No. 5, pp. 37–41.

[14] Pushkov R.L., Obukhov A.I. *Application of a high-level language preprocessor for CNC systems for processing complex contours.* Proceedings of the X International Conference "Systems for design, technological preparation of production and management of the stages of the life cycle of an industrial product (CAD/CAM/PDM - 2010)", 2010, pp. 213–216.

[15] Pushkov R.L., Salamatin E.V., Evstafieva S.V. *Practical aspects of using a high-level language in a CNC system to implement group processing.* Automation in industry, 2018, No. 5, pp. 31–34.

Received: 12.02.2024
Accepted: 07.05.2024

MACHINE SCIENCE

ISSN: 2227-6912
E-ISSN: 2790-0479

2024, № 1 Pages 24-35

GROWTH DYNAMICS OF STEEL PRODUCTION USING INNOVATIVE TECHNOLOGIES (overview)

Arif MAMMADOV[1,a*], Nizami ISMAYILOV[2,b], Agil BABAYEV[1,c], Mukhtar HUSEYNOV[1,d], Ilham ALİYEV[1,e]

[1]Department of Metallurgy and Materials Technology, Azerbaijan Technical University, Baku, Azerbaijan
[2]Azerbaijan State Marine Academy, Baku, Azerbaijan

E-mail: [a]ariff-1947@mail.ru, [b]nizism@mail.ru, [c]aqil.babayev@aztu.edu.az, [d]muxtar.53@mail.ru [e]ilham.aliyev@aztu.edu.az

https://doi.org/10.61413/QMRR2817

Abstract: In the conditions of new realities, the main trends of the transition to innovative technologies in the world metallurgical industry, including steel production, were analyzed. The importance of using metallized iron in steel production is justified. The state of steel production in the world's leading countries was evaluated based on modern literature sources and statistical indicators. The main features of the transformation that will lead to the correction of the strategic development vector of the ferrous metallurgy industry in the conditions of tough competition and protection policy have been determined. It has been shown that despite the slow progress of the decarbonization process in the world metallurgical production, strategic orientations are aimed at the application of technological innovations and preservation of social and environmental priorities.
Keywords: *new realities, metallized iron, steel production, main trends, statistical indicators*

Introduction.

In the conditions of globalization and new realities, tough competition and sanctions, as well as protectionist policies of national states, a number of trends are observed in the world ferrous metallurgy industry, including steel production. Statistical indicators characterizing the state of steel production in the world's leading countries provide sufficient grounds for assessing the objective picture [1,2].

It is noted that new innovative technologies have a number of advantages compared to the classic scheme of steel production. Thus, the use of a certain amount of metallized iron as a charge material in steel production allows solving the shortcomings of the classical scheme, including shortening the technological chain and reducing the dependence on coke use. The widespread application of electromelting in steel production has already made the abandonment of blast furnace technology, which is very harmful to the environment, in the main leading countries of the metallurgical industry [3-5]. That's why currently there is a strong growth dynamics of metallized iron production in the countries of the world. The advantages of metallized iron in electrosmelting in comparison with other components of the charge highlight its role in quality steel production [6].

After the post-pandemic period, the analysis of the development dynamics of steel production in the countries of the world from this context is of scientific and practical importance. The dynamic development of steel production with the application of electrosmelting, based on innovative technologies, including nanotechnologies, has been strongly observed in the Republic of Azerbaijan in recent years.

Taking this into account, the analysis of the growth dynamics of steel production in the world with the use of innovative technologies made by us allows to evaluate the directions of future development in this field.

Main part.

It is known that the main components of metal scrap for electric steelmaking processes are cast iron, black metal scraps and metallized raw materials (Direct Reduction Iron - DRI). An overview of the ranges of technological changes in the steelmaking industry is shown in table. It can be seen from the table that the greater variability of the charge is typical for the electro- steeling process.

Table 1.Share of steelmaking processes, %

Indicators	Oxygen converter process	Electro-steeling process	Marten (scrap-ore) process	Marten (scrap process)
Share of the process in world steelmaking	69,8	29,0	1,2	
The share of the steelmaking process in the CIS	64,6	21,1	14,3	
Typical charge, %: - liquid cast iron - black metal scraps - metallized raw materials (DRI)	 75-80 20-25 -	 0-30 30-100 0-70	 25-55 25-75 -	
Max. share scraps in metallic slag	28	100	45	15

Thus, the classic production scheme of steel can be described as follows (Fig.1).

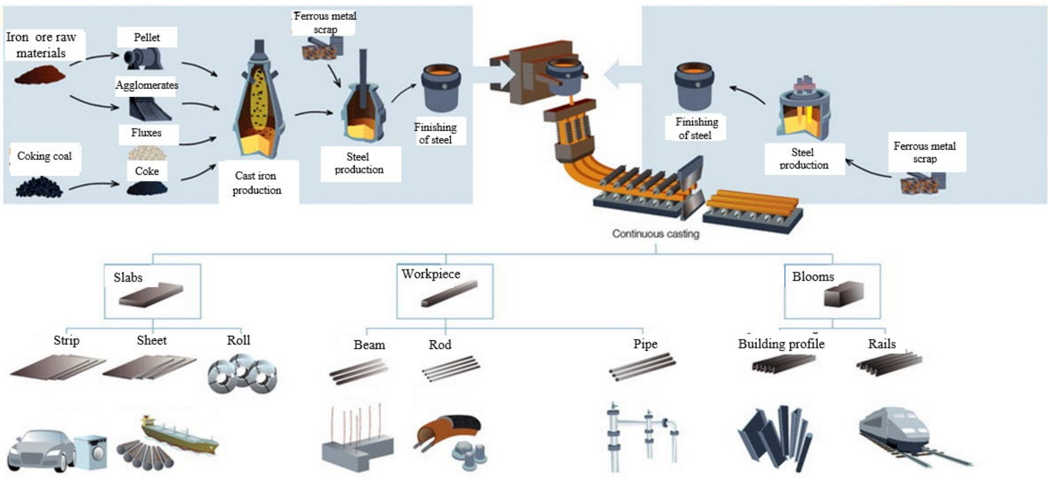

Figure 1. The classic scheme of steel production

The following advantages of the classical scheme can be indicated: high degree of iron separation; high specific productivity; high heat f.i.e.; efficient use of energy resources. Disadvantages of the classic scheme include: high capital costs; the need for preliminary crushing of the shale; coke usage costs; low quality of ferrous scrap.

New processes of obtaining iron.

The main reasons for the emergence of new processes of iron production are the shortcomings of the classic scheme, including the need to shorten the technological chain and reduce the dependence on coke. That is why the new processes are called "direct purchase of iron" or "cokeless metallurgy".

New processes of obtaining iron are divided into solid-phase and liquid-phase processes according to the type of semi-product produced, the share of the latter is very small, ie 5...6% of all non-coke metallurgy. Iron ore and iron ore logs are taken as primary raw materials in the new processes. Gasification products of natural gas or coal are used as a regenerator. Coal is used as a heat source in liquid phase processes. The scheme of steel production from metallized product is shown in fig. 2 is presented.

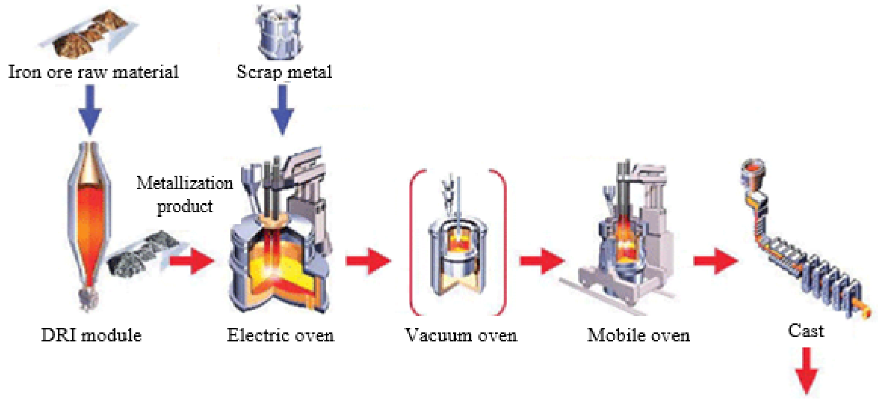

Figure 2. Scheme of steel production from metallized product

It should be noted that numerous ideas and various implementation schemes have created numerous names of processes and products of alternative metallurgy. Let's list the most used of them: DRI (Direct Reduced Iron), SI, SPI (Sponge Iron), HBI (Hot Brignetted Iron), HDRI (Hot Direct Reduced Iron), CDRI (Cold Direct Reduced Iron), etc. In general, the scheme of production of metallized products is shown in Fig. 3 is presented.

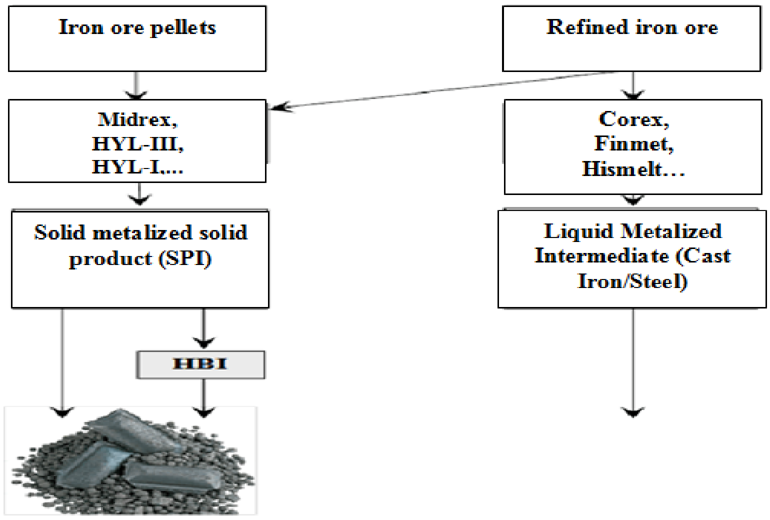

Figure 3. Scheme of metallized product production

Fig. 4 shows the development dynamics of direct iron reduction processes in the total volume of DRI production during 2005-2010: (https://trends.rbc.ru/trends/innovation).

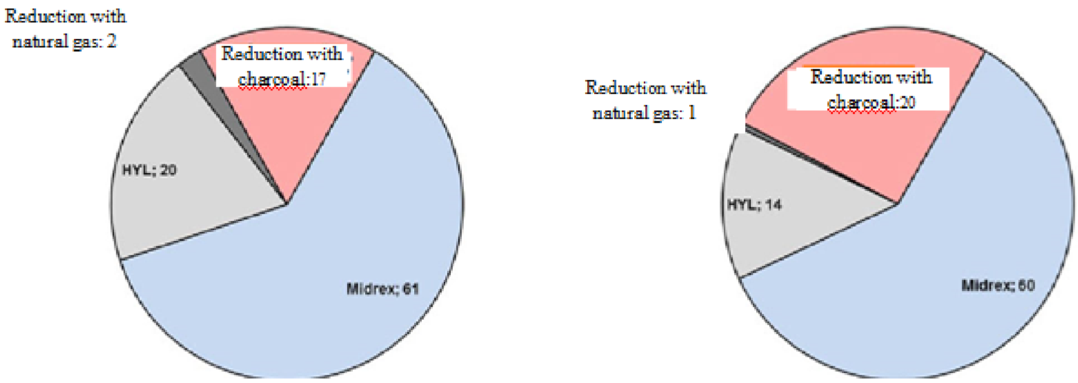

Figure 4. Development dynamics of DRI production

The technological scheme of the production of metallized products imposes certain requirements on the raw materials used and imposes some restrictions:

- the metallization process is carried out in counterflows of solid materials and gases;
- crushing of the two materials is required to improve gas permeability of the shale.

Thus, the main disadvantages of new metallized iron production processes are: low specific capacity of aggregates; the need to use high amounts of iron and low amounts of loose rock and mixed shale; high demand for energy carriers and oxygen; high requirements for storage and transportation conditions.

Non-furnace iron procurement facilities are mainly typical for developing countries (India, Venezuela, Iran, Mexico, Saudi Arabia) with small steel production and consumption. The dynamics of DRI production in a number of world countries are presented in the corresponding diagrams (Fig. 5 - Fig. 9).

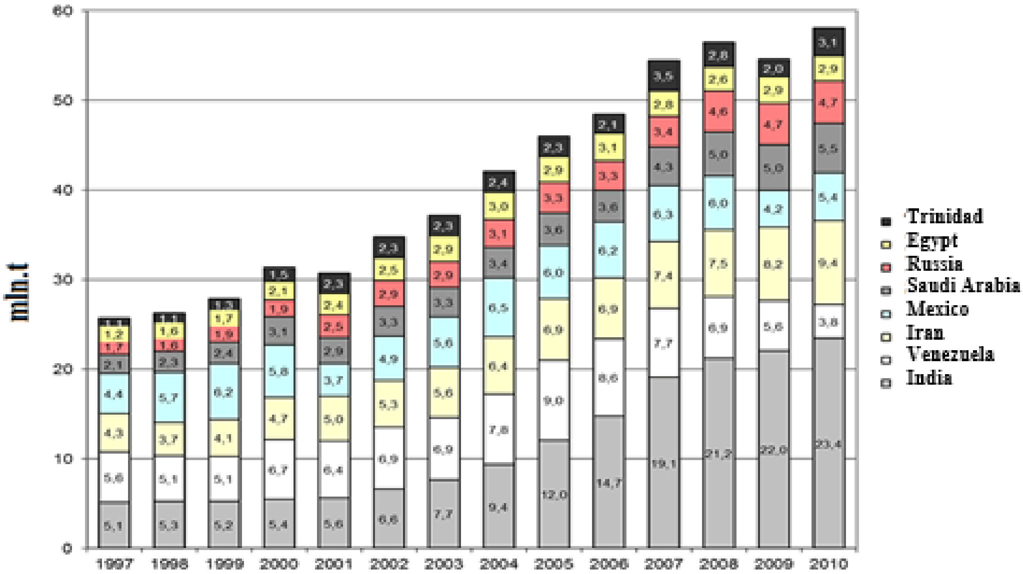

Figure 5. Dynamics of DRI production in a number of countries

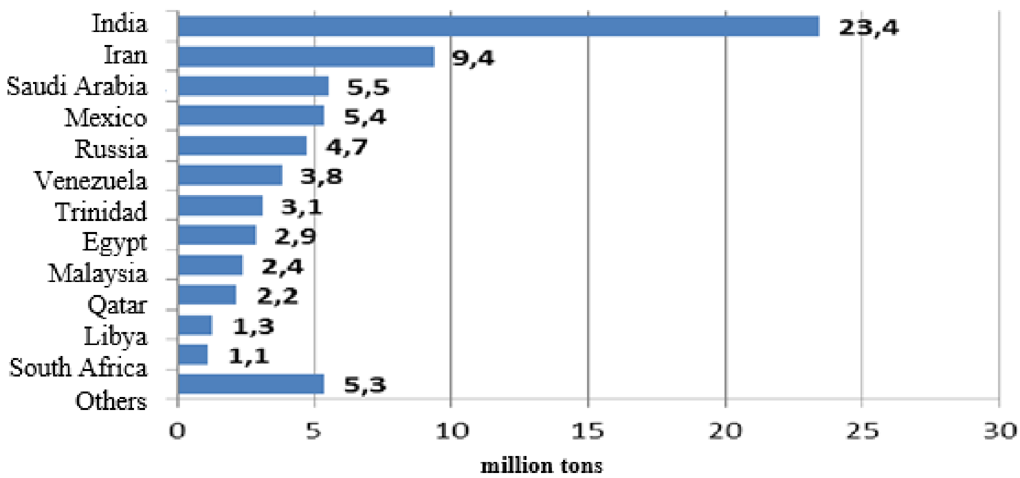

Figure 6. Production of DRI in some countries in 2010

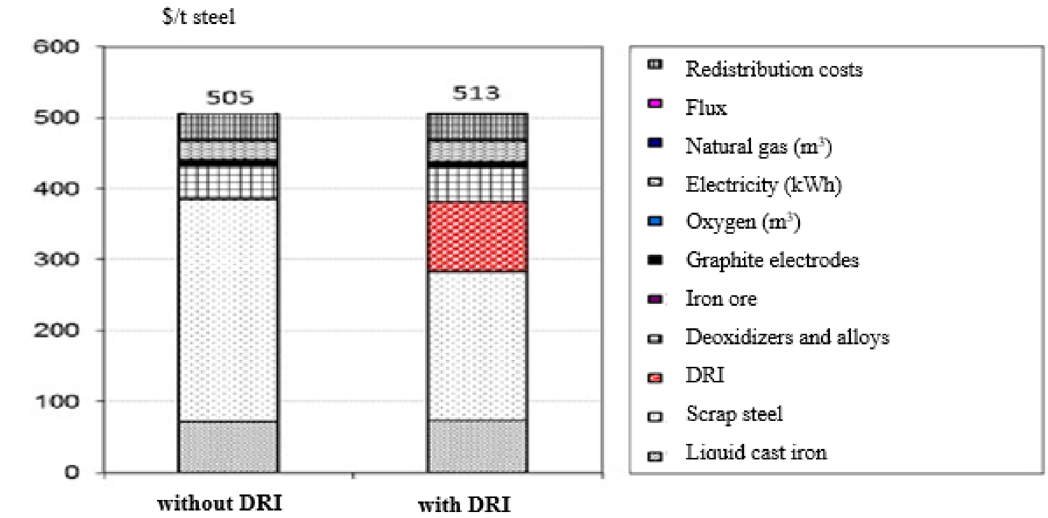

Figure 7. Cost of DRI production in the world

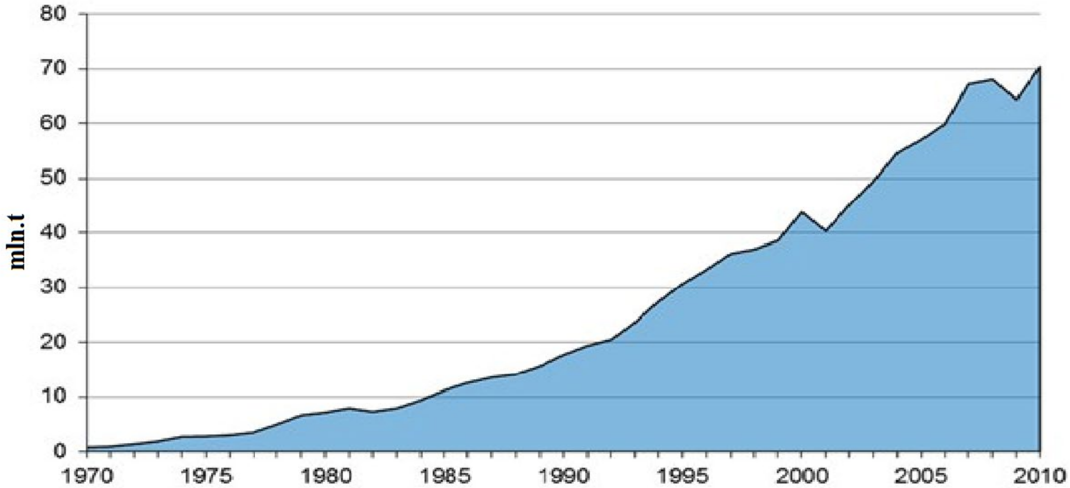

Figure 8. Volume of world trade of DRI by product types

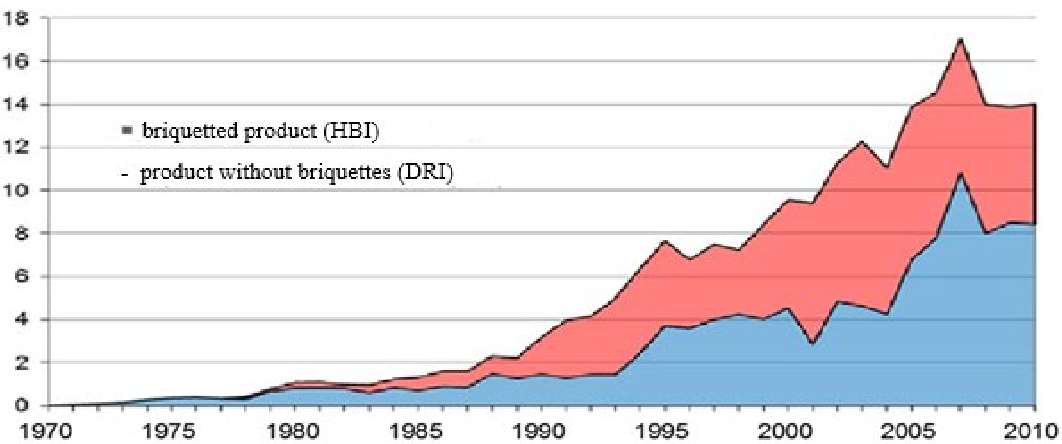

Figure 9. Transportation share of DRI production

It is clear that the main consumer of DRI is the production of electropolishing, because the share of DRI in the metallurgy can reach 70%. DRI has a number of advantages over other components of the system:

- stability of chemical composition; low sulfur and phosphorus;
- absence of elements prone to liquefaction (lead, copper); high spreading weight;
- the possibility of being fed to an electric furnace without stopping the melting process;
- protection of electrodes from mechanical damage.

The disadvantages of using DRI in electric furnaces are:

- increase in energy consumption (every 10% DRI: +15kW.s/t);
- increase in electrode consumption (every 10% DRI: +0.2 kg/t);
- reduction of healthy metal yield (every 10% DRI: - 0.4%);
- increase in thawing time (every 10% DRI: + 2.5 min);
- an increase in the heat load on the masonry of the furnace.

The pros and cons of DRI production and application are reflected in the price of DRI. Replacing 30% of scrap metal with similarly priced DRI increases steelmaking costs by about \$8 per ton (Fig. 10). To ensure efficiency, the price of DRI should be ~7% lower than the price of high-quality scrap metal.

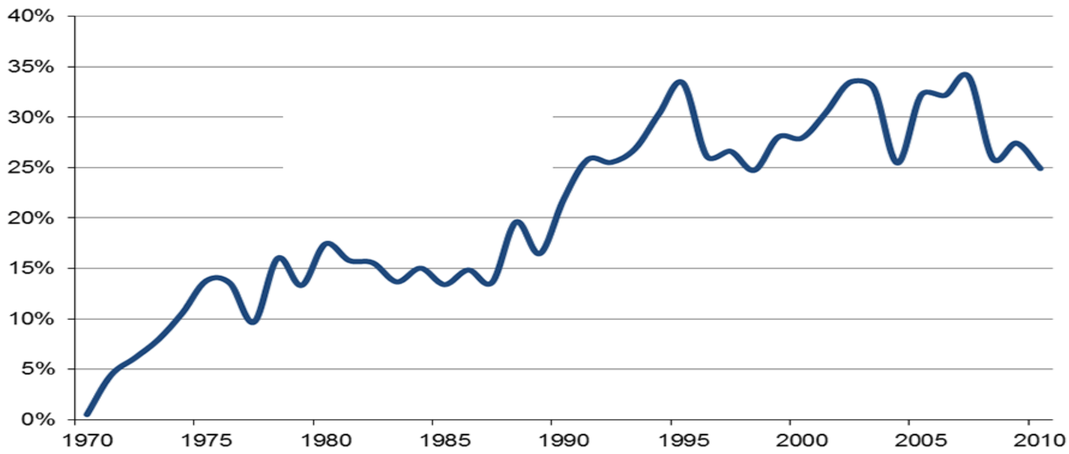

Figure 10. Cost of steel with and without DRI

The price dynamics of DRI and scrap metal in 2009-2012 is presented in fig. at 11:

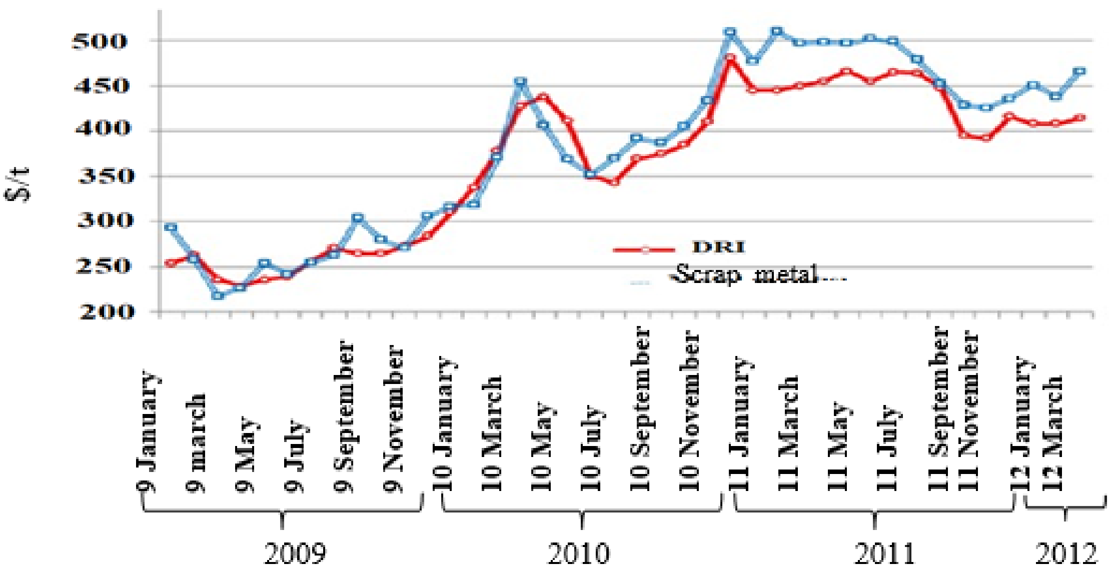

Figure 11. Price dynamics of DRI and metal scrap

[7] - in the "Metallurgical" scientific and technical bulletin, an analysis of the general trends of the development of the Russian and world metallurgical industry in the first quarter of 2023 was carried out. Factors affecting the results of the industrial sector were evaluated and forecasts for the upcoming period were given. It is noted in the bulletin that in 2023, the world prices of steel products continued to increase, but a certain decrease was observed against the background of the recovery of the Chinese economy.

The prices of non-ferrous metals and alloys are formed under the influence of fluctuations in the dollar exchange rate and the threat of a possible decrease in the growth of the world economy. World steel production decreased by 0.1% during the investigated period. However, China and India increased their production of steel products, but other countries saw a slight decrease. A bigger decline was seen in metallurgy in sister Turkey, and the main reason for this can be explained by the devastating earthquake in the south-east of the country.

Russian metallurgical production increased in the first quarter mainly due to non-ferrous metallurgical output, although ferrous metallurgical output decreased due to a sharp drop in exports. In non-ferrous metallurgy, there was an increase in the production volume of gold, silver and primary aluminum, copper and zinc, but a decrease in nickel production was observed due to repairs at "Norilsk Nickel" enterprises.

Despite the significant decrease in the production of large-diameter pipes in Russia, the production of steel pipes in general increased again at a record level. Experts believe that metallurgical production in 2023 may remain at the level of 2022, provided that the stability of the world economy is ensured.

In works [8-10], considerations were put forward about the future of Russian metallurgy. It is noted that in recent years the metallurgical industry in Russia has been developing and updating more actively than other sectors. New technologies and innovative solutions make it possible to improve product quality, increase production efficiency, and reduce production costs. The article focuses on the following recent innovations in Russian metallurgy.

1. Use of nanotechnologies in steel production. The use of nanoparticles in steel production processes is considered one of the most promising technologies. Nanoparticles make it possible to improve the important properties of metal, such as strength, corrosion resistance, and resistance to thermal effects.

2. Development of electrometallurgy. Electrometallurgy is characterized as a progressive technological process that opens wide opportunities for obtaining metals and alloys from their oxides and other by-products. In recent years, this technology has gained more popularity due to its undoubted advantages over the traditional blast furnace technology. The fact is that electro-metallurgy has the possibility to be applied in the production of rare metals and alloys that are difficult to obtain by traditional methods.

3. Application of new materials for construction and construction sector. Modern construction materials should be strong and light at the same time. One of the materials that meet such requirements is sandwich type composite steel. Sandwich-type composite steel consists of several layers of different materials, which make the steel strong as well as light. Composite steel also makes the product resistant to various types of corrosion and has sufficient longevity.

4. Development of new types of equipment for the metallurgical industry. Modern metallurgical equipment should be more efficient and easy to use. In this context, one of the last successful operations can be considered a device for automatic welding under high pressure. This technology allows welding metal structures with high speed and precision.

Thus, the article concludes that despite all the difficulties, the development of Russian metallurgy continues. New technologies and innovative technical solutions make it possible to increase production efficiency, improve product quality and reduce production costs. Based on these trends, the metallurgical industry will continue to develop and will be able to maintain its position as one of the leading sectors in the country's economy.

In cases no. [11-14] (Black metals, 2022, №2, DOI 10.17580/chm.¬2022.02.13) trends and prospects in the market of ferrous metals are analyzed in the context of the impact of the world crisis. The article examines the current state of the world and Russian ferrous metal markets. Special attention is paid to the formation of the metallurgical product price. Research is based on statistical and comparative analysis, as well as rating and prognostic assessment methods.

It was determined that at the beginning of 2020, the main blow to the world metallurgical industry was the decrease in demand for metals and alloys against the background of the collapse of the economic activity of many states and entities within the framework of anti-coronavirus restrictions.

The reasons for the sudden increase in demand and prices in the market of ferrous metals in 2021 have been determined. The serious recovery of developed countries after lifting the lockdown in their economies, the implementation of long-term infrastructure projects, the shortage of metal resources in the world, the transition of the metallurgical industry to the "green" economy, etc. reasons are given. On the basis of established trends and expert opinions, perspectives of production, consumption and price formation in the market of metals, alloys and metal products were predicted.

In the article "Analysis of trends in the world metal complex in the post-pandemic era: ferrous and non-ferrous metallurgy" (Innovation and investment, No. 3, 2021), the following results were obtained [15-21]:

- the world steel market faced difficulties during the pandemic and showed a trend of decreasing production and consumption; however, the pandemic itself did not have a serious long-term negative impact on the field;
- the revival of the metallurgical market has already been observed in the second quarter of 2020, which can be mainly attributed to the gradual recovery of business activity in China;
- the restoration of economic activity in the fields of steel consumption has led to an increase in the price of metal products and demand for steel in the world market;
- cross-border restrictions have led to greater localization of a number of production and operations during the pandemic and post-pandemic period;
- the need for maximum protection of human resources has created an opportunity to optimize supply chains due to robotization, automation, remote control and electronic commerce.

Thus, unlike many other industries, the ferrous and non-ferrous metallurgy industry has been in a pre-crisis state since the second half of 2019. This situation was reflected in the decrease in demand and prices for basic metal products. Although the negative impact of the pandemic was significant, it did not have a dramatic negative impact on the field.

In the post-pandemic period, the field quickly recovered its potential, and the main indicators of the metal market showed stable growth. The management systems of metallurgical companies have undergone significant changes, which has created the basis for increasing the efficiency of adaptation to modern world realities for the long term.

In the article **“Analysis of trends of the world metallic complex in the period of post-**

pandemic recovery: black and non-ferrous metallurgy" by A.C. Kharlanov, published in issue No. 3 of 2021, interesting facts attract attention [17].

The article shows that as a result of the spread of the coronavirus infection, product production in the world metallurgical industry decreased in 2020 to 1,850 million in 2019. 1,799 million from t. t, partially restored in 2021 to 1,900 mln. t, and 1,988 million in 2022. t organized.

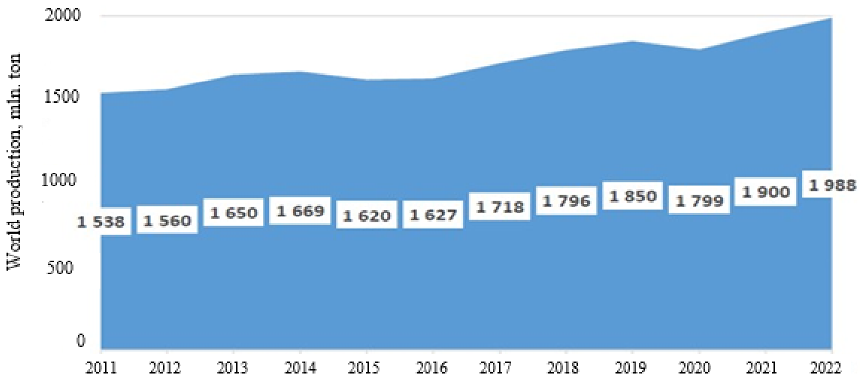

Figure 12. Dynamics of steel production in the world in 2011-2022

Fig. 12, the dynamics of steel production in the world in 2011-2022 is described based on the data of Worldsteel website. Fig. In the 13th, the dynamics of the annual growth of steel production in the world during the same period is presented. Fig. 14 shows the annual dynamics of world steel consumption in 2011-2022. Again, the dynamics of steel production and consumption in the world for that period is shown in fig. It was presented on the 15th. Fig. Figure 16 shows the dynamics of iron ore price changes in the world market in 2016-2023.

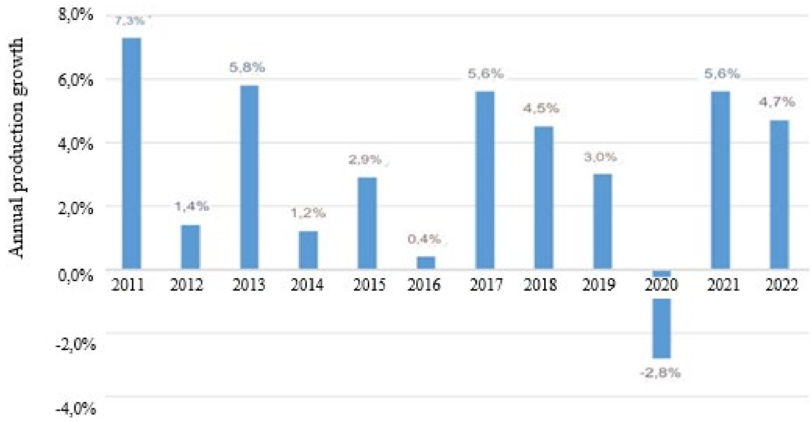

Figure 13. Dynamics of annual growth of steel production in the world in 2011-2022

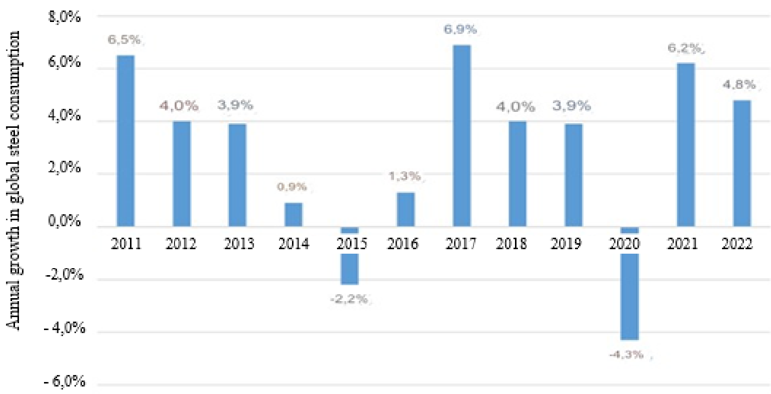

Figure 14. Annual dynamics of world steel consumption in 2011-2022

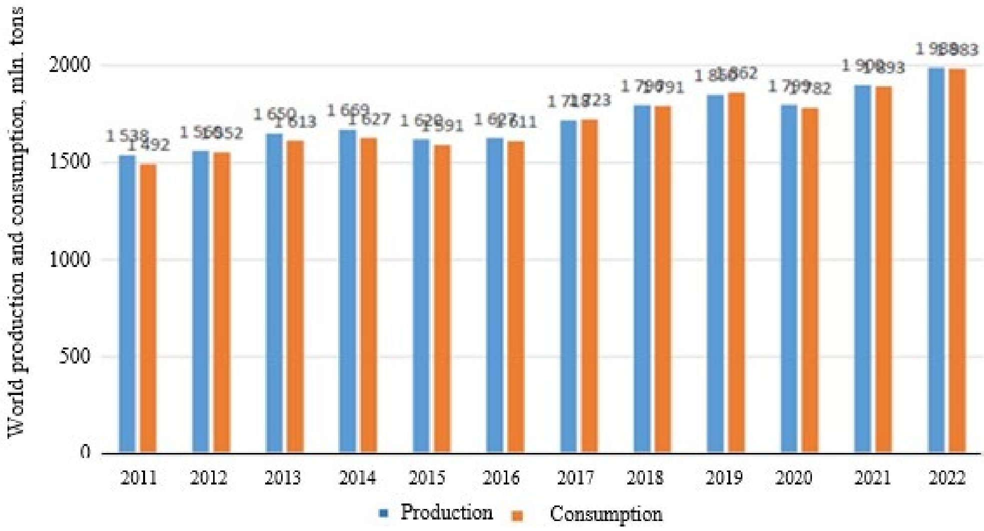

Figure 15. Steel production in the world in 2011-2022 and dynamics of consumption

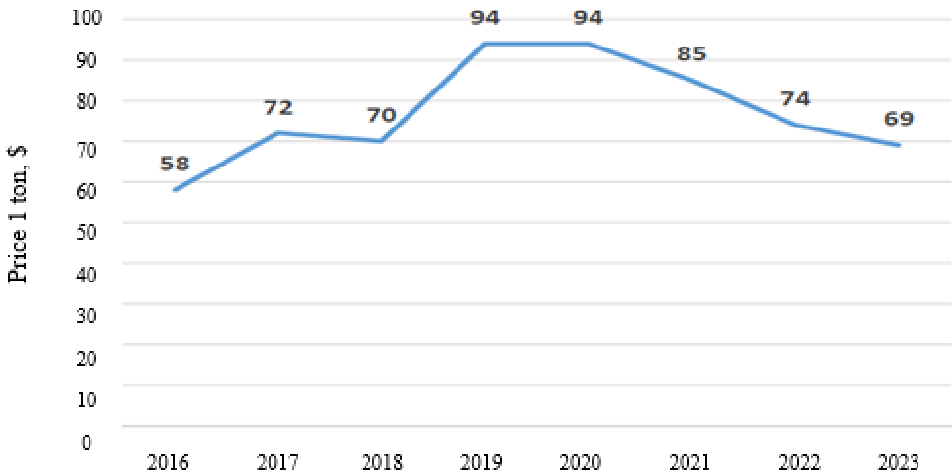

Figure 16. Iron ore on the world market in 2016-2023 price changes

Result.

1. The advanced methods of metallized iron production, which determine the growth dynamics of steel production in the world with the application of innovative technologies, have been analyzed, and their positive and negative aspects have been examined. It was determined that the purchase of non-blast iron can be considered effective mainly for the production of electrosteel. Therefore, the volume of metallized iron production increases at an increasing rate every year and contributes to steel production.

2. The modern state of the world's ferrous metallurgy was analyzed, new trends in steel production were determined under the conditions of globalization and new reality, tough competition and sanctions, as well as protectionist policy. The objective picture was evaluated based on the statistical indicators characterizing the state of metallurgical production in the world's leading countries. It has been shown that the development of ferrous metallurgy is characterized by the new reality of the modern world, constant change, geopolitical instability, constantly increasing tension and complexity.

Funding Acknowledgements.

This article was created under the support of the Azerbaijan Science Foundation - Grant No. AEF - MCG - 2023 - 1 (43) - 13(01)1-M-01.

REFERENCES

[1] Chebotarev Sergey, Korotchenko Anna. Metallurgy of the future: what awaits the industry in the era of the 4th industrial revolution // using the example of NLMK Company //up-pro.ru/strateg

[2] Review of the metallurgy industry for the 1st quarter of 2023 // Bulletin Metallurgy: trends and forecasts, RIA Rating, 2023, issue No. 50, rating@rian.ru

[3] Harlanov A.S. *Analysis of trends in the global metallurgical complex during the post-pandemic recovery period*. Economics and business, 76-83.

[4] *Development of electrometallurgy - ferrous and non-ferrous metallurgy*. metallome.ru

[5] Vladimir Safonov, Alexey Smirnov (DNTU). *Where are the leaders of electrometallurgy heading?* read-metal.com

[6] Budanov I.A. *Management of the Development of Metallurgy and the Global Metal Market*Studies on Russian Economic Development. 2020. Vol. 31, No.6. pp. 663–673.

[7] Zinovieva N.G. *Ferrous metallurgy of the world and Russia in a pandemic. Ferrous metallurgy.* Bulletin of scientific, technical and economic information. 2020. T. 76, № 7. pp. 657–664.

[8] *London Metal Exchange /LME - prices. Central metal portal of the Russian Federation.* URL: https://www/metallicheckiy-portal.ru/index-cen-lme (date of the application: 24.11.2021)

[9] *World Steel Association. World Steel in Figures.* URL: https://www.worldsteel.org/steel-by-topic/statistics/World-Steel-in Figures.html

[10] Tarnavsky V.V. *Chinese acceleration*. Metal supply and sales.2020. № 11. pp. 86

[11] Kaukin A. S., Kosarev V. S., Miller E. M. *Metallurgical industry in 2020 and early 2021. Monitoring the economic situation in Russia* // Trends and challenges of socio-economic development. 2021. T. 144, № 12. pp. 16–20.

[12] *Federal State Statistics Service (Rosstat).* URL: https://rosstat.gov.ru

[13] *The pace of economic recovery in Russia is accelerating.* Russian Economic Report (World Bank Group). 2021. No. 45. P. 88.
URL: https://www.vsemirnyjbank.org/ru/country/russia/publication/rer

[14] Adno Yu.L. *World metallurgy 2020: consequences and lessons of the pandemic*. Ferrous metals. 2021. No. 8. pp. 61–67.

[15] *"Russian Steel" - results of 2020: the situation in the industry*. Metals of Eurasia. 2021. No. 1. P. 4–5

[16]Tarnavsky V.V. *There would have been no happiness, but misfortune helped*. Metallosnabzhenie and sales. 2020. No. 12. P. 18

[17] Kharlanov A.S. *Analysis of trends in the global metal complex during the post-pandemic recovery period: ferrous and non-ferrous metallurgy*. Innovations and investments. 2021. No. 3. P. 76–83

[18] Bolotin M. *On the prospects of hydrogen metallurgy*. Metal supply and sales. 2021. No. 2. P. 86

[19] Fedoseev S.V., Tsvetkov P.S. *Key factors of public perception of carbon dioxide capture and disposal projects*. Notes of the Mining Institute. 2019. No. 237. P. 361–368

[20] Pei M. *SSAB is determined to take leadership in the global transition to “green” steel* . Metals of Eurasia. 2021. No. 4. P. 16,17.

[21] Rakhlis T.P., Skvortsova N.V., Koptyakova S.V., Balynskaya N.R. *Development of Microelectronics on the Circumstances of the Innovative and Technological Growth of the Russian Economy*. International Business Management. 2016. Vol. 10, Iss. 4. P. 401–407

Received: 13.01.2024
Accepted: 17.06.2024

MACHINE SCIENCE

ISSN: 2227-6912
E-ISSN: 2790-0479

2024, № 1 Pages 36-45

ANALYSIS OF ERRORS OCCURRING DURING TOOTH MILLING OPERATIONS AND TECHNOLOGICAL SYSTEM FACTORS AFFECTING THE ACCURACY OF TOOTH PROCESSING

Michael PASHKOV[1,a], Ilya AVVAKUMOV[2,b], Heyran ABBASOVA[3,c*], Elgun SHABİYEV[3,d], Irada ABBASOVA[3,e]

[1]KAMAZ PJSC, Naberezhnye Chelny, Russia
[2]Department Design and technology of machine-building industries of Kazan National Research Technical University named after A.N.Tupolev – KAI, Naberezhnye Chelny, Russia
[3]Department of Machine Building Technology, Azerbaijan Technical University, Baku, Azerbaijan

E-mail: [a]mikh-pashkov@mail.ru, [b]iiavvakumov@kai.ru [c]abbasova.heyran@aztu.edu.az, [d]elgun@aztu.edu.az, [e]i.abbasova@aztu.edu.az*

https://doi.org/10.61413/MRKD7906

Abstract: The article discusses the issues of determining and analyzing errors in the formation of gears by gear hobbing in the conditions of large-scale machine-building production. An analysis of some errors was carried out. The work identified the following main types of errors that arise during the machining of gears: radial, tangential, axial, producing surfaces. Each of these types has been analyzed in sufficient detail, and a table of the influence of errors in the technological system on the main parameters of the producing surface of the tool has been compiled. In addition, the work analyzes and systematizes the factors of the technological system that affect the accuracy of the formation of gears. All errors are considered in one small period of time and then approximated in time. This approach avoids the problem of heterogeneity of errors. Thus, a generalized universal model of the structure of machine errors is formed. Next, by obtaining mathematical models for each error, a model of the errors of the technological system is formed. The article provides a classification of hob gear cutters. Here we distinguish involute, convolute and Archimedean cutters. The article states that the errors in the relative positions of each conjugated point of the generating and machined contours are composed of: a) errors in the relative position of the tool and the workpiece in space, created by inaccuracies in the manufacture and setup of the machine and fixtures, as well as inaccuracies in the rolling movements; b) errors in the profile of the generating contour (tool) itself. It is indicated that in the manufacture of gears using the profile copying method, the errors of the tool itself and the location of the tool and the workpiece on the machine, the geometric accuracy and rigidity of the machine are of greatest importance. When machining gears using the rolling method, the kinematic and dynamic accuracy of the machine increases. An analytical dependence is provided—a formula—that considers a combination of factors affecting the accuracy of the tooth profile to varying degrees. The provisions put forward in this work in terms of accounting and systematization of gear machining errors play an important role. In conclusion, the article provides recommendations for improving the quality of processing of gear teeth, as well as constructing a three-dimensional model of the interaction of three elements of the technological system: machine - hob gear cutter - workpiece.

Keywords: *gears, gear machining, machining errors, gear cutting tools.*

Introduction.

One of the important tasks facing researchers is the ability to control the precision of manufacturing parts. Error minimization is a special case of part manufacturing quality management.

Ensuring the accuracy of gears at the stages of roughing is an integrated task, the solution of which depends on many parameters: technological preparation of production, applied processing methods, technical and technological discipline in production.

Research.

The task facing the researchers is to determine the dependencies of the precision of the toothed crown on the errors of the technological system, tool, basing, workpiece, etc.

These include the manufacturing error of the worm cutter (f_{fr}), the error of installing the milling cutter on the machine ($f_{\text{ins.fr.}}$), blank error ($f_{\text{workp.}}$), the error of installing the workpiece on the machine ($f_{\text{ins.workp.}}$), machine error ($f_{\text{mach.err.}}$), measurement error ($f_{\text{meas.}}$).

In accordance with GOST 1643-81, *the error of the f_{fr}* tooth profile is the normal distance between the two nominal end profiles closest to each other, between which the actual end active profile of the tooth of the gear is placed. The actual end profile of a tooth is understood as the line of intersection of the actual lateral surface of the tooth of a gear wheel with a plane perpendicular to its working axis [1].

Thus, the calculated error of the tooth profile of the gear is a function of:

$$f_{fr.calc.} = F(f_{fr}, f_{inst.fr.}, f_{\text{workp.}}, f_{\text{ins.workp.}}, f_{\text{mach.err.}}, f_{\text{meas.}}) \quad (1)$$

In accordance with GOST 1643-81, the tolerance for tooth profile error f_{f}.

Accordingly:

$$f_f \geq f_{fr.calc.} = F(f_{fr}, f_{inst.fr.}, f_{\text{workp.}}, f_{\text{ins.workp.}}, f_{\text{mach.err.}}, f_{\text{meas.}}) \quad (2)$$

After analyzing the existing error calculation methods, the following were identified:

1. Systematic errors:

- errors of the workpiece- errors of manufacture, basing;
- machine errors- errors in the manufacture of individual components and their relative location, taking into account their wear during operation;
- errors resulting from the forces and moments acting during processing.

2. Random errors- uneven properties of the material of the workpiece, tool, etc.

Random errors have an effect on the occurrence of scattering of the workpiece sizes processed under the same conditions [2, 3, 4, 5]. The size dispersion is due to many random causes that cannot be accurately determined beforehand and that manifest themselves simultaneously and independently of each other. Such reasons include fluctuations in the hardness of the workpiece material, fluctuations in the temperature regime of processing, elastic squeezing of the elements of the technological system under the influence of cutting forces, etc.

The analysis shows that processing errors are not fully taken into account when calculating dimensional chains. Moreover, the errors selected manually from the reference literature are not systematized, implicit, automatic calculations of dimensional circuits, taking into account the errors that occur during machining, are insufficiently developed.

Automated calculation of errors in this case is difficult, because it is necessary to simultaneously take into account the causes of errors and the laws of their change over time. It is proposed to consider the process of forming the lateral surface of the tooth of the gear ring of the wheel at a specific time, and then the resulting functional dependencies change over time. In this case, all errors can be considered static. Random errors at a particular time can be taken as constant values. The dynamic errors under these conditions depend only on the cutting parameters.

Accounting for errors and determining the type of their relationship can be achieved by introducing intermediate coordinate systems (IC). According to the differentiation method, errors are identified that occur at a certain level, starting from the coordinate system of the machine further towards the tool and the workpiece to the cutting point. The beginning of the SC node shows the spatial position of this node relative to the coordinate systems of the previous nodes and the machine as a whole.

Each CI characterizes a specific *i*-th node of the machine tool system, thus the error of the i-th link is unambiguously described in the corresponding SC. And the interrelationships of the SC with each other determine the accumulated error. Geometrically, the accumulated error is a vector with a beginning in the (*i*-1)-th SC and an end in the *i*-th SC. The choice of the origin of coordinates for each SC is carried out in accordance with the standard coordinate system of the gear milling machine, which minimizes errors and reduces the number of SC.

In order to determine the "degree of contribution" of the error of a particular node to the total error, all intermediate errors are systematized on the one hand according to the object of influence of the error - the location of the workpiece or tool. In order to ensure the completeness of information about errors, the differentiation (detailing) of the technological operation into individual elements is carried out according to the method of differentiation of TP into structural elements.

Differentiation is carried out by "sequential movement" from the point of contact between the tool and the workpiece, moving from the consideration of microsystems to macrosystems. An error vector is calculated at each level (as the geometric sum of all error vectors taken into account at this level).

All errors are considered in one small period of time and then approximated in time. This approach makes it possible to circumvent the problem of heterogeneity of errors. Thus, a generalized universal model of the machine error structure is formed. Further, by obtaining mathematical models for each error, a model of the errors of the technological system is formed.

Consider the static error of the profile of a worm gear cutter.

Roughing of the gear rings of cylindrical wheels is mainly carried out by worm gear cutters.

The cutting edges (RC) of worm cutters are located on the surface of the coils of various types of worms. These worms are called the main ones.

As is known, depending on the type of the main worm, worm gear cutters are classified as involute, convolute and Archimedean.

The exact geometric shape of the main worm is determined by the condition of proper engagement of this worm and the gear wheel. Since proper engagement with an involute gear wheel forms only one type of worm- an involute worm, an involute worm must be adopted for theoretically accurate profiling of the worm.

The main advantage of this worm is the presence of an involute profile in the end section, and a complex curved profile in the axial or normal section to the turns of the worm. Therefore, theoretically correct profiling of the worm cutter will be ensured when the cutting edges are positioned on the surface of the coils of the involute worm [6].

However, at present, in the manufacture of worm cutters, the main worms are used, which are shaped approximately according to Archimedean or convolute worms.

The worm closest to the involute, Archimedean, is distinguished by a rectilinear trapezoidal profile in the axial section and a curved profile along the Archimedean spiral in the end section. This feature makes it easy to manufacture and control Archimedean worm cutters.

The convolute worm has a rectilinear trapezoidal profile in a normal section along the turn, or in the hollow of the turns. In the same sections, a profile is set for worm cutters profiled on the basis of convolute worms.

In general, the theoretical profile of the cutting edge of a worm gear cutter, which is the line of intersection of the main involute screw and the front flat surface, is curved. Since the manufacture of a cutter with a curved RC of a given profile is quite difficult, in practice their profile is approximated by a straight line, a circular arc, three rectilinear sections or a hyperbola [7, 8].

In the article Lazebnik I.S. [9], the organic error of the profile of the cutting edge of the milling cutter resulting from processing is considered.

The simplest and most common in practice is the profiling method, which consists in approximating the theoretical profile of the RC by a straight line segment. However, the value of the OP may be unacceptably large. If the approximating straight line passes through a point lying on the average calculated cylinder and is tangent to the theoretical profile of the RC at this point, then the maximum OP is observed at the points of the RC furthest from the specified point.

The accuracy of the profile of the RC worm cutter depends not only on the profiling method, but also on the method of backing the teeth.

The most common is radial backing with a disk circle, in which the angle Σ of the intersection of the axes of the cutter and the circle is equal to the angle (γ_{mo}) lifting the helical line of the main worm of the milling cutter on the middle design cylinder. With this method of backing, there is an error in the profile of the milling cutter tooth, which cannot be completely avoided, but can be reduced by choosing the parameters of the grinding wheel at a given angle Σ.

The calculated error of the milling tooth profile, according to I.S. Lazebnik, is determined by errors that arise as a result of approximate profiling and backing of the milling tooth [9]. The calculated error of the milling cutter tooth profile f_Σ in the axial direction and $f_{\Sigma n}$. The normals are determined from the expressions:

$$f_\Sigma = \Delta f - f, \quad f_{\Sigma n} = \Delta f_n - f_n \tag{3}$$

where Δf- the organic error measured in the axial direction; Δf_n and f_n- OP and deviation of the tooth profile from the straight line caused by occlusion, measured according to the normal.

Let's set the task of determining the error of the profile of a milling cutter with a front angle not equal to zero ($\gamma_B \neq 0$).

The planes A-A, B-B and C-C intersect the axis of the milling cutter and the intersection points of the circle with a diameter of dm0 with the front surface, respectively, for the new non-threaded milling cutter, in the design section and for the fully re-threaded milling cutter (fig.1). Let's denote the angles between the planes of sections by φ_1 and φ_2.

For a non-overfilled milling cutter, the radii of the circles of the protrusions of the depressions are greater than the corresponding radii in the calculated section by an amount:

$$\Delta_{r_1} = \frac{K_{z_0}\varphi_1}{2\pi} \tag{4}$$

For fully reworked cutters, the specified radii are respectively equal:

$$\Delta_{r_2} = \frac{K_{z_0}\varphi_2}{2\pi} \tag{5}$$

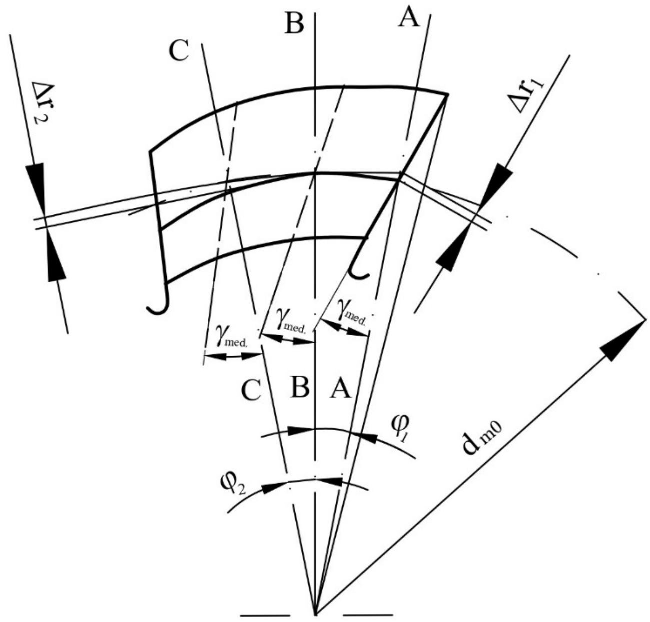

Fig.1. The scheme for determining the error of the tooth profile of the milling cutter with $\gamma_6 \neq 0$

The plane of the section B-B is symmetrical with respect to the planes A-A and B-B, thus the

$$\Delta_{r_1} = \Delta_{r_2} = \frac{K_{z_0}\varphi}{2\pi} \tag{6}$$

angles $\varphi_1 = \varphi_2 = \varphi$ and.

With overflows of error Δf_n, f_n and accordingly $f_{\Sigma n}$ they may change. Obviously, all other things being equal, the change in error $f_{\Sigma n}$ with overflows, the greater the value, the more K, z_0 and φ.

Many elements of the technological system have an impact on the accuracy of dental treatment. The article discusses the nature and classification of gear processing errors, as well as their impact on the accuracy of the gear being processed. A table of the influence of errors in the technological system on the main parameters of the producing surface of the tool is presented.

The accuracy of gear processing of cylindrical gears, as well as the accuracy of mechanical processing in general, is influenced by the following main factors [10]:

1. The accuracy of manufacturing the elements of the technological system (TS) — machine tool, attachment, tool, workpiece.
2. The accuracy of the machine settings and the installation of tools and workpieces.
3. Elastic deformations of TC elements due to instability of cutting forces and non-rigidity of these elements.
4. Wear, thermal deformations of vehicle elements during processing, redistribution of internal stresses in the workpiece during various operations, etc.

The geometric, kinematic and dynamic components of machine precision are distinguished. The geometric accuracy of the machine is determined by the accuracy of the dimensions, shape and relative position of the machine elements in a static state. The kinematic and dynamic accuracy of the machine is manifested during its operation. The first is determined by the accuracy of the mutual superposition of all elements of the vehicle during the entire processing time of the part, the second by fluctuations in the values of the kinematic accuracy of the machine due to the non—rigidity of its elements and periodic changes in the forces acting on them. The kinematic and dynamic accuracy of the machine has a particularly great influence on the accuracy of tooth processing when processing teeth using the rolling method.

The accuracy of the shape, dimensions and location of the lateral surfaces of the teeth is determined by the accuracy and constancy of the mutual positions of the producing contour and the product at each moment of time. The errors in the relative position of each conjugate point of the producing and processed contours consist of: a) errors in the relative position of the tool and the workpiece in space created by inaccuracies in the manufacture and configuration of the machine and tooling, as well as inaccurate running-in movements; b) errors in the profile of the producing contour (tool) itself.

The kinematic accuracy of the machine does not matter in machines operating using the free-rolling method (gear shaving, tooth-honing, tooth-rolling, tooth-grinding, etc.), since the running-in movement on these machines occurs as a result of direct engagement of the tool and the product.

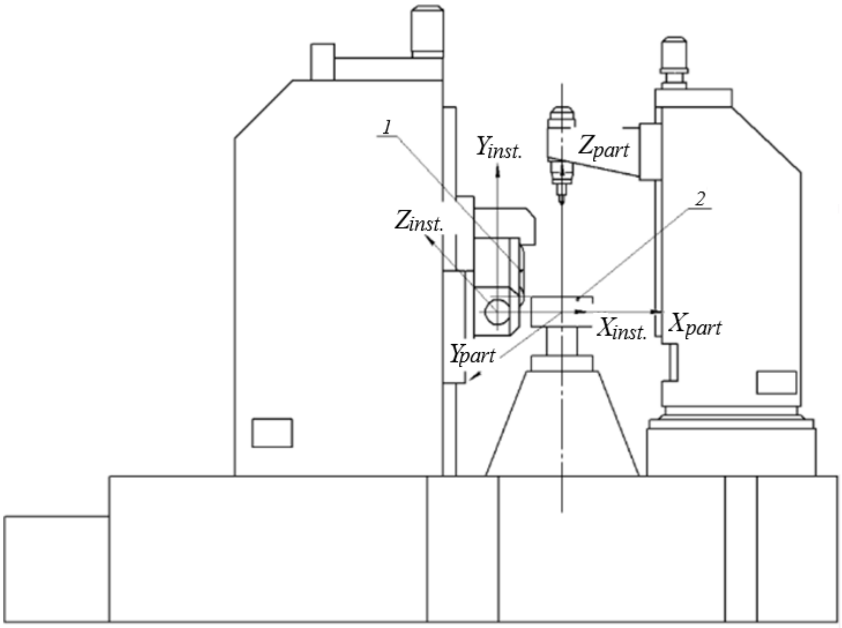

Fig.2 Technological system of the gear milling machine: 1- hob gear cutter, 2-gear

In the manufacture of gears according to the method of copying the profile, the errors of the tool itself and the basing of the tool and the preparation on the machine, the geometric accuracy and rigidity of the machine are of paramount importance. In the manufacture of gears by the rolling method, the importance of the kinematic and dynamic accuracy of the machine increases.

The nature and classification of dental processing errors

All the processes of shaping and finishing the teeth of cylindrical gears are intermittent and periodic due to the intermittent location of the teeth of the wheel on its crown, the limited number of teeth of the tool, the nature of the interaction of the wheel and the tool during tooth processing. Sinusoidally varying gear working errors also occur due to the reasons of harmonic errors of rotating elements of the vehicle, the gear working machine (gears, shafts, blanks, tools, etc.) and errors of the teeth of the workpiece that occurred during previous operations.

Practice shows [10] that in real gears, a limited number of harmonic vibrations are noticeably manifested, caused by: a) wheel installation errors during tooth formation; b) the beating of the dividing wheel in the gear machine; c) the beating of the worm of the dividing transmission of the machine; d) the beating of the gear cutting tool; e) the axial beating of the lead screw.

These inaccuracies are found accordingly: a) by the radial runout of the gear ring; b) by the accumulated error of the circumferential pitch measured from the base during gear processing; c) by the longitudinal stripes observed on the bevel-toothed wheels, or cyclic errors of the corresponding frequency; d) by sinusoidally varying profile errors; e) by the undulation of the lateral surface of the teeth of the bevel-toothed wheels.

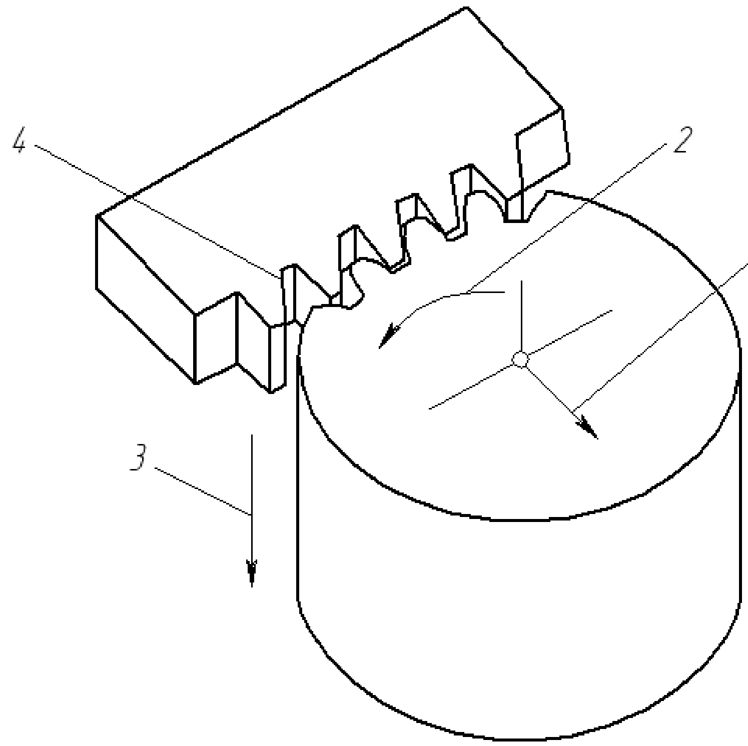

Fig. 3 Four types of errors in dental treatment: 1- radial, tangential, axial, producing surface

Other periodic errors [11] have little effect under normal conditions and appear only when their values significantly exceed the technically permissible norms. The effect of all random errors, which do not have a periodic nature of change, is one percent of the total error of the wheel and can be considered separately with sufficient accuracy.

The periods of fluctuations of the components of the periodic error of the wheel are interconnected by the ratio:

$$T_1 = 2T_2 = 3T_3 = ... = iT_i \tag{7}$$

where T_1 - the period of the main oscillation is equal to 2πn; n - the number of revolutions of the wheel during gear cutting; T_2, T_3, …, T_i - the periods of the components of the wheel error.

Consideration of wheel errors in the form of a periodic function allows a new approach to solving a number of practical problems. The most significant of them are: finding product errors based on particular sinusoidal vibrations acting during the manufacture of gears; finding the correct methods for measuring the total periodic error of the wheel and decomposing it into a number of separate harmonic components during technological analysis to determine the period, amplitude and initial phase in order to detect the primary sources of the total periodic error of the wheel; finding links between periodic error and its manifestation during operation of this gear in transmission in the form of noise, vibrations, dynamic loads.

The effect of individual errors that occur during gear processing can be reduced to four types

(Fig. 3): a) a change in the radial distance between the tool and the gear being processed — radial machining errors; b) a violation of the rolling of the tool and the product or inaccuracies of division — tangential machining errors; c) errors in tool movement along the axis of the product — axial processing errors; d) deviations of the producing surface of the tooth working tool — errors of the producing surface.

Radial error tooth treatments occur due to errors in the basing of the product on the machine, the radial runout of the tool and periodic fluctuations in the position of the spindle of the product (table swing) or the tool. Radial machining errors are characterized by the fact that they remain constant in any axial section of the wheel. Many examples can be given of the causes of errors in the basing of the workpiece on the machine: the beating of the centers of the machine relative to the axis of rotation of the table, the beating of the center sockets of the workpiece relative to its mounting necks, the beating of the mandrel of the machine table relative to the axis of rotation, the beating of the part due to the gap when it is placed on the mandrel, the separation of the technological and installation base, for example, during alignment workpieces on the machine according to its outer diameter.

Similar reasons cause radial runout of the tool: runout of the tool spindle seats, runout of the mandrel under the tool, gap of the tool landing on the neck or mandrel, tool manufacturing error.

Tangential error [11, 12, 13] tooth processing occurs mainly due to a violation of the rolling of the tool and product in machines operating by the rolling method, or due to division errors in machines with a dividing mechanism. The sources of these errors are errors in the links of the kinematic chain of machine tools and mainly the final worm pairs or dividing discs of machine tools and lead screws that are included in the rolling chain. The tangential processing errors remain constant along each contact line.

The axial error of the gear processing occurs mainly due to inaccuracies in the machine guides, the misalignment of the workpiece axis, and in some cases due to errors in the kinematic chain of the machine. The axial machining errors remain unchanged in each end section of the wheel. These errors cause a violation of the longitudinal contact, and in skew-toothed wheels, the high-altitude contact of the teeth.

Errors in the producing surface of the tool arise due to the use of approximate methods of profiling the tool [9] or errors in its manufacture and sharpening. In addition to these errors, wheel inaccuracies related to the influence of the intermittency of the cutting process due to the feed and the finiteness of the number of cutting edges of the tool should also be included here [14]. Any deviation of the shape of the producing surface of the tool from the exact surface creates a profile error on the product, and when cutting bevel wheels, also an error of the contact line. Inaccuracies in the profile angle of the producing surface of the tool also cause deviations in the engagement pitch and direction of the contact line on the product, which leads to non-smooth operation of the straight-toothed wheels and a violation of the high-altitude contact of any wheels.

The influence of errors in the technological system on the main parameters of the tool's producing surface is shown in Table 1.

Table 1. The influence of errors in the technological system on the main parameters of the producing surface of the tool

Errors of the technological system		The angle of intersection between the axes of the tool and the product, in º	The parameter of the screw surface of the product	The center-to-center distance between the tool and the workpiece, in mm
		ε	P	A_w
Radial errors	Errors in the installation of the workpiece	+	-	+
	Tool installation errors:	+	-	+
Tangential errors	- misalignment of the milling cutter axis;	-	+	-
	- radial runout of the cutter.	-	+	-
	Kinematic error of the dividing wheel	-	+	+
	The periodic error of the dividing wheel	-	+	+
	Kinematic and geometric eccentricity of the workpiece	-	+	-
Axial errors	Periodic error (swing) the table	+	-	+
	Cyclic errors of the worm and the dividing gear wheel of the machine	+	-	+
	The inclination of the guides of the tool carriage in the longitudinal plane	+	+	+
	Tilt of the table guides in the longitudinal plane	+	+	+
	The inclination of the guides of the tool carriage in the transverse plane	+	-	+
	Tilt of the table guides in the transverse plane	-	+	-
	The end runout of the base end of the workpiece	-	+	-
Errors of the producing surface of the tool	Inaccuracies inherent in the slicing method			
	Inaccuracy of the milling cutter tooth profile	-	+	-
	The number of cutting edges of the cutter	-	+	-
	Changing the shape of the cutting edges of the cutters as a result of their wear	-	+	-
	Inaccuracy in the manufacture or reworking of the tool			
	Inaccuracy of the milling cutter's producing profile (PP)	-	+	-
	Deviation of the front surface of the milling cutter tooth	-	+	-
	The error of the helical line and the steps of the mill rails	-	+	-
	Single tool pitch errors (corresponding to local shear of the cutting edge)	-	+	-
	Inaccuracy of the inclination or pitch of the screw chip grooves of the tool	-	+	-
	The error of the cutter installation			
	The runout of the main cylinder in the manufacture of a milling cutter relative to the control collars	-	+	+
	The runout of the mandrel of the gear cutting machine relative to the axis of rotation	+	+	+
	Non-concentricity of the hole in the mill and the mandrel of the machine	+	+	+

Conclusions.

The considered method makes it possible to construct with sufficient accuracy a three-dimensional model of the interaction of three elements of the technological system: a machine tool - a worm gear cutter- a workpiece. The technique allows us to take into account the relationship and the vector direction of the errors that occur.

The influence of errors in the technological cutting system on the calculated parameters of the producing surface of the tool has been established.

REFERENCES

[1]. Markov A.L. *Measurement of gears*. Leningrad.: Mechanical Engineering, Leningrad branch, 1977, 276 p.

[2]. Koshin, A.A., Yusubov, N.D. *Elements of matrix theory of multitool processing accuracy in three-dimensional setups.* Bulletin of mechanical engineering, no. 9, 2013, pp. 13-17.

[3]. Yusubov, N.D., Abbasova, H.M. *Full-factor matrix model of accuracy of dimensions performed on multi-purpose CNC machines*. Obrabotka metallov (tekhnologiya, oborudovanie, instrumenty) = Metal Working and Material Science, vol. 23, no. 4, 2021, pp. 6-20.https://doi.org/10.17212/1994-6309-2021-23.4-6-20

[4]. Yusubov N., Abbasova, H., Khankishiyev, İ. *Entwicklung einer Projektierungstheorie für die Mehr-werkzeugbearbeitung mit den Möglichkeiten der modernen CNC-Werkzeugmaschinen*. Forschung im Ingenieurwesen, no. 85, 2021, pp. 661-678. https://doi.org/10.1007/s10010-021-00478-7

[5]. Simonova L.A. *Managing the processing of a batch of parts*. Naberezhnye Chelny, 2004, 114 p.

[6]. Tsvis Yu.V. *Profiling of a cutting running-in tool.* M.: MASHGIZ, 1961, 155 p.

[7]. Tsepkov A.V. *Profiling of backed tools*. M.: Mechanical Engineering, 1979, 150 p., ill.

[8]. Romanov V.F. *Calculations of gear-cutting tools*. M.: Mechanical engineering, 1969, 252 p.

[9]. Lazebnik I.S. *Minimizing the error of the tooth profile of a worm gear cutter*. ISSN 0038-9811. Machines and tools No.4. 1990.

[10]. Yakimov A.V., Smirnov L.P., Boyarshinov Yu.A. Perov E.N., Naparyin Yu.A. *The quality of manufacture of gears*. M.: Mechanical engineering, 1979, 191 p.

[11]. Starzhinsky V.E. Kane M.M. *Production technology and methods of quality assurance of gears and gears*. St. Petersburg: Profession, 2007 830 p.

[12]. Rasulov N.M., Shabiyev E.T. *Instability ın cutting depth grinding teeth cogwheels by copying*. Proceedings of Higher Educational Institutions. Machine Building. BMSTU, 2016, No. 12 p. 79-86

[13]. Rasulov N.M., Shabiyev E.T. *Increasing the grinding efficiency gear teeth by copying based management depth of cut*. Proceedings of Higher Educational Institutions. Machine Building. BMSTU, 2017, No. 2 p. 90-97

[14]. Taits B.A. *Production of gears*. M.: Mechanical engineering, 1990, 463 p.

Received: 01.03.2024
Accepted: 01.06.2024

MACHINE SCIENCE

ISSN: 2227-6912
E-ISSN: 2790-0479

2024, № 1 Pages 46-57

THEORETICAL AND PRACTICAL ASPECTS OF THE APPLICATION OF THE DYNAMIC PROGRAMMING METHOD IN OPTIMAL CONTROL PROBLEMS

Viktor ARTEMYEV [1,a], Natalia MOKROVA[1,b], Anar HAJIYEV[2,c*]

[1]Federal State Budgetary Educational Institution of Higher Education Russian Biotechnological University, Moscow, Russia

[2]Department of Machine design and industrial technologies, Azerbaijan Technical University, Baku, Azerbaijan

E-mail: [a]artemyevvs@mgupp.ru, [b]mokrovanv@mgupp.ru, [c*]anar_hajiyev_1991@mail.ru

https://doi.org/10.61413/GIPV6858

Abstract: The article examines the dynamic programming method based on the principle of optimality, analyzes the theoretical aspects of the method, as well as its use for analyzing a wide range of systems whose behavior in the future can be fully or statistically predicted based on their current state. The research results suggest that dynamic programming is used to solve a variety of tasks, including, but not limited to, the development of algorithms in the fields of machine learning, automated management and the definition of a management strategy for production systems. The paper presents aspects of the application of the dynamic programming method to solve practical problems of optimal process control, demonstrating its effectiveness and versatility in conditions of real operational constraints.

Keywords: *dynamic programming, mathematical model, object control, system behavior.*

Introduction.

The mathematical description of the technological object determines the formulation and methods of solving the optimal control problem. The mathematical model of the control object is usually presented in the form of differential equations or systems of equations describing the dynamics of changes in the state of the system under the influence of external and internal factors. Object management involves the search for such a strategy of influencing the system, which will lead to optimal modes of conducting technological operations in accordance with the specified criteria [1, 2]. The purpose of building a management algorithm is to optimize the operation of an object in accordance with specified efficiency criteria [3], which includes minimizing costs, maximizing productivity or achieving a certain quality of management [4].

The increasing volumes of production systems and their complexity lead to the need to formulate tasks for adapting management facilities to changing operating conditions of the facility [5], expanding the requirements for its efficiency and reliability. The management of complex systems using traditional methods becomes ineffective [6, 7]. Which leads to the need to develop new approaches and management methods [8] capable of ensuring high adaptability and optimal behavior of the object in real time [9]. To solve this problem, a dynamic programming method is used, which allows us to effectively find optimal management strategies based on the Bellman optimality principle [10]. To implement effective management, it is necessary to integrate a system with various levels of control, from monitoring and analytics to active process management [11, 12]. A systematic approach combining data from all levels and subsystems is the basis for managerial decision-making

Formulation of the problem.

The dynamic programming method is used for a wide class of problems in the theory of optimal automatic control systems [13, 14, 15].

Consider the problem of controlling an object with the equation

$$\frac{dx}{dt} = f(x,u) \tag{1}$$

where x is an n-dimensional vector with coordinates $x_{1,\dots,}x_n$, and u is an r–dimensional vector with coordinates $u_{1,\dots,}u_r$. Let

$$u \in \Phi(u), \tag{2}$$

and it is required to minimize the functional

$$Q = \int_0^T G\left[x(t),u(t)\right]dt, \tag{3}$$

where, for example, we will consider T fixed for now.

The dynamic programming method is based on the optimality principle formulated by R. Bellman for a wide range of systems whose future behavior is completely or statistically determined by their state in the present. Therefore, it does not depend on the nature of their "prehistory", i.e. the behavior of the system in the past, as long as the system is currently in this state.

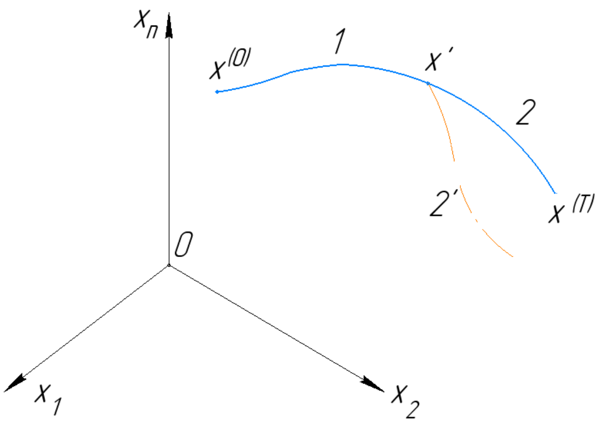

Figure 1. Illustration of the optimality principle

To illustrate, consider the optimal trajectory in the n-dimensional phase space of Fig. 1 with the initial and final values of the vector x equal to x^0 at $t = t^0$ (usually $t_0 = 0$) and $x^{(T)}$ at $t = T > t_0$. Let the initial conditions $x^{(0)}$ be given; the value of $x^{(T)}$, generally speaking, is unknown. Note some intermediate point x' of the trajectory corresponding to $t = t'$, where $t_0 < t' < T$, and call the section of the trajectory from $x^{(0)}$ to x' the first (1) in Fig. 1, and from x' to $x^{(T)}$ is the second (2). For the second section, as an independent trajectory from (3), we get $\int_{t'}^{T} G[x,u]dt$. The trajectory is optimal with the minimum value of the integral. The integral is minimal. The principle of optimality can be formulated as follows: the second section of the optimal trajectory is, in turn, the optimal trajectory.

Thus, the initial state of the system is x' at the initial moment of time $t = t'$, then regardless of how the system came to this state, its optimal subsequent movement will be trajectory 2. Let's assume the opposite, then criterion (3), considered for the time interval from *t* to *T*, will be the smallest is not for trajectory 2, but for some other trajectory $2'$, starting from point x', and shown by a dotted line in Fig. 1. But in this case, it would be possible to build a "better" trajectory than trajectory 1-2, and for the initial task it is only necessary to choose the control u so that trajectory 1 and then 2 are described. We proceeded from the optimality of trajectory 1-2. The contradiction proves the impossibility of the existence of trajectory 2, providing a lower value of *Q* than trajectory $2'$. So, trajectory 2 is optimal.

The optimality principle formulated above is a very general prerequisite for an optimal process, valid for both continuous and discrete systems. Only in the case when the endpoint is set c' from the first section at $t = t'$, the first section is also the optimal trajectory in itself. In this case, the state of the system at the time under consideration is understood to be the state corresponding to the point x' at time $t = t'$.

Let's say the motion of a controlled object is characterized by a first-order equation

$$\frac{\mathrm{d}x}{\mathrm{d}t} = f_1(x,u), \tag{4}$$

where *x* is the only coordinate of the system, and *u* is the only control action limited to some area (2). Let the initial condition $x(0) = x^{(0)}$ be given. Let's assume that we need to find a control law *u(t)* that minimizes the integral

$$\mathrm{Q} = \int_{\mathrm{t}_0}^{\mathrm{T}} \mathrm{G}_1(\mathrm{x},\mathrm{u})\,\mathrm{dt} + \varphi_1\left[x(T)\right], \tag{5}$$

where t_0 will usually be considered equal to zero, and the value of $T = const$. Let's replace the continuous system with a discrete-continuous one from the point of view of convenience of machine calculations, as well as determining the class of functions under consideration. The main scope of the dynamic programming method lies precisely in the field of discrete-continuous or purely discrete systems, or systems approximated to them.

We divide the interval *(0, T)* into *N* equal sections of small length Δ and consider only the discrete values $x = x(k)$ and $u = u(k)\,(k = 0,1,\ldots,N)$ at time points $t = 0, 1\Delta, 2\Delta, \ldots, k\Delta \ldots, (N-1)\Delta, N\Delta = T$. Then the differential equation (4) of the object can be approximately replaced by an equation in finite differences

$$\frac{x(k+1) - x(k)}{\Delta} = f_1\left[x(k), u(k)\right], \tag{6}$$

or

$$x(k+1) = x(k) + f\left[x(k), u(k)\right], \tag{7}$$

were

$$f\left[x(k), u(k)\right] = \Delta f_1\left[x(k), u(k)\right]. \tag{8}$$

The initial condition remains the same:

$$x(0) = [x]_{t=0} = x^0. \tag{9}$$

The integral (5) is approximately replaced by the sum

$$Q=\sum_{n=0}^{N-1}G\left[x(k),u(k)\right]+\varphi\left[x(N)\right] \tag{10}$$

were

$$\begin{cases} G\left[x(k),\ u(k)\right]=G_1\left[x(k),\ u(k)\right]\Delta, \\ \varphi\left[x(N)\right]=\varphi_1\left[x(N\Delta)\right]=\varphi_1\left[x(T)\right] \end{cases} \tag{11}$$

The task is to determine the sequence of discrete values of the control action and, i.e., the values *u (0)* and *u (1)* ..., *u (N – 1)* minimizing the sum (10) under conditions (2), (7) and (9). Thus, it is required to find the minimum of the function of many variables and the method of dynamic programming makes it possible to reduce this operation to a sequence of minimizations of a function of one variable.

We realize the movement from the end of the process, from the moment $t = T$, to its beginning. We consider the moment $t=(N-1)\Delta$. The values $u(i)$ $(i=\ 0,\ 1\ldots,N-2)$, except for the last $u(N-1)$, have already been implemented in some way, and some value $x(N-1)$ corresponding to the moment $t=(N-1)\Delta$ has been obtained. According to the principle of optimality, the impact of $u(N-1)$ does not depend on the "background" of the system and is determined only by the state of $x(N-1)$ and the purpose of management. Consider the last section of the trajectory from $t=(N-1)\Delta$ to $t=N\Delta$. The value of $u(N-1)$ affects only those terms of the sum (10) that relate to this section. Denote the sum of these terms by Q_{N-1}:

$$Q_{N-1}=G\left[x(N-1),u(N-1)\right]+\varphi\left[x(N)\right] \tag{12}$$

From (7) we get

$$x(N)=x(N-1)+f\left[x(N-1)\right] \tag{13}$$

Therefore, $x(N)$ also depends on $u(N-1)$. Let's find an acceptable value $u(N-1)$ satisfying (13) and minimizing the value Q_{N-1}. Denote the found minimum value Q_{N-1} by S_{N-1}. This value obviously depends on the state of the system at $t=\ (N-\ 1)$, i.e. on the value of $x(N-1)$ included in (12) and (13). So, $S_{N-1}=S_{N-1}\left[x(N-1)\right]$. Let's write an expression for S_{N-1}:

$$\begin{aligned} \mathrm{S}_{\mathrm{N}-1}\left[\mathrm{x}(\mathrm{N}-1)\right] &= \min_{u(n-1)\in\omega(u)} Q_{N-1} = \min_{u(n-1)\in\omega(u)}\left\{G\left[x(N-1),u(N-1)\right]+\varphi\left[x(N)\right]\right\} = \\ &= \min_{u(n-1)\in\omega(u)}\left\{G\left[x(N-1)\right]+\varphi\left[x(N-1)+f\left[x(N-1),u(N-1)\right]\right]\right\} \end{aligned} \tag{14}$$

To define S_{N-1} is required to minimize only the variable $u(N-1)$, S_{N-1} we get a function from $x(N-1)$, then fix the resulting value. Let's move on to the penultimate section, considering two sections – the last and the penultimate, note that the choice of $u(N-2)$ and $u(N-1)$ affects only the summands (10) included in the expression

$$Q_{N-2}=G\left[x(N-2),u(N-2)\right]+\{G[x(N-1),u(N-1\}]+\varphi\left[x(N)\right]\} \tag{15}$$

The value $x(N-2)$ at the initial moment of the penultimate interval, obtained as a result of the prehistory of the process, will be considered set. It follows from the principle of optimality that only the value of $x(N-2)$ and the goal of control – minimizing Q_{N-2} – determine optimal control in the area under consideration. Let's find the value S_{N-1} – the minimum of Q_{N-2} by $u(N-2)$ and $u(N-1)$. But the minimum of $u(N-1)$ in (15) has already been found for each value of $x(N-1)$, and the latter depends on $u(N-2)$. In addition, when minimizing Q_{N-1}, the corresponding optimal value $u(N-1)$ is found along the way; we denote it by $u^*(N-1)$. If you also consider that the rst term in (15) does not depend on $u(N-2)$, we can write:

$$S_{N-2}\left[x(N-2)\right]=\min_{\substack{u(N-2)\in\omega(u)\\ u(N-1)\in\omega(u)}} Q_{N-2}=\min_{u(N-2)\in\omega(u)}\left\{G\left[x(N-2),u(N-2)\right]+S_{N-1}\left[x(N-1)\right]\right\}=$$

$$=\min_{u(N-2)\in\omega(u)}\{G\left[x(N-2),u(N-2)\right]+S_{N-1}-f\left[x(N-2),u(N-2)\right]]\}$$

because of (7) implies $x(N-1)=x(N-2)+f\left[x(N-2),u(N-2)\right]$.

Note that the minimization is performed using one variable $u(N-2)$. In this case, we find $u^*(N-2)$ – the optimal value of u $u(N-2)$ – and the value S_{N-2} – the minimum of the function Q_{N-2}. Both $u^*(N-2)$ and S_{N-2} are functions of $x(N-2)$. Now we fix the value of S_{N-2}. It is important to note that the found optimal value $u^*(N-2)$ minimizes the entire expression in the curly bracket of the formula S_{N-2}, and not specifically the summand $G\left[x(N-2),y(N-2)\right]$. Therefore, a strategy in which each value of $u(N-j)$ is chosen by minimizing only a specific term $G\left[x(N-j),y(N-j)\right]$ in the sum (10) is not at all optimal. The optimal strategy takes into account the ultimate goal, i.e. minimizing the entire expression in the curly bracket, depending on $u(N-j)$.

Let's continue the procedure of moving from the end to the beginning of the interval *(T, 0)*. Taking into account the third section from the end requires consideration of that part of the sum *Q*, which depends on $u(N-3)$. Let's denote this part by Q_{N-3}:

$$Q_{N-3}=G\left[x(N-3),u(N-3)\right]+$$
$$+\left\{G\left[x(N-2),u(N-2)\right]+G\left[x(N-1),u(N-1)\right]+\varphi\left[x(N)\right]\right\}$$

Based on expression (13), we write $x(N-2)=x(N-3)+f\left[x(N-3),u(N-3)\right]$. Next, the minimum of the expression in the curly bracket in the expression Q_{N-3} is $\mathrm{S}_{N-2}\left[\mathrm{x}(\mathrm{N}-2)\right]$. Therefore, the minimum S_{N-3} of the expression Q_{N-3} is equal to

$$S_{N-3}\left[x(N-3)\right]=\min_{u(N-3)\in\omega(u)}\left\{G\left[x(N-3),u(N-3)\right]+S_{N-2}\left[x(N-3)\right]\right\}=$$

$$=\min_{u(N-3)\in\omega(u)}\{G\left[x(N-3),u(N-3)\right]+S_{N-2}-f\left[x(N-3),\, u(N-3)\right]]\}$$

Passing in a similar way to $S_{N-4},\ldots,S_{N-k}$, we obtain the recurrent formula

$$\begin{gathered} S_{N-k}\left[x(N-k)\right]=\min_{u(N-k)\in\omega(u)}\{G\left[x(N-k),u(N-k)\right]+ \\ +S_{N-k+1}\left[x(N-k)\right]+f\left[x(N-k),\,u(N-k)\right]\} \end{gathered} \tag{16}$$

In parallel, we determine the optimal value of $u*$, depending on $x(N-k)$

$$u^*(N-k)=u^*\left[x(N-k)\right] \tag{17}$$

And the minimizing expression in curly bracket (16). Calculating by formula (16) sequentially S_{N-k} for $k=$ 1, 2, $\ldots, N$, we come to determine the optimal value of $u*(0)$, i.e. the value of the control action required at the initial moment of time. Simultaneously with determining the value of $u(0)$, we obtain S_0, i.e. the minimum value of the criterion *Q* under optimal control. The analytical expression of the minimization results turns out to be impossible; therefore, this procedure is performed numerically. The solution process is transferred to an object of any order *n* with equation (1) and any number of control actions $u_l\ (l=1,\ldots,r)$. It is only necessary to replace the scalars *x*, *u*, *f* in the above formulas with vectors *x*, *u* and *f*. In this case, vectors should be introduced for the kth instant of time $t=k\Delta$

$$\begin{cases} x(k)=\{x_1(k),\ldots,x_n(k)\}, \\ u(k)=\{u_1(k),\ldots,u_r(k)\}. \end{cases} \tag{18}$$

Here $u_j\ (N-k)$ is the *j*-th control action, and $x_j\ (N-k)$ is the *j*-th coordinate at the moment $t=(N-k)\Delta$.

Let's replace the differential equations (1) with equations in finite differences, and the integral (3) with the sum. Then the reasoning, which is completely similar to the above, shows that formula (16) is replaced by the expression

$$\begin{gathered} S_{N-k}\left[x(N-k)\right]=\min_{u(N-k)\in\omega(u)}\{G\left[x(N-k),u(N-k)\right]+ \\ +S_{N-k+1}\left[x(N-k)\right]+f\left[x(N-k),\,u(N-k)\right]\} \end{gathered} \tag{19}$$

The calculation procedure is similar if in *f* it clearly depends on time.

Next, at each stage, we find the minimum of the function *r* of the variables $u_1(N-k),\ldots,u_r(N-k)$, the optimal values are the scalar S_{N-k} and the vector $u^*(N-k)$ - the essence of the function of the vector $x(N-k)$, i.e. the function *n* variables $x_1(n-k)_{,}\ldots,x_n(n-k)$.

Dynamic programming is not a solution to any problem, at one time the method was not used because of the so-called curse of dimensionality. With the development of computer technology, instead of analytical patterns, it became possible to search for solutions in the form of graphs or tables, i.e. calculation procedures until the desired result is obtained. The simpler the calculation procedure, the better the method. Dynamic programming is characterized by a radical simplification of the calculation procedure in comparison with the direct method of solving the problem. Indeed, the problem of minimizing the sum (10) can be considered as the problem of minimizing the function of *N* variables $u(0),u(1),\ldots,u(N-1)$.

To solve the minimization problem, it is necessary to express each *x(k)* as a functional dependence on all previous control actions $u(0)$, $u(k-1)$ (and initial conditions) using formula (7), i.e. to find a solution for *x(k)* in general form. As a result of such a replacement, expression (10) will become more complicated, and finding the smallest of possibly several minima with a large number of variables is also difficult.

Meanwhile, dynamic programming allows you to replace the minimization of a complex function of many variables with a sequence of minimizations. At the same time, in each of the minimization processes, the minimum of a much less complex function of one or more variables (*n* variables for an object of the nth order) is determined. Therefore, using dynamic programming, it is possible to solve a number of problems that are unsolvable by direct minimization. It does not follow from the above that the direct method is always unacceptable, it is applicable with a limited number of variables. In general, dynamic programming provides a significant rationalization of calculations compared to the direct method. In this case, the solution can be extremely cumbersome. Indeed, at each stage of calculations, it is necessary to find and memorize the functions $S_{N-k}(x)$ and $S_{N-k+1}(x)$, i.e., in general, two functions of *n* variables. Memorizing such functions for large values of n requires a significant amount of memory and in difficult cases is practically achievable only with the help of any approximations.

The described technique is transferred without fundamental changes to optimal systems with random processes. To illustrate, let's consider an example in which, in addition to *u*, a random disturbance *z* acts on an object of the first order. Then equation (7) will be replaced by equality

$$x(k+1) = x(k) + f\left[x(k), u(k), z(k)\right] \tag{20}$$

where *z(k)* are the discrete values of the disturbance. Now *x(k)* and criterion (10) become random variables. Therefore, as a new criterion *Q*, the value of which needs to be minimized, we choose the mathematical expectation of expression (10), and we also introduce *z* into the number of arguments *G* for generality:

$$Q = M\left\{\sum_{n=0}^{N-1} G\left[x(k), u(k), z(l)\right] + \varphi\left[x(N)\right]\right\} \tag{21}$$

Here *M* is the mathematical expectation. In this example, we will consider the values *z(i)* and *z(j)* for *j* to be independent and assume that the densities of distributions $P\left[z(0)\right], P\left[z(1)\right), \ldots \ldots, P\left[z(N)\right]$ are known. Using the proposed method, we first find a function for each fixed $x(N-1)$

$$\begin{gathered}
S_{N-1}\left[x(N-1)\right] = \min_{u(N-1)\in\omega(u)} Q_{N-1} = \\
= \min_{u(N-1)\in\omega(u)} M\{G\left[x(N-1), u(N-1), z(N-1)\right] + \\
+\varphi\left[x(N-1) + f\left[x(N-1), u(N-1), z(N-1)\right]\right]\} = \\
= \min_{u(N-1)\in\omega(u)} \int_{-\infty}^{\infty} P\left[z(N-1)\right]\{G\left[x(N-1), u(N-1), z(N-1)\right] + \\
+\varphi\left[x(N-1) + f\left[x(N-1), u(N-1), z(N-1)\right]\right]\} dz(N-1).
\end{gathered} \tag{22}$$

When minimizing, the optimal value of $u^*\left[x(N-k)\right]$ is determined simultaneously. Having memorized $S_{N-1}\left[x(N-1)\right]$, we find the following function

$$S_{N-2}\left[x(N-2)\right]=\min_{u(N-2)\in\omega(u)} M\{G\left[x(N-2),u(N-2),z(N-2)\right]+$$
$$+S_{N-1}\left[x(N-1)\right]\}=\min_{u(N-2)\in\omega(u)} \int_{-\infty}^{\infty} P\left[z(N-2)\right]\{G\left[x(N-2),u(N-2),z(N-12)\right]+ \tag{23}$$
$$+S_{N-1}\left[x(N-2)+f[x(n-2),u(N-2),z(N-2)\right]\}dz(N-2).$$

The solution methodology turned out to be essentially the same as for regular systems. A similar technique is applicable to an object of any order. We can also consider more general problems in which $\mathrm{P}\left[z(i)\right]$ are unknown in advance, and some optimal procedure for processing observations allows us to accumulate information about the densities of distributions.

Solution of the problem

The dynamic programming method, with some additional assumptions, can be applied to the study of continuous systems. Let the motion of an object be characterized by the equations

$$\frac{\mathrm{d}x}{\mathrm{d}t}=f(x,u,t). \tag{24}$$

At the initial moment of time t_0, the vector *x* is equal to $x^{(0)}$, and the optimality criterion has the form, $T =$ *const*

$$Q=\int_{t_0}^{T} G(x,u,t)\,\mathrm{d}t \tag{25}$$

Let's assume that an optimal trajectory has been found leading from the starting point $x^{(0)}$ to the end point $x^{(T)}$. The minimum value of the criterion *Q* corresponding to the optimal trajectory is denoted by $S\left(x^{(0)},t^{(0)}\right)$. According to the principle of optimality, the section of the trajectory from the point x corresponding to the moment $t>t_0$ to the endpoint $x^{(T)}$ Fig. 2 is also the optimal trajectory, and the part of the criterion *Q* corresponding to this section and the time interval from *t* to *T* has the minimum possible value.

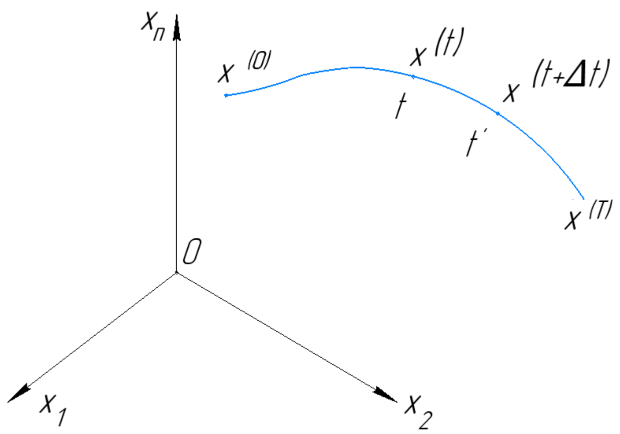

Figure 2. Illustration of the optimality principle, continuous case

Let's denote this value by $S\left[x(t),t\right]$. Let $\Delta\mathrm{t}$ be a small period of time, and $S\left[x(t+\Delta\mathrm{t}),t+\Delta\mathrm{t}\right]=S\left[x',t'\right]$ be the minimum value of the part of the integral *Q* that corresponds to the optimal area trajectories from point $x(t+\Delta t)=x'$ to the end point $x^{(T)}$ and, consequently, the time interval from $t+\Delta t=t'$ to *T*. The ratio between $S[x',t']$ and $S[x,t]$ is completely analogous to formula (19); you just need to write $S[x,t]$ instead of $S_{N-k}[x(N-k)]$, $S[x',t']$ instead of $S_{N-k+1}[x(N-k+1)]$, finally, $G[x(t),u(t),t]\Delta t$ instead of $G[x(N-k),u(N-k)]$. The last substitution was made in the first of the equations (11). Since Δt is a small but finite period of time and replacing the differential equation with an expression in finite differences is inaccurate, it is necessary to add the expression $0_1(\Delta t)$ to some equality, i.e. the magnitude of the order of smallness is higher than Δt:

$$\lim_{\Delta t\to 0}\frac{0_1(\Delta t)}{\Delta t}=0 \tag{26}$$

Instead of (19) can be written:

$$S[x,t]=\min_{u(t)\in\omega(u)}\{G[x,u,t]\Delta t+S[x',t']\}+0_1(\Delta t) \tag{27}$$

The dependence of (27) is possible to obtain and regardless of the discrete case discussed above. Indeed, according to the definition

$$S[x,t]=\min_{u(t)\in\omega(u)}\int_t^T G(x,u,\tau)\,d\tau \quad (t\le\tau\le T) \tag{28}$$

Here *S* is the minimum value of the integral obtained on the set of all permissible controls $u(\tau)$ in the range from *t* to *T*. The integral (28) can be represented as the sum of two terms corresponding to the intervals from *t* to $t+\Delta t$ and from $t+\Delta t$ to *T*. Since Δt is small, you can write

$$S[x,t]=\min_{u(t)\in\omega(u)}[G(x,u,t)\Delta t+\int_{t'}^T G(x,u,v)\,dv]+0_1(\Delta t) \tag{29}$$

where Δt is considered small, and $0_1(\Delta t)$ is of the order of smallness higher than Δt. Since the first term in the square bracket (29) depends only on the value of *u(t)* at time *t*, and only the integral in the square bracket also depends on the values of *u(v)* in the interval of change of *v* from $t'\neq t+\Delta t$ to *T*, then you can write

$$\begin{aligned} S[x,t]&=\min_{u(t)\in\omega(u)}[G(x,u,t)\Delta t+\min_{u(t)\in\omega(u)}\int_{t'}^T G(x,u,t)\,dv]+0_1(\Delta t)= \\ &=\min_{u(t)\in\omega(u)}\{G(x,u,t)\Delta t+S[x',t']\}+0_1(\Delta t) \end{aligned} \tag{30}$$

Here, under the sign of the minimum is the value *u(t)* at time *t*, formulas (30) and (27) coincide. Just as in (19), it should be noted that $x'=x(t+\Delta t)$ depends on *u(t)*. From (24) we find for small Δt

$$x'=x(t+\Delta t)=x(t)+\frac{dx}{dt}\Delta t+0_2(\Delta t)=x(t)+f[x(t),u(t),t]\Delta t+0_2(\Delta t), \tag{31}$$

where $0_2(\Delta t)$ is a value of the highest order of smallness compared to Δt. Formula (31) is similar to expression (17).

Now suppose that the function $S(\cdot)$ really exists, is continuous and has partial derivatives with respect to the variables $x_i\ (i=1,\dots,n)$, and with respect to *t*, i.e. all $\partial S/\partial x_i\ \ (i=1,\dots,n)$ and $\partial S/\partial t$ exist, the validity of the subsequent conclusion depends on the validity of the given assumption. If the latter is not justified, then the reasoning is only heuristic in nature. However, there are cases when the assumption is unfair, and the application of dynamic programming to continuous systems needs, as shown in a number of works, in general, additional justification.

Substitute the expression x' from (31) into formula (27) and decompose $S[x',t']$ into a Taylor series in the vicinity of point *(x, t)* we get:

$$\begin{aligned} S\ [x',t'] &= S\left[x(t+\Delta t),t+\Delta t\right]= \\ &= S[x(t\{+f\left[x(t),u(t),t\right]\Delta t+0_2(\Delta t);t+\Delta t]= \\ &= s\left[x,t\right]+\sum_{i=1}^{n}\frac{\partial S\left[x,t\right]}{\partial x_i}f_i\left[x,u,t\right]\Delta t+\frac{\partial S\left[x,t\right]}{\partial t}\Delta t+0_3(\Delta t), \end{aligned} \tag{32}$$

where $0_3(\Delta t)$ is the value of higher order of smallness compared to Δt. We can write the formula in a more compact, introducing the gradient of the function *S(x, t)* is a vector with the coordinates of $\partial S/\partial x_i\ \ (i=1,\dots,n)$

$$grad\, S=\left(\frac{\partial S}{\partial x_1},\dots,\frac{\partial S}{\partial x_n}\right) \tag{33}$$

Then (32) takes the form

$$\begin{aligned} S\left[x',t'\right] &= S\left[x(t+\Delta t),t+\Delta t\right]= \\ &= S\left[x,t\right]+grad\, S\left[x,t\right],f\left[x(t),u(t),t\right]\Delta t+\frac{\partial S\left[x,t\right]}{\partial t}\Delta t+0_3(\Delta t) \end{aligned} \tag{34}$$

Substituting (34) and (27) and taking out the values $S[x,t]$ and $\partial S/\partial t$, independent of *u(t)*, the formula takes the form:

$$-\frac{\partial S\left[x,t\right]}{\partial t}=\min_{u(t)\in\omega(u)}\left\{G\left[x(t),u(t),t\right]+grad\, S\left[x,t\right],f\left[x(t),u(t),t\right]\right\}+\frac{0_4(\Delta t)}{\Delta t} \tag{35}$$

where $0_4(\Delta t)$ is a value of the highest order of smallness compared to Δt. Now let's aim Δt to zero, since $0_4(\Delta t)$ obeys condition (26), then the last term in the right part (35) disappears at $\Delta t\to 0$. Therefore, in the limit we get

$$-\frac{\partial S\left[x,t\right]}{\partial t}=\min_{u(t)\in\omega(u)}\left\{G\left[x(t),u(t),t\right]+grad\, S\left[x,t\right],f\left[x(t),u(t),t\right]\right\} \tag{36}$$

Expression (36) is called the Bellman equation and is a partial differential equation.

To concretize the theoretical calculations, let's look at an example. Let $r=1$ and $n=\ 2$ be in the special case, and $G=G(x_1,x_2)$ and the only control action is denoted by *i*. The equations of the object are:

$$\frac{\partial x_1}{\partial t}=f_1=ux_1+x_2,\frac{\partial x_2}{\partial t}=f_2=u^2 \tag{37}$$

Then equation (36) takes the form ($S[x,t]$ replaced by *S*)

$$-\frac{\partial S}{\partial t}=\min_{u}\{G(x_1,x_2)+\frac{\partial S}{\partial x_1}\left(ux_1+x_2\right)+\frac{\partial S}{\partial x_2}u^2 \quad (38)$$

Assuming that $\partial S/\partial x_2>0$, we find the minimum of the curly bracket in *u*, equating the derivative to zero. The optimal value $u*$ that minimizes the square bracket we write in the form

$$u^*=-\frac{1}{2}x_1\frac{\partial S}{\partial x_1}\frac{1}{\partial S/\partial x_1} \quad (39)$$

Substituting (39) the expression in equation (38), we obtain the partial differential equation:

$$-\frac{\partial S}{\partial t}=G\left(x_1,x_2\right)+\frac{\partial S}{\partial x_1}x_2-x_1^2\frac{(\partial S/\partial x_1)^2}{4\partial S/\partial x_2} \quad (40)$$

The partial differential equation (40) can be solved, since the boundary conditions are known for it, *S[x,t]* is a known function. For example, for criterion (5) it is $\varphi_1\left[x,\left(T\right)\right]$, since for $t_0=T$ the integral in (5) is zero. For criterion (25), the function *S[x,t]* is zero. Knowing the boundary function *S[x,t]*, it is possible to integrate equation (40) by some known method. One of the usual methods of approximate integration consists in discretizing the problem and solving the resulting recurrence relations of the form (19). In some cases, it is possible to find an approximate solution in another way or even obtain an exact solution in a closed form. The resulting value of $u*$ represents optimal control.

Results and conclusions.

Based on equation (36), dependence (38) is obtained, which describes the change in the function *S* [*x, t*] over time depending on the parameters x_1 and x_2, as well as the control parameter *u*. This equation minimizes an expression involving the function $G(x_1,x_2)$, linear and quadratic terms by *u*. The derivative of *u* is zero, which makes it possible to find the optimal value of $u*$, which minimizes this expression, when substituted in (38), we obtain dependence (40), solved under given boundary conditions for *S* [*x, t*]. The boundary conditions for *S* [*x, t*] can be different, depending on the context of the problem, as indicated in studies with criteria (5) and (25). Using these conditions, equation (40) can be integrated by various methods. One of the most common approaches is the discretization of space and time and the subsequent solution of recurrence relations. It is also possible to find an approximate or exact solution to the equation in a closed form.

Finding the optimal control is an important result, since it allows not only to solve the partial differential equation, but also to optimize the control process depending on the given conditions and parameters of the system [16]. This emphasizes the importance of accurately determining the function *S* [*x, t*] and its initial or boundary values for the successful application of optimal control methods.

REFERENCES

[1]. Moiseev N.N. *Mathematical problems of system analysis.* – M.: Nauka, 1981, – 488 p.
[2]. Negojce K. *Application of systems theory to control problems*. –M: Mir, 1981, – 179 p.
[3]. V.A. Besekersky. E.P. Popov. *Theory of automatic control systems*. – St. Petersburg: Profession, 2003. – 752 p.
[4]. Avvakumov, S.N., Kiselev, Y.N. *Some algorithms of optimal control.* Proc. Steklov Inst. Math. 255 (Suppl 2), S1–S15 (2006). https://doi.org/10.1134/S0081543806060010.
[5]. Boris S. Mordukhovich, M. Ebrahim Sarabi. *Variational analysis and full stability of optimal solutions to constrained and minimax problems, Nonlinear Analysis: Theory, Methods &*

Applications. Volume 121, 2015, Pages 36-53, ISSN 0362-546X, doi.org/10.1016/j.na.2014.10.013

[6]. Kosheleva I.V., Danilov A.I., Mokrova N.V. *Decomposition control of a cascade of catalytic reforming reactors. / Advances in chemistry and chemical technology.* Volume XVI. 2002. No. 1 (18). p.32-33.

[7]. Mokrova N.V., Volodin V.M. Justification for the choice of methods for solving the problem of optimal control of complex processes. Bulletin of TSTU, 2006. Volume 12. 22-28 p. ISSN 0136-5835.

[8]. Mokrova N.V., Volodin V.M. *Modeling of decomposition control of multi-stage processes*. / Chemical and oil and gas engineering. 2007. No. 2. p.17-19. ISSN 0023-11-26. Mokrova N.V., Volodin V.M. *Analysis of high-end complex chemical technological system check-out*. Chemical and Petroleum Engineering. 2008. № 2. C. 3 – 5. ISSN 0023-11-26.

[9]. Bellman R. *Dynamic programming* . Transl. from English – M.: Izdatinlit, 1960. – 400 p.

[10]. Hu Wen-Tsen., Umbetov U. *Decentralized control of multidimensional objects with decomposition by situations.* News of the National Academy of Sciences of the Republic of Kazakhstan, Physics and Mathematics Series, 2007, No. 1, pp. 82 – 85.

[11]. Volodin V.M., Guseva A.Yu. *Optimal control of multi-stage processes with complex flow structures.* Chemical and petroleum engineering. No. 3. 1997. pp. 20 – 21.

[12]. Wilco van Harselaar, Niels Schreuders, Theo Hofman, Stephan Rinderknecht. *Improved Implementation of Dynamic Programming on the Example of Hybrid Electric Vehicle Control*, IFAC-PapersOnLine, Volume 52, Issue 5, 2019, Pages 147-152, ISSN 2405-8963, doi.org/10.1016/j.ifacol.2019.09.024.

[13]. A. S. Maksimov, S. D. Savostin, V. S. Artemyev. *SCADA systems* . – Kursk: Closed Joint Stock Company "University Book", 2023. – 127 p. – ISBN 978-5-907776-95-1.

[14]. V. Artemyev, A. Medvedev, V. Yaroshevich. *Investigation of optimal control of variable systems in the dynamic spectrum.* Machine Science. – 2023. – Vol. 12, No. 1. – P. 68-75.

[15]. V. Artemyev, S. Mokrushin, S. Savostin [et al.].*Processing of time signals in a discrete time domain.* Machine Science. – 2023. – Vol. 12, No. 1. – P. 46-54.

[16]. V. S. Artemyev, M. N. Makhiboroda, S. L. Yablochnikov [et al.]. *Implementation of Adaptive Control with Parametric Uncertainty*. Intelligent Technologies and Electronic Devices in Vehicle and Road Transport Complex (TIRVED), Moscow, 10–11 november 2022. – Moscow: IEEE, 2022. – P. 9965505. – DOI 10.1109/TIRVED56496.2022.9965505.

[17]. A. Haag, M. Bargende, P. Antony, F. Panik. *Iterative refinement of the discretization of the dynamic programming state grid*. In 16. Int. Stuttgarter Symposium, Springer (2016), pp. 145-154.

[18]. Wei Zhou, Lin Yang, Yishan Cai, Tianxing Ying. *Dynamic programming for New Energy Vehicles based on their work modes part I: Electric Vehicles and Hybrid Electric Vehicles.* Journal of Power Sources, Volume 406, 2018, Pages 151-166, ISSN 0378-7753, doi.org/10.1016/j.jpowsour.2018.10.047

[19]. Mokrova N.V. *Problem of optimum control of manufacture of the activated coals.* Ugol. 2007. №7. c.72-74. ISSN: 0041-5790.

Received: 06.02.2024
Accepted: 22.05.2024

MACHINE SCIENCE

ISSN: 2227-6912
E-ISSN: 2790-0479

2024, № 1 Pages 58 – 65

THE INFLUENCE OF DEFECTS ON THE PHYSICO-MECHANICAL PROPERTIES OF POLYMER COMPOSITE MATERIALS AND PRODUCTS

Rasim BASHIROV[1,a*], Fuzuli RASULOV[1,b], Ilhama HAMDULLAYEVA[1,c], Nijat ISMAILOV[1,d]

[1]Department of special materials and tools Azerbaijan Technical University, Baku, Azerbaijan

E-mail:[a]rasim_agma@aztu.edu.az, [b]resulovfr@gmail.com, [c]İlhame.hemdullayeva@aztu.edu.az, [d]nicatismayilov1994@mail.ru

https://doi.org/10.61413/EFRI7341

Abstract: The issues of the formation of physical and mechanical properties in polymer composite materials consisting of reinforcement (glass fiber) and a matrix (resin) are considered. The reasons causing failures in polymer composite materials of the specified type and products based on them are given. The dependence of the average strength and ultimate relative strain of monofilaments on their length and diameter has been studied. The effect of defects on the surface of reinforcing glass fibers on their strength has been studied. It is shown that with an increase in the length of glass fiber, defects of various types are formed on its surface. An empirical formula for the rate of fiberglass cracking is given. It is shown that the second stage of the glass fiber destruction process is poorly described by a power function with a constant exponent when the level of unloading stresses changes. The dependence of the nominal voltage on the actual voltage in glass fibers is obtained for various values of the coefficients of variation. It is shown that the main processes of interaction between the resin and the fiber occur either at their interface or in the border zone.

Keywords: *length, diameter, polymer composition. matrix, fiber, strength, elongation, failure, cracking*

Introduction.

The problem of quality and reliability of materials, products and structures is one of the pressing problems of modern scientific and technological development. This problem is very important for products and structures made from structurally inhomogeneous heterogeneous materials, which include polymer-based composite materials. These materials are characterized, along with high performance characteristics, by significant variability in physical and mechanical properties, the existence of various defects in them, and heterogeneity of composition and structure. Therefore, when designing products and structures from these materials, it is necessary to significantly increase the safety factors, which lead to an increase in their metal consumption, as well as in cost [1,2,3,4,5]. Of particular importance in solving the problem of quality and reliability of products and structures made of polymer composite materials (PCM) are effective methods and means of control. In this case, the greatest attention is paid to non-destructive methods and means of control. Thus, the use of non-destructive methods and control means allows for express analysis of the emerging technological characteristics of the product material and structure during its manufacturing process without any testing or stopping the production process. This ensures stability of the values of technological modes and contributes to a significant reduction in the number of defects formed in the finished structure.

Discussion of results.

In the figure and table. The dependence of the average strength of microfibers on the length and diameter of the fiber is given.

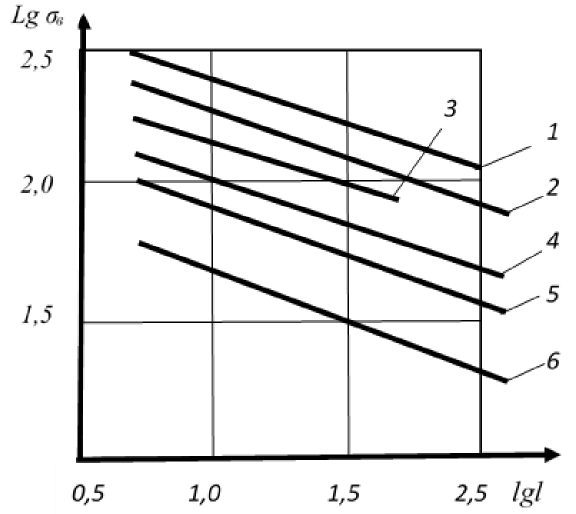

Figure. 1. The dependence of the average strength σ_b of monofilaments on their length: l - monofilament diameter; d=5μm; 2-d=6.0 μm; d=12.4 μm; 4-d=22.0 μm; 3-d=40μm; 6-d=120μm;

Table.1. Strength of the fiber depending on its diameter and length.

Length of fiber l, mm	Diameter of fiber d, µm	Tensile strength σb, MPa
5	9,0	1550
10	9,7	1250
20	10,0	1200
45	9,0	1160
90	9,6	750
190	9,6	850
1600	10	700

This study shows that the elastic modulus of PCM is not affected by the diameter and length of the fibers, that is, the elastic modulus of the fibers practically does not depend on their size. [6,7,8]. The dependence of strength and ultimate (failure) relative deformation on fiber diameter is shown in Figure 2, from which it can be seen that the dependence is linear until failure; with increasing fiber diameter, the ultimate deformation decreases. [9,10,11].

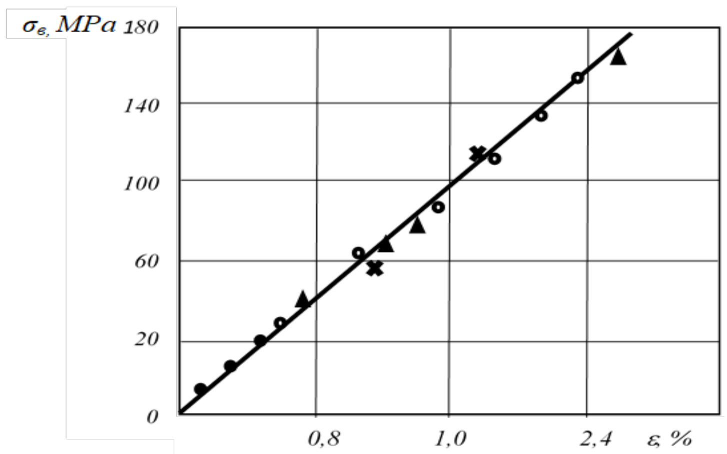

Figure. 2. Dependence of strength σ_b and maximum relative deformation ε on fiber diameter: ● – d = 100 μm; Δ – d =50 μm; ✖ - d=20 μm; o- d=20 μm.

From the data given in Table 1 it is clear that with increasing length of a fiber of constant diameter, a change in these parameters occurs due to defects randomly distributed along its length.

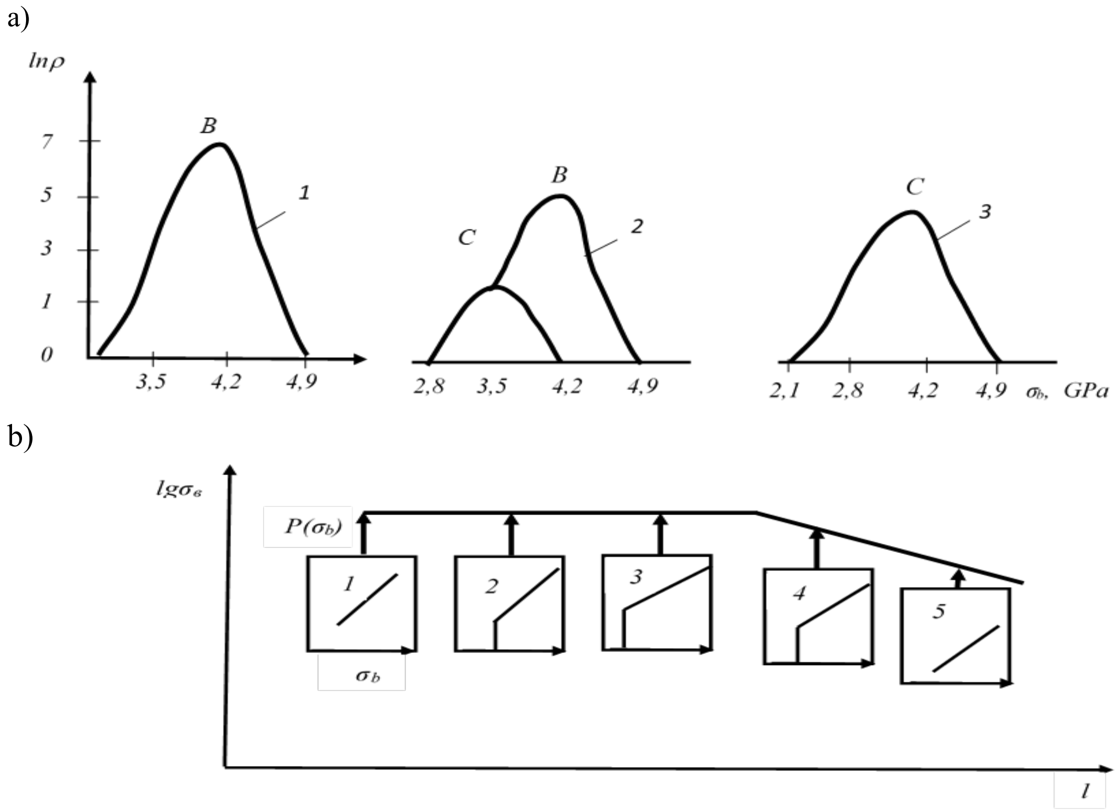

Figure. 3. Effect of defects on the strength of glass fibers:
a – probability density curves of strength limits,
b – integral distribution curves of strength limits in the presence of defects of types A and C.

We have made a classification of glass fiber defects, which are divided into three main types: A - internal submicrocracks measuring 10-4 cm; B and C surface cracks of various sizes. Moreover, the size of type B defects is smaller than the size of type C defects, which are less common. It was found that in fibers with a length of 10-2 to 10 cm, mainly type B defects are observed, but the presence of type A and C defects is also possible. In fibers over 10 cm in length, type C defects are predominant. Apparently, fibers with a length of less than 10-2 cm should contain type A defects, but it is very difficult to experimentally determine the presence of this type of defects on fibers of such length.

We also considered the influence of defects on the strength of the fiber, the length of which changed from 0.05 to 1.5 cm. It was found that the probability density curves of the tensile strength of glass fibers with a length ℓ of up to 0.05 cm. (curve l, Figure 3, a) have one maximum, which indicates the influence of only type B defects, and the integral dependence represents a straight line (Graph 1, Figure 3, b). As the length of the glass fiber increases, defects of types B and C appear on its surface; at the same time, the probability density curve of the strength limits already has two maxima (curve 2, Fig. 3, a) and in the integral dependence (graph 2) a turning point is observed, depending on the ratio of the number of failures caused by defects of type B and C.

From Figure 2b (graphs 2, 3, 4) it is clear that with increasing length, some of the glass fibers are destroyed by type B defects, and some by C defects, since they are most dangerous and characteristic of long fibers. The probability density curve of the strength limits in this case has one maximum (curve 3, Fig. 3, a) and the corresponding integral curve (graph 5, Fig. 2 a) does not have a break, but its slope differs from the slope of the curve in graph 1. As the length of glass fibers increases, the direction of the slope of the curves changes towards lower failure stresses, while the minimum strength can be found when testing long fibers.

It should be noted that the process of fiber failure (failure) depends on its defects and environmental conditions (temperature, moisture, vacuum, etc.). The process of statistical destruction at the initial temperature occurs in two stages. Initially, cracks develop from defects existing in the composition, and then the process of fiber destruction proceeds at an increasing speed [12,13,14]. In this case, the cracking rate is well described by the empirical dependence, which for an E-glass fiber with a diameter of 10 μm and a length of 25 m has the following form (5).

$$V = R_1 \sigma_h^n + V_0,$$

where σ_H - normal stress, R_1 - a constant, n - an exponent (for fibers of various types the values are n = 16÷26); V_0 – the cracking rate at zero stress.

The second stage of the destruction process is poorly described by a power function with a constant exponent even when the stress level changes. Therefore, based on correlation analysis, it was found that the dependence of voltage on time in logarithmic coordinates can be represented linearly. However, the behavior of a fiber bundle under load is different from that of a monofilament. When considering PCM as a statically indeterminate system consisting of fibers, which is characterized by random strength values, in general, the load on the bundle Q can be represented in the form

$$Q = N \int_{\varepsilon}^{\infty} d\varepsilon_b \int_0^{\infty} f(\varepsilon_1 E)\psi(\varepsilon_b E) dE,$$

where N - initial number of fibers in the bundle; $f(\varepsilon_1 E) -$ fiber load function; $\int_{\varepsilon}^{\infty} d\varepsilon_b \int_0^{\infty} \psi(\varepsilon_b E) dE -$ the number of fibers remaining when a quasi-equilibrium state is reached.

If the stress distribution in the bundle and the law of plane sections is valid, the relationship between the total load on the bundle Qi and the load on individual i fiber q_i can be represented in the form

$$Q_i = N q_i \int_{q_i}^{\infty} p(q) dq,$$

where *p(q)* - probability density of failure loads for fibers.

The failure load Q_{max} for a fiber bundle at $q_r = q_{kr}$ is equal to

$$\frac{d}{dq}\left\{ q_{kr} \int_{q_i}^{\infty} p(q) dq \right\} = 0.$$

If the probability of fiber exceeding the failure load is indicated

$$p(q) = \int_0^q p(q) dq = a\left(\frac{1}{q}\right) = a(\omega),$$

where *a(ω)* changes from 1 to 0 when placing the fibers included in the bundle and characterizes the degree of destruction of the bundle, then the load on the bundle

$$Q = N \frac{1}{\omega} \left[1 - a(\omega)\right]$$

where *a(ω)=1-Q ω/N* at a constant force there will be a linear relationship between a(ω) and ω.
The conditions for determining the maximum load will have the form

$$Q = \frac{N\left[1 - a(\omega)\right]}{\omega}, \quad \frac{d\left[1 - a(\omega)\right]}{d_{\omega} \omega_{max}} = 0.$$

It should be noted that for large N and any fiber strength distribution function, if the probability of fiber failure p(q) is such that 1–p(q) tends to zero faster than 1/q, the distribution of average failure stresses for bundles asymptotically tends to normal distribution with mathematical expectation

$$\overline{q}_b = q_{\max}\left[1 - p(q_{\max})\right]$$

and standard deviation

$$S_{qb} = q_{\max}\sqrt{\frac{1}{N}p(q_{\max})\{[1 - p(q_{\max})]\}}$$

The maximum stress can be determined by maximizing the value represented as the product of the force in the fiber and the number of unbroken fibers, i.e.

$$\frac{d}{dq}\{q[1 - p(q)]\}_{q=q_{\max}} = 0.$$

When determining the failure load on a large bundle, knowing the strength limits of the fibers, it is possible to arrange the failure loads in a variation series in decreasing order, q1>q2>q3...>qr. Equilibrium condition will be as follows in the form

$$Q \leq q_r,$$

where r is the sequence number of the thread in the row.

Then the maximum load can be determined by the formula

$$Q_{max}=max[rq_r].$$

This formula can be confirmed by research results. In this regard, the behavior of a bundle of parallel glass fibers, the strength of which is distributed according to the normal law, was studied. It was found that the maximum load on the beam

$$Q_{\max} = Nq_{kp}\int_{q_{k_r}}^{\infty}\overline{p}(q)dq$$

and the rated load on the fiber at the start of rapid rupture

$$q_H = \frac{Q_{\max}}{N} = q_{kp}\int_{q_{k_r}}^{\infty}\overline{p}(q)dq$$

is determined from the maximization condition i.e.

$$\frac{dQ}{dq_{kp}} = \int_{q_{kp}}^{\infty} p(q)dq - q_{kp}p(q_{kp}) = 0.$$

This equation is a function of q_{kp} and can be solved graphically.

We also obtained the dependence of the nominal stresses σ_H in the fibers on the actual σ, which has the form $\sigma_H = \sigma\int_0^{\infty} p(\sigma)d\sigma$. Graphically this dependence is shown in Fig. 4. From this dependence it is possible to find the stresses corresponding to the maximum effective load on the bundle depending on the dispersion of the monofilament strength, Curves 1-5 correspond to coefficients of variation 0; 90; 17.5; 30 and 75% σ_K^{l} и $\sigma^{//}$- intervals of possible equilibrium states σ_{kmax} and σ_{Hmax} - failure points.

Regardless of the dispersion, curves 1-5 intersect at the point ($\bar{\sigma}$, $\bar{\sigma}$/2), which indicates that any beam can withstand a load that gives a normal voltage $\bar{\sigma}$ /2. Thus, the minimum load can be determined by the formula

$$Q_{\min} = \frac{\overline{\sigma}}{2}Nf,$$

where *f* the cross-sectional area of one fiber, $\bar{\sigma}$ - the average strength of the fibers in the bundle.

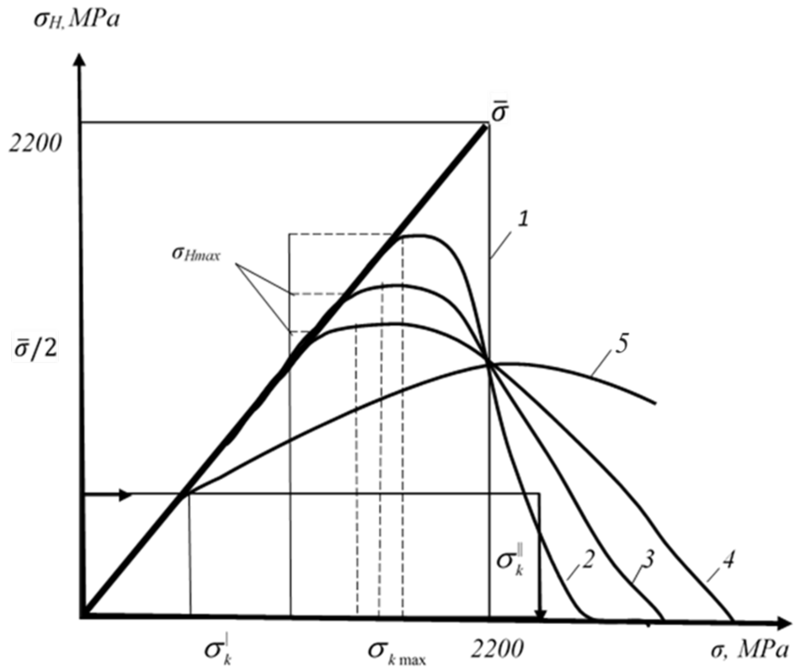

Figure. 4. Dependence of the nominal stress σ_H on the actual stress σ in glass fibers at different values of the coefficients of variation

The results of research are considered to explain the physical process of the behavior of unbonded fibers when exposed to a load. It should be noted that the process of destruction of PCM fibers differs from the destruction of a bundle of fibers in that the destruction of a fiber at any point in the bundle means its weakening and leads to an increase in effective stress, while the destruction of individual PCM fibers (connected bundle) occurring in different sections leads to redistribute the load on fibers located closely in the rupture zone. Therefore, the main role in ensuring collaboration in the forming fibers is played by the binding polymer matrix. In this case, the main interaction processes between the matrix and the fiber occur either at the interface or in the border region [15,16]. The main characteristic of this interaction is the interlayer shear strength of the composition.

In addition to the adhesive characteristics of the fiber, the surface structure of the fibers and their chemical composition play a significant role in increasing the interlayer shear strength. Thus, in work [2] it is shown that the destruction of fiberglass does not occur at the glass-resin boundary, but along the binder layer located near the fibers (at a distance of 1-2 μm) where the weakening of the strength of the binder is caused by the inhibitory effect of the fibers on the curing process of the binders. The relationship between adhesive strength and tensile strength of PCM has also been established [17,18,19]. A similar relationship for oriented fiberglass plastics based on various binders is shown in Figure 5.

The solidity and high shear strength of PCM is ensured mainly by the binding, i.e., polymer matrix, therefore special requirements are placed on it not only in terms of adhesive properties, but also in terms of deformation [20,21].

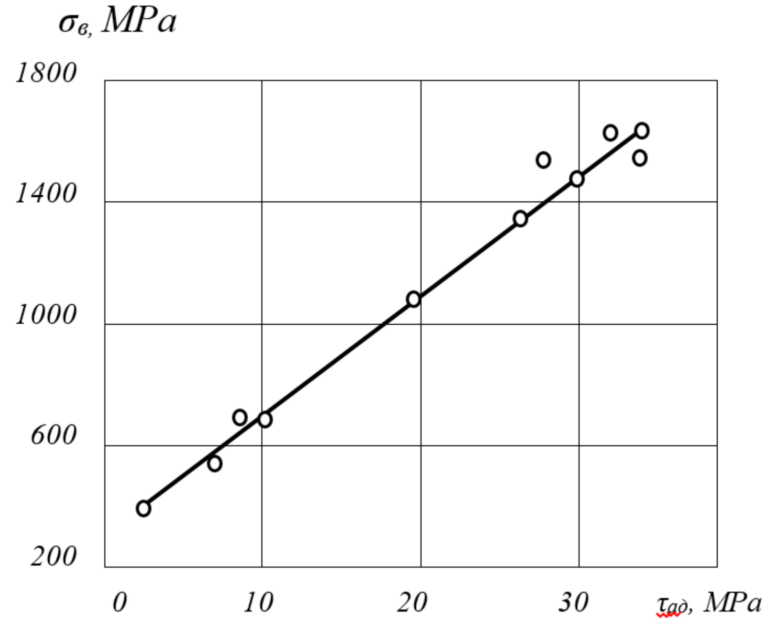

Figure. 5. Dependence of adhesive strength $\tau_{ад}$ on tensile strength $\sigma_{в}$ PCM.

For PCM, the optimal fiber content (50 - 75%) is that the relative elongation of the matrix should be 6-15 times greater than in the fiber. In order to eliminate cracking and increase the load-bearing capacity of shells made of oriented fiberglass with a volumetric fiber content of 30-70%, we recommend that the relative elongation of the binder be 4-26%.

Conclusions. 1. It has been shown that the strength of a fiber in PCM depends on its diameter, i.e., the larger the fiber diameter, the lower its strength, which is determined by the nature and location of defects on the surface. The relationship between strength and maximum relative deformation also depends significantly on the fiber diameter. Higher values of these parameters are achieved with small fiber diameters.

2. The strength of fiberglass reinforcement depends on the nature of the defects on its surface. It has been established that surface defects are the most dangerous for long fibers. However, the behavior of a fiber bundle under load is different from that of a monofilament. The stresses corresponding to the maximum effective load on the bundle depend on the strength dispersion of the monofilaments.

3. The main interaction processes between the matrix and the fiber depend on the adhesion characteristics, surface structure and chemical composition of the fibers. It has been established that the weakening of the strength of the matrix in PCM is caused by the inhibitory effect of fibers on the process of hardening of the binders. In addition, there is a relationship between adhesive strength and tensile strength of PCM.

REFERENCES

[1] Yu.M. Lakhtin, V.P. Leontiev, *Materials Science*. Textbook for higher technical educational institutions, M.: Mechanical Engineering (1990) 528 pp.

[2] A.T. Mamedov, R.K. Mekhtiev, *Modification of a fiber composite reinforced with unidirectional orthotropic fibers, weakened by straight cracks during longitudinal shear.* Mechanics of composite materials and structures, volume 23.4 (2017) 579-590.

[3] Y.N.Kakhramanly, Z.N. Guseinova, B. A. Mamedov et al., Physico-mechanical properties of modified polymatrix polymer compositions. Plastics 1-2 (2018)12-15.

[4] Rao PD, Kiran CU, Prasad KE. Effect of fiber loading and void content on tensile properties of Keratin based randomly oriented human hair fiber composites. Int J Compos Mater 2017;7:1 36-43.

[5] S.R. Rakhmanov, A.T. Mamedov, A.N. Bespalko et al., *Mechanical engineering materials.* Monograph, AzTU (Baku, 2017) 410 pp.
[6] B.N. Arzamasov, V.I. Makarova, G.G. Mukhin, Materials Science. *Textbook for universities*. Publishing house of MSTU im. N.E. Bauman (Moscow, 2001) 648 pp.
[7] A.V. Markov, S.V. Vlasov, P*rinciples of selection of polymer materials for the manufacture of products. Polymer materials.* Products, Equipment, Technologies 6 – 8 (2004) 17 – 29.
[8] Yu.K.Mashkov, O.V.Kropotin, O.A. Kurguzova*, Creation of a polymer antifriction nanocomposite based on polytetrafluoroethylene with increased wear resistance.* Omsk Scientific Bulletin 2 (120) (Omsk, 2013) 86 – 89.
[9] Saba N, Paridah MT, Abdan K, Ibrahim NA. *Effect of oil palm nano filler on mechanical and morphological properties of kenaf reinforced epoxy composites.* Construct Build Mater 2016;123: 15-26.
[10] Yahaya R, Sapuan S, Jawaid M, Leman Z, Zainudin E. *Effect of fibre orientations on the mechanical properties of kenafearamid hybrid composites for spall-liner application.* Defence Technol 2016; 12:52-8.
[11] Saba N, Paridah M, Jawaid M. *Mechanical properties of kenaf fibre reinforced polymer composite: a review.* Construct Build Mater 2015;76:87-96.
[12] Saba N, Mohammad F, Pervaiz M, Jawaid M, Alothman OY, Sain M. *Mechanical,morphological and structural properties of cellulose nanofibers reinforced epoxy composites.*Int J Biol Macromol 2017;97:190-200.
[13] Sassoni E, Manzi S, Motori A, Montecchi M, Canti M. *Novel sustainable hemp-based composites for application in the building industry: physical, thermal and mechanical characterization.* Energy Build 2014;77:219-26.
[14] Senthilkumar K, Saba N, Rajini N, Chandrasekar M, Jawaid M, Siengchin S, Alotman OY.*Mechanical properties evaluation of sisal fibre reinforced polymer composites:* a review,.Construct Build Mater 2018;174:713-29.
[15] Costa ML, *Rezende MC, De Almeida SFM. Effect of void content on the moisture absorption in polymeric composites.* Polymer Plast Technol Eng 2006;45:691-8.
[16] Yu.K. Mashkov, O.V. Kropotin, O.A. Kurguzova, *Anti-friction polymer composite material.* Russian Federation Patent 2525492 C2. No. 2012146766/05; application 05/10/2014; publ. 08/20/2014, Bulletin. No. 23/. (RU. 2014) 3 p.
[17] N.S. Enikolopov, *Composite polymer materials*. Nature 8 (1980) 62-67.
[18] S.A.Abasov, M.A. Ramazanov, *Strength properties of polymers and compositions based on them.* Proceedings of the National Academy of Sciences of Azerbaijan. ser. Fm. and technical sciences. 5 (1) (Baku, 2003) 161-164.
[19] N.T.Kakhramanov, R.V. Alieva, *Aging and stabilization of polymers.* Elm (Baku, 2007) 260 pp.
[20] Y.M.Bilalov, Y.S.Kakhramanly, A.S. Jafarov, *Mechanism and kinetics of crystallization of incompatible polymer mixtures.* News of Azerbaijan Higher Technical Institutions 1 (Baku, 1999) 32-38.
[21] S.N. Ermakov, T.P. Kravchenko, *Molecular polymer-polymer compositions, some aspects of production* 12 Plastic masses (2003) 21-25.

Received: 16.02.2024
Accepted: 02.05.2024

MACHINE SCIENCE

ISSN: 2227-6912
E-ISSN: 2790-0479

2024, № 1 Pages 66-73

INCREASING THE ACCURACY OF PROCESSING PARTS ON CNC LATHES

Agasi AGAYEV[1,a*], Govhar ABBASOVA[1,b]

[1]Department of Machine building technology, Azerbaijan Technical University, Baku, Azerbaijan

E-mail: [*a]agasig@aztu.edu.az, [b]govher.abbasova@aztu.edu.az

https://doi.org/10.61413/NYXB4393

Abstract: The article examines the effect of the movement trajectory of the cutting tool on the longitudinal cross-sectional accuracy of the details processed on digitally controlled (DC) lathes. Opportunities to improve the accuracy of details are analyzed. The article investigates the influence of the trajectory of the cutting tool on the accuracy of the longitudinal section of parts processed on lathes with computer numerical control (CNC). The possibilities of increasing the accuracy of parts are analyzed. The article describes a method for calculating the trajectory of a turning tool on a machine with numerical control to compensate for elastic deformation when processing of the workpiece. In the process of turning bodies of rotation with low rigidity, elastic deformations occur under the action of cutting force, which negatively affects the accuracy of the machined surface. As a result, an error appears in the form of barrel-shaped, saddle-shaped, or a combination of these errors, depending on the stiffness machine and its individual parts. Based on the calculation of deformation at a constant depth of cut, it is proposed to determine the error, which must be further compensated using the given calculation method. It allows compensation to be carried out by predistortion the trajectory at the stage of programming the control program. Thus, during the turning process, the required diameter will be obtained with minimal errors, which in turn will have a positive effect on the reduction additional processing to remove form errors and improve the quality of part processing.

Keywords: *processing accuracy, shape error, machining, workpiece, part, machine tool, cutting tool, trajectory.*

Introduction.

The development of all branches of mechanical engineering and instrument making is characterized by a continuous increase in requirements for the precision of manufacturing parts and product assembly. The issue of increasing accuracy in all technological operations is considered relevant. Increasing the accuracy of milling, as well as the accuracy of machining operations, starting with roughing operations, allows us to minimize the number of processed operations on the surfaces of parts, save material, and also reduce labor costs. In addition, it should be noted that with increasing accuracy of machining parts, labor costs for assembling machines and devices are minimized due to partial or complete elimination of transfer operations. All this requires a special careful approach to ensuring and increasing accuracy at each stage of product creation - at the design stage, the manufacturing stage, as well as at the assembly and testing stages [1].

Studying the possibilities of increasing the accuracy of machining. The quality of the product as a whole directly depends on the precision of manufacturing of each of its parts. Among the well-known groups of parts, one of the parts that require increased manufacturing accuracy are parts processed on lathes. Because many of these parts are subjected to a variety of stresses, inaccurate preparation increases the corrosion and failure of the parts. Turning today remains a more labor-intensive operation in the manufacture of parts of this type.

The accuracy of detailing is understood as its compliance with the requirements for the drawing in terms of linear and angular dimensions, geometric shape, waviness and unevenness [2-5].

The process of mechanical processing of parts with pastes is accompanied by the occurrence of errors from the influence of systematic and random factors. One of these factors is the elastic deformation of the elements of the technological system (machine-layout-tool-part) under the influence of the cutting force. As a result, the position of the cutting tongue of the tool relative to the processed paste changes. A change in the cutting force and rigidity of the technological system during the movement of the cutting tool leads to deformation of its elements, as a result of which shape errors, as well as size variations, occur on the processed surfaces of individual pastes, as well as in batch pastes [5].

Increasing accuracy usually leads to increased labor intensity and cost of manufacturing parts. When designing operations for preparing parts, it is necessary to take into account errors that may occur during machining and be sure to determine the possibilities for their reduction or compensation. The general basic methods for improving machining accuracy are as follows:[6-9]:

- with increasing rigidity of the technological system;

-reducing the cost of construction errors (using the principle of overlapping bases; correct choice of price and direction of compression force, etc.);

- increasing the accuracy of tool adjustment by size;

- with the correct choice of material for the cutting part, optimization of cutting mode elements and increasing the wear resistance of the cutting tool through the use of cooling and lubricating fluids;

- reducing the influence of temperature deformations of the machine, tool and paste on the accuracy of machining;

- using active controls and various automatic debuggers;

- with the introduction of management systems.

Precision control in flexible manufacturing using CNC machines to improve production culture in modern industrial enterprises is more typical. Accuracy control gradually, as a result of the improvement of modern CNC installations, there is a need to move to software control of the accuracy of machining.

In this regard, important issues include the study of factors influencing the accuracy of machining, the study of the causes of errors and the patterns of their change. This is especially true for parts mounted on consoles and centers during turning.

A very important and pressing problem is the study of the law of change in errors that arise when processing parts mounted on lathes in consoles and centers, and the determination of the equidistance of the trajectory of the cutting tool in accordance with the law of change in error, as well as the study of software control of the error that may arise. [10-13]

Increasing the accuracy of machined parts can be achieved by studying the causes of errors, as well as partial and complete prevention of elastic deformations of the paste, taking into account the cutting force, the rigidity of the technological system and the method of installation of the paste. Figure 1 shows methods for increasing the accuracy of machining shaft-type parts on CNC lathes.

Formulation of the problem.

Increasing the accuracy of parts processed on CNC lathes. In CNC lathes, when processing the outer surfaces of plates of low hardness, the bending of the tip and the compression of its cutting force under the action of the radial organizer P_y lead to their deformation under the influence of this force. Their deformation in the diametrical direction when the rods are cantilevered (for example, in a lathe chuck) is determined by the following well-known expression (1) [4]:

$$\Delta x = \frac{P_y \cdot l^3}{3 \cdot E \cdot J} \tag{1}$$

here, E-modulus of elasticity of the formation material, N/mm^2; J is the moment of inertia of the cross section of the mold, mm^4; l is the distance between the point of application of the cutting forand the place of attachment of the form, mm (Fig. 1).

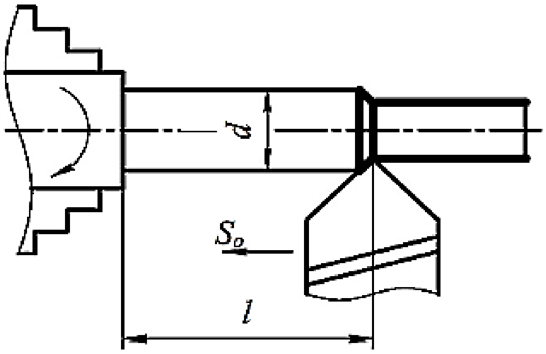

Figure 1. Scheme of processing a shape fixed in a chuck on a lathe

As the distance l increases, the deformation of the shape increases significantly, which leads to an increase in shape errors in the longitudinal cross section of the shape (or part).

The radial organizer of the cutting force during the top processing operation is determined by expression (2) below [4]:

$$P_y = 10 \cdot C_p \cdot t^x \cdot S_0^y \cdot V^n \cdot K_p \tag{2}$$

here, C_p, K_p are coefficients; x, y, n are strength indicators. When upper processing of molds made of structural steels for bits made of hard alloy $C_p = 243$, $x = 0{,}9$, $y = 0{,}6$ and $n = -0{,}3$; and for bits made of high-speed steels $C_p = 125$, $x = 0{,}9$, $y = 0{,}75$ and $n = 0$ [4].

The coefficient K_P is determined by the expression below (3)[4, s. 96-103]:

$$K_p = K_{M_p} \cdot K_{\varphi P} \cdot K_{\gamma P} \cdot K_{\lambda P} \cdot K_{rP} \tag{3}$$

here, is a coefficient depending on the tensile strength of the material being processed; - coefficients depending on the geometric parameters of the cutting tongue of the bit. $K_{M_p} \cdot K_{\varphi P} \cdot K_{\gamma P} \cdot K_{\lambda P} \cdot K_{rP}$

For bits made of hard alloy and high-speed steel with a planning angle $\varphi = 45^0$, an inclination angle of the leading edge $\gamma = 10^0 ... 20^0$, an inclination angle of the main cutting edge $\lambda = 0^0$ and a tip radius $r = 2$ mm $K_{\varphi P} = K_{\gamma P} = K_{\lambda P} = K_{rP} = 1$; , where $\sigma_B \langle 600$ MPa, $m = 0{,}35$ (for high-speed steel bits) and $m = 0{,}75$ (for hard alloy bits); t, S_0, V - respectively depth of cut (mm), longitudinal gear (mm/cycle) and cutting speed (m/min). $K_{M_P} = \left(\frac{\sigma_B}{750}\right)^m$

In CNC lathes, it is possible to compensate for shape errors that arise during processing, and in some cases, positional errors, by first changing the trajectory of the cutting tool using a numerical control program (NC-numerical Control).

There are three known ways to compensate for errors in the shape of parts:
- correction of the trajectory of movement of the cutting tool when performing the last working stroke;
- change in transmission and resulting cutting force during the movement of the cutting tool;
- correction of the trajectory of the cutting tool to obtain an uneven cutting depth when performing the last working stroke to process a given working surface.

Solution of the problem.

Let us assume that the shape of the surface to be formed corresponds to straight line 1 (Fig. 3). The actual shape of the surface, formed as a result of elastic deformation of the mold during processing, will correspond to curve 2. In order to compensate for the shape error, a correction is made to the tool path taking into account the current value of the shape error. To do this, the trajectory must necessarily correspond to curve 3, which is considered a mirror image of curve 2 if you look at straight line 1, corresponding to the nominal contour of the part. Since the specific operation of a lathe does not allow the tool to move along a smooth curve, the actual tool movement curve will be stepped (curve 4 in Fig. 2).

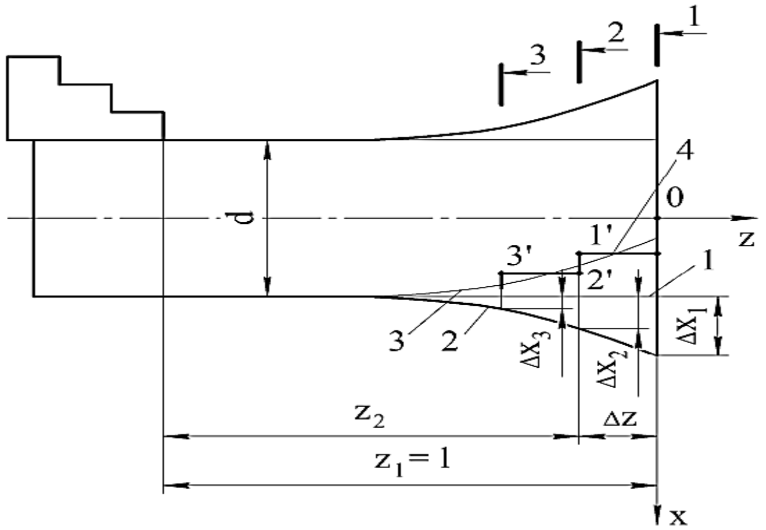

Figure 2. Scheme of formation and compensation of errors in the shape of the cantilever fastening in the chuck

The adjusted trajectory ($1^/$, $2^/$, $3^/$, ... support points) can be written in several blocks of the control program. Therefore, at the support points, the transfer motion of the tool approaches zero at short intervals, and the cutting force decreases. This is due to the formation of ring-shaped marks on the treated surface. In addition, the contour formed as a result of the influence of the stepwise nature of the tool movement becomes non-linear after processing. Therefore, it is more advisable to use this method only for roughing or primary surface treatment.

The deformation of the shape in any kth cross section (Fig. 1) can be calculated using the following expression (4):

$$\Delta x_k = \frac{P_y \cdot (l-(k-1)) \cdot \Delta z^3}{3 \cdot E \cdot J} \tag{4}$$

here, l is the distance between the side surfaces of the cams and the mold, mm; ΔZ - distance between adjacent cross sections, mm.

If the deformation of the shape in any cross section is less than half the discreteness of coordinates in the diametrical direction on CNC machines, then in this section and in the section with a higher number the deformation is assumed to be zero.

The coordinates of the support points of the adjusted cutting tool path will be determined by the following expression (5):

$$\left.\begin{array}{l} point\,1^{/}; x=\dfrac{d}{2}-\dfrac{\Delta x_1+\Delta x_2}{2}; z=-\Delta z \\ point\,2^{/}; x=\dfrac{d}{2}-\dfrac{\Delta x_2+\Delta x_3}{2}; z=-\Delta z \\ for point\,k^{/}, if k even number: \\ x=\dfrac{d}{2}-\dfrac{\Delta x_k+\Delta x_{k+1}}{2}; z=-(k-1)\cdot\Delta z \\ for point\,k^{/}+1, if k even number: \\ x=\dfrac{d}{2}-\dfrac{\Delta x_k+\Delta x_{k+1}}{2}; z=-k\cdot\Delta z \end{array}\right\} \tag{5}$$

here, d is the nominal diameter of the part, mm; - the distance between cross sections at which the shape deformation is calculated, mm. Δz

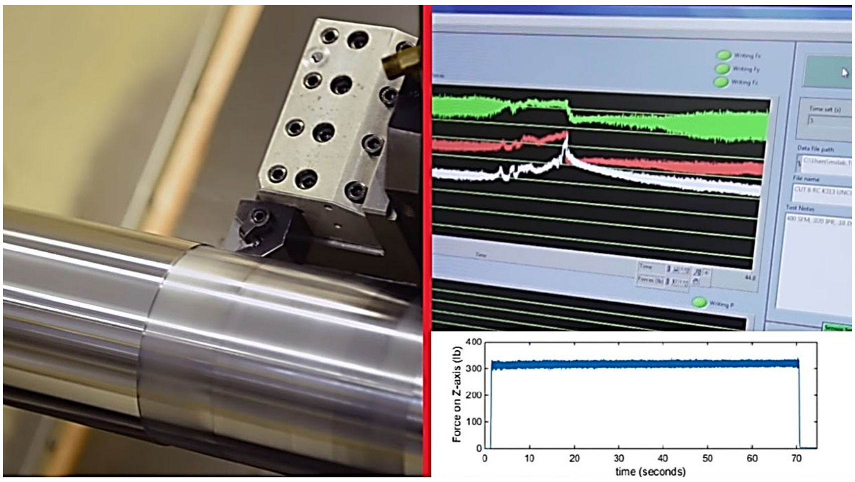

Figure 3. Measurement of cutting force using Kistler's RCD dynamometer

The shape error of the workpiece is calculated as the difference between the largest dmax $d_{\max}$ and smallest dmin $d_{\min}$ diameters according to (6):

$$\Delta_f = d_{\max} - d_{\min} \tag{6}$$

For the experimental implementation of the problem posed in the article, the study was conducted on the SL-10 digital program controlled machine of the HAAS company. Rods made of Steel 45 material with a length of 8÷12 mm were taken for the study. A three-punch cartridge was used as a clamping arrangement. The Kistler RCD dynamometer was used to determine the value of the cutting force applied to the pasta during processing (figure 3).

Table 1. Displacement of the axis of the stick workpiece

In the current sections of the passage of length L (x), mm	Axis displacement -y, mm J=0,05 sm^4 d=10 mm				Cutting force P_y, N	Processing modes		
	theoretical	experience	without compensation	with compensation		t, mm	S, mm/per	n, dövr/min
10	0,00063	0,00055	0,00032	0,0002	198	0,5	0,3	500
20	0,005	0,0044	0,0021	0,0012				
30	0,017	0,014	0,008	0,004				
40	0,04	0,036	0,014	0,008				
50	0,078	0,068	0,004	0,02				

During the experiment, the value of the displacement of the cutting force of the rod in 5 equal parts along the length from the value of the component P_y was calculated using expression (2) and written in table 1. Then, according to these values, the dependence graph $y = f(L)$ reflecting the theoretically calculated displacement was constructed (figure 4).

Then, $t = 0{,}5$ mm of the pastes, in processing modes $S = 0{,}3$ mm/cycle and $n = 500$ cycles/min, processing was carried out without taking into account the center axis shape error compensation scheme (figure 2). During processing, the values of the central axis displacement in 5 equal parts along the length of the workpieces measured by the indicator are written in table 1. On the basis of these values, the $y = f(L)$ dependency graph was constructed for processing the center axis shape error without considering the compensation scheme (figure 4).

Then, the processing of the stick pashto was carried out in the same processing modes, taking into account the shape error compensation scheme of the central axis (figure 2). Again, with the same rule, the values of the displacements of the central axis of the workpieces in 5 equal parts along the length were measured and written in table 1. On the basis of these values, the dependence graph $y = f(L)$ for processing was built taking into account the compensation scheme for the shape error of the central axis (figure 4. - curve). In all these experiments, the range of shear force variation was $P_y = 157...256N$.

As can be seen from figure 4, the value of the displacement of the axis increases as the price of the transitions along the length of the plate increases at the value of the cutting force $P_y = const$ At a large value of the moment of inertia, the value of the displacement is small, and at a small value of the moment of inertia, the value of the displacement is large. Comparing the graphs constructed with a known dependence for the determination of the deformation of the central axis of the cantilever fixed part, it is known that the difference between the processing modes with and without taking into account the compensation scheme for the central axis shape error is $10 \div 12\%$.

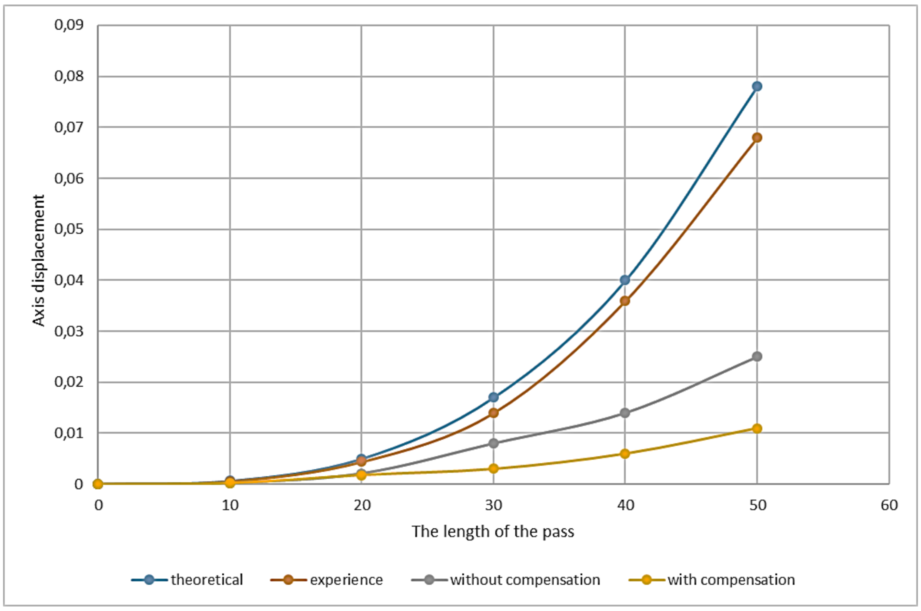

Figure 4. The graph of the displacement of the axis of the stick workpiece as a function of length.

Results and conclusions.

The article explores the possibility of compensating for shape errors that arise during processing on CNC lathes, and in some cases, for errors in relative position, by first changing the trajectory of the cutting tool using a digital control program (NC-numerical control), with which the circuit was built formation and compensation of errors in the shape of a fixed plate fixed to the chuck by a console. Since ensuring accuracy in machining and assembly processes is considered one of the important issues, this paper examines the factors affecting the machining accuracy in turning and how they can be prevented. To this end, the article analyzes the factors influencing the accuracy of machining during turning of parts to which the console is attached, and explains ways to reduce them. Elastic deformations that occur in the technological system due to the action of the cutting force have been identified; special attention is paid to the occurrence of shape errors as a result of bending of the central axis of the workpiece during processing. To compensate for the error by adjusting the value of the cutting force (an organizer that can be taken into account in the control program) in order to reduce the cost of the error arising from the deformation of the shape axis under the influence of the cutting force, it is proposed to implement this issue through the NC program.

REFERENCES

[1]. A. A. Matalin. *Mechanical engineering technology*, Petersburg. : Publishing House “Lan”, 2016. 512 p.

[2]. A. G. Suslov, V. F. Bezyazychny, Yu. V. Panfilov. *Surface engineering of parts*. Mechanical Engineering, 2008. 318 p.

[3]. A. A. Panov, V. V. Anikin, N. G. Boym, *Metal cutting. Technologist's Handbook.* Mechanical Engineering: Mechanical Engineering-1, 2004. 784 p.

[4]. A. M. Dalsky, A. G. Suslov, A. G. Kosilova and others; edited by A. M. Dalsky, A. G. Kosilova, R. K. Meshcheryakov, A. G. Suslov. *Handbook of mechanical engineering technologist:*

in 2 volumes T. 1, 2 / – 5th ed. reworked and additional – M.: Mashinostroenie-1, 2001.
[5]. Yusubov N.D. *Experimental determination of cutting force during turning*. Mechanical engineering technology. Moscow. 2003 No. 3(43), pp. 23-25. http://www.virste.ru/gurnal.php?idname=5&idgurnal=119
[6]. Bogatenkov, S.A., Sazonova, N.S., Yusubov, N.D. et al. *Increasing the Productivity of Multitool Machining on Automated Lathes by Optimizing the Machining Plan.* Russ. Engin. Res. 41, 1071–1074 (2021).
https://doi.org/10.3103/S1068798X21110046
[7]. P. P. Serebrenitsky, *A short reference book for mechanical engineering technologists*, St. Petersburg.: Polytechnic, 2007. 951 p.
[8]. P. P. Serebrenitsky, A. G. Skhirtladze. *Programming for automated equipment.* M.: Higher School, 2002. 592 p.
[9]. V.F. Guryanikhin, V.N. Agafonov. *Design of technological operations for processing workpieces on CNC machines: textbook.* Ulyanovsk: Ulyanovsk State Technical University, 2002. 60 p.
[10]. Karabulut, A. *Determination of diametral error using finite elements and experimental method* / A. Karabulut // METALURGIJA. – 2010. – Vol. 49. – Iss. 1. – P. 57–60. 11.
[11]. Pisarciuc, C. *The use of statistical process control to improve the accuracy of turning* / C. Pisarciuc // 20th innovative manufacturing engineering and energy conference (IMANEE 2016). Ser. Materials Science and Engineering. – IOP Publishing Ltd, 2016. – Vol. 161. DOI: 10.1088/1757-899X/161/1/012011
[12]. A. Swic, D. Wolos, J. Zubrzycki, *Accuracy Control in the Machining of Low Rigidity Shafts.* Industrial and service robotics et al. // Applied Mechanics and Materials. 2014. Vol. 613. p. 357. DOI: 10.4028/www.scientific.net/AMM.613.357
[13]. A. Swic, D. Wolos, G. Litak, *Method of control of machining accuracy of low-rigidity elastic-deformable shafts* // Latin american journal of solids and structures. 2003. Vol. 23, iss. 3. p. 221-232. DOI: 10.1016/S0307-904X(02)00122-1
[14]. A. Swic, A. Gola, D. Wolos, M. Opielak, *Micro-geometry Surface Modeling in the Process of Low-Rigidity Elastic-Deformable Shafts Turning* // Iranian journal of science and technology-transactions of mechanical engineering. 2017. Vol. 41, iss. 2. p. 159–167. DOI: 10.1007/s40997-016-0050-4
[15]. A.V. Phan, L. Baron, J.R.R. Mayer, G. Cloutier, *Finite element and experimental studies of diametral errors in cantilever bar turning* // Applied mathematical modeling. 2003. Vol. 27, iss. 3. pp. 221–232.

Received: 20.11.2023
Accepted: 21.05.2024

MACHINE SCIENCE
ISSN: 2227-6912
E-ISSN: 2790-0479
2024, № 1 Pages 74-80

CdMnSe THIN FILMS FOR SOLAR ENERGY CONVERTERS

Matanat MEHRABOVA[1,2,a*], Nizami HUSEYNOV[2,b], Vladimir KOCHEMIROVSKY[3,c], Aygun KAZIMOVA[4,d], Afin NAZAROV[5,e], Vusala POLADOVA[2,f]

[1]*Engineering Physics and Electronics Department, Azerbaijan Technical University, Baku, Azerbaijan

[2] "Transformation of Renewable Energy Sources laboratory", Institute of Radiation Problems, Baku, Azerbaijan;

[3]Higher School of Law and Forensic Enginering, Peter the Great St. Petersburg Polytechnic University, St.Petersburg, Russia;

[4]Physics Department, Ganja State University, Ganja, Azerbaijan;

[5]Epitaxial Layers And Structures Laboratory, Institute of Physics, Baku, Azerbaijan

E-mail: [a]metanet.mehrabova@aztu.edu.az, [b]nizamiphys@gmail.com, [c]vako4@yandex.ru, [d]aygunkazimova2019@gmail.com, [e]afinnazarov@yahoo.com, [f]poladova-vusale@bk.ru

https://doi.org/10.61413/TUBL2352

Abstract: The studied semiconductor structure for photovoltaic cells is composed of SnO_2-coated glass and CdMnSe thin film. A study is made by examining the photoluminescence from the surface of the CdMnSe thin film with laser power and sample temperature for an as-grown, then an air-annealed thin film, and undergone $CdCl_2$ treatment. Thin films of $Cd_{1-x}Mn_xSe$ (x=0.05) were grown on a glass substrate. The lifetime of charge carriers under pulsed illumination was determined from the kinetic decay of the photocurrent. The study of relaxation curves of nonequilibrium photoconductivity under the influence of laser radiation confirmed the presence of two recombination channels - intrinsic and impurity. Photocurrent relaxation occurs through fast and slow recombination channels. The fast relaxation time τ = 13 μs associated with the intrinsic transition, and the slow relaxation time is due to impurity excitation and τ = 20 μs. The photoluminescence spectra of thin films of $Cd_{1-x}Mn_xSe$ (x=0.05) were studied. The observed emission lines can be divided into three parts. Emission lines with maxima λ_1 = 868 nm, λ_2 = 888 nm and λ_3 = 933 nm, which are caused, respectively, by an optical transition in the region of the edge of the absorption band, an acceptor level located in the band gap and an optical zone-band transition or annihilation of free excitons.

Keywords: *Thin film, semimagnetic semiconductor, lifetime, recombination center, photoluminescense*

Introduction.

One of the current trends in the development of alternative energy is building photovoltaics, which involves the integration of solar panels with residential buildings or industrial facilities. As a rule, such devices are assembled on a rigid basis, but assembling panels on a flexible basis would significantly reduce their specific weight and also facilitate installation.

In recent years, the market demand for solar modules has increased significantly. Strong competition among manufacturers in the world market requires continuous improvement of the technical parameters of solar cells and reduction of their prices.

The vast majority of solar cells currently produced for commercial purposes are made of silicon (Si). Photoelements made of Si solids are widely used, as their absorption, spectral characteristics correspond to the spectral characteristics of solar radiation and the theoretically calculated maximum efficiency under standard conditions is 30%. 91% of the energy of light flux falling through silicon, i.e. the part of the solar spectrum with a wavelength of 1.1 μm and shorter, can be converted into electricity. Their main drawback is the high cost of silicon ingots due to the expensive operation of the cutting technology [1].

GaAs and CdTe compounds attract the attention of many researchers as a very promising material. Because of their use, it was possible to obtain a very large efficiency. Although GaAs have a number of advantages over silicon, they also have some disadvantages, such as brittleness and high density. At large values of the band qap E_g, its ability to convert long-wavelength rays is limited (it absorbs rays with a wavelength less than 0.9 μm). CdTe-based solar cells are more durable and strong [1,2].

In recent years, low dimension semiconductor structures have been the subject of researchers by many scientific centers around the world [3-10]. In order to obtain high quality and inexpensive solar cells, it is important to have the following conditions: replacement of massive crystals with thin-films, proper selection and development of thin-film technology. By replacing massive crystals with thin-film structures, the total amount of material used for structures obtained on different substrates can be reduced by 100 or even 1000 times. On the other hand, the transition to thin films simplifies the requirements for the crystallographic quality and purity of the material, reducing the resistance, which is one of the main parameters of the solar cell. For this reason, the choice of the optimal value of the layer thickness is a key factor, and this can be achieved by the molecular beam condensation method.

In recent years, new types of materials have been used for solar cells. For example, copper-indium-diselenide, GaAs, CdS, CdTe, CdSe, etc. thin-film photovoltaic elements based on them. These solar cells have been used for commercial purposes in recent years, and their production technology is constantly evolving. Over the last decade, the efficiency of such thin-film structures has almost increased for 2 times.

The material for the absorbing layer of flexible solar cells can be thin films based on cadmium selenide (CdSe). The advantages of this material include an optimal band gap of ~1.71 eV, as well as a high absorption coefficient of solar radiation ($\sim 5 \cdot 10^5$ cm^{-1}) [11].

Thin films of semimagnetic semiconductors based on Cd are of particular interest for the purpose of using these materials in photovoltaics [12,13]. Many physical properties of semiconductors are determined by the nature, state and location of local levels in the band gap. The study of current-voltage characteristics (CVC) and thermally stimulated current (TSC) spectra does not fully allow us to judge such important parameters as the capture center, depth, concentration and capture cross sections, as well as information about the nature of the distribution of local levels in the band gap of high-resistance materials.

Over the last few years, solar cells based on thin films of CdMnSe semimagnetic semiconductors (SMSC) are of great interest. These materials have unique properties: high photosensitivity at room temperature, the wide band gap and the ability to control a number of physical properties by changing the concentration of the transition metal element in the sample, etc.

The study of recombination processes is a necessary essential stage in the study of the physical properties of semiconductor materials and devices based on them. It is the mechanism of charge carrier recombination that determines the features of the occurrence of photoelectric, luminescent and injection phenomena that underlie most areas of practical use of semiconductors. In this work, the recombination processes of charge carriers in thin films of semimagnetic semiconductors $Cd_{1-x}Mn_xSe$ are investigated.

Experiments and discussions.

In this work, solid solutions of $Cd_{1-x}Mn_xSe$ (x = 0.05) were synthesized and thin films on their basis were grown on a glass substrate with a conduction SnO_2 layer at a source temperature T_{sour} = 1100 K, substrate temperature T_{sub} = 670 K using the molecular beam condensation (MBC) method in a vacuum installation УВН-71-Р3 in a vacuum of 10^{-4} Pa [14,15]. Ni contacts were deposited on thin films. The type of conductivity was determined by the t.e.m.f, which showed that the obtained $Cd_{1-x}Mn_xSe$ thin films have p-type conductivity.

The crystal structure of the obtained thin films was studied by X-ray diffraction method on an XRD Broker, D8 ADVANGE, Germany. In the X-ray diffraction patterns of $Cd_{1-x}Mn_xSe$ thin films, all diffraction peaks confirm that the thin films have a sphalerite-type cubic structure with a lattice parameter of a = 6.05 Å. (Fig. 1).

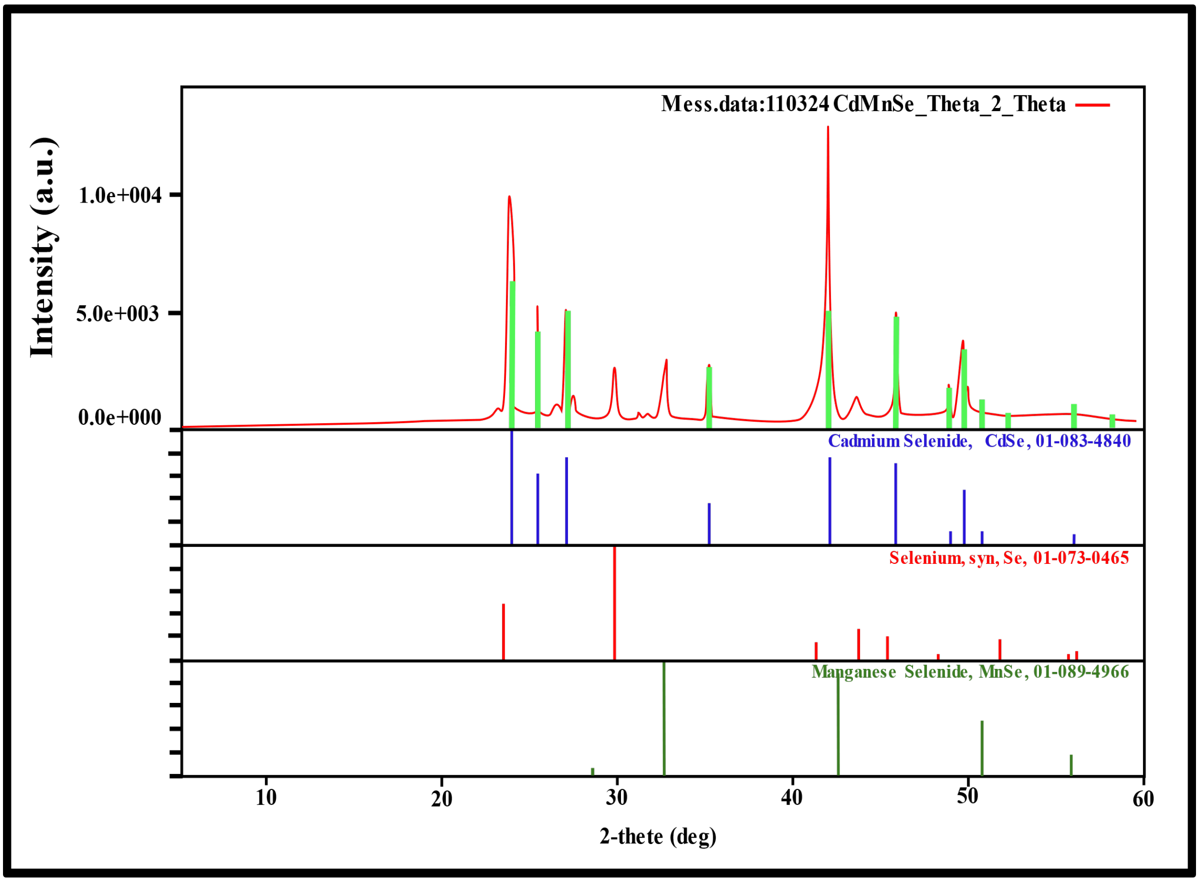

Figure 1. XRD spectrum of CdMnSe thin films

In order to determine the recombination mechanism, parameters of recombination centers and processes of electronic transitions in $Cd_{1-x}Mn_xSe$ (x=0.05) films, we used a complex of stationary and kinetic research methods. To obtain kinetic characteristics, semiconductors were illuminated with short pulses (t~10^{-6}s) of LEDs. The photoelectric signal, caused by a change in the potential of the semiconductor under the influence of pulsed illumination, after preliminary amplification by a broadband transistor amplifier, was fed to the input of the oscilloscope and recorded by a computer (Fig. 2). The time resolution of the selective circuit was no worse than 10^{-8} s, which made it possible to record the signal in a time interval of 10^{-8}÷10^{-2} s.

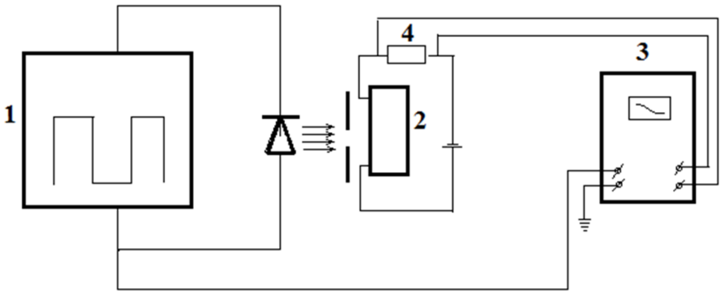

Figure2. Block diagram of the installation for measuring the kinetics of the photoelectric effect: 1 –generator; 2 – cell; 3 – amplifier with polarization unit; 4 – oscilloscope

In Fig. 3 shows the photocurrent relaxation curve in $Cd_{1-x}Mn_xSe$ (x=0.05). The study of the relaxation curves of nonequilibrium photoconductivity under the influence of laser radiation also confirms the presence of two recombination channels in $Cd_{1-x}Mn_xSe$ (x=0.05) - intrinsic and impurity. Photocurrent relaxation occurs through fast and slow recombination channels. The fast relaxation time τ, which is ~13 µs, is associated with the intrinsic transition, and the slow relaxation time is due to impurity excitation and is τ ~20 µs.

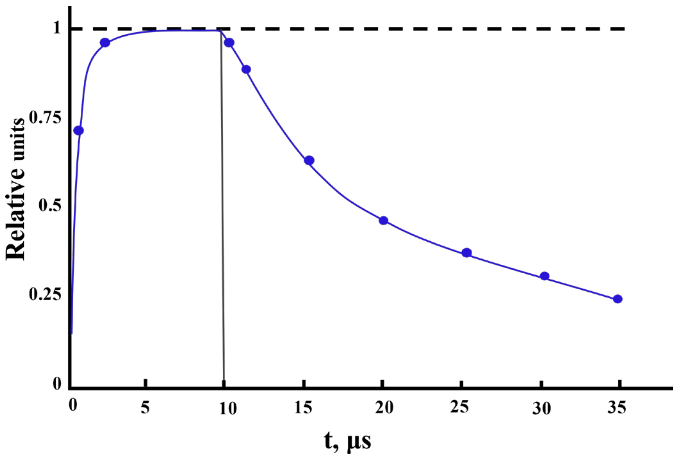

Figure 3. Kinetics of photocurrent changes for $Cd_{1-x}Mn_xSe$ (x=0.05) at room temperature.

All these studies have clearly shown that for high-resistance CdMnSe crystals, the main role in recombination processes is played the various types of recombination centers: fast (s-) and slow (r-) – sensitive. Under pulsed illumination, the lifetime of charge carriers is determined from the kinetic decay of the photocurrent. The study showed that the decay of the photocurrent is not monoexponential, which indicates the presence of several types of recombination. Depending on the energy state of these centers, the effective lifetime was 10^{-6}-10^{-3} s.

It was considered possibility of estimating the lifetime of nonequilibrium charge carriers in a surface layer with defects. In the presence of several types of recombination, the effective carrier lifetime can be found from the expression

$$\frac{1}{\tau_{eff}} = \sum_i \tau_i$$

For a thin film of $Cd_{1-x}Mn_xSe$ (x=0.05), taking into account the introduced structural defects and the influence of the surface, the effective lifetime can be determined as

$$\frac{1}{\tau_{eff}} = \frac{1}{\tau_l} + \frac{1}{\tau_s}$$

Where $\frac{1}{\tau_s} = \frac{2s}{d}$; τ_l - taking into account the recombination of carriers on structural defects in the thin film, τ_s - surface lifetime; s - surface recombination rate; d - plate thickness. Analyzes have shown that the lifetime is τ =13-20 μs, and the surface recombination rate $s = 40\frac{sm}{s}$.

To measure photoluminescence, a pulsed Nd:YAG laser with built-in 2nd and 3rd harmonic generators designed to generate radiation with wavelengths of 1064, 532 and 335 nm was used as a radiation source. The laser pulse duration was 10 ns with a maximum power of ~12 MW/cm^2. The radiation intensity was varied using calibrated neutral light filters. Using a lens, the incident laser beam was focused onto the surface of the sample with a spot diameter of ~2.0 mm. The luminescence spectra of thin films of $Cd_{1-x}Mn_xSe$ (x=0.05) were studied using an M833 automatic monochromator with dual dispersion (spectral resolution ~0.024 nm at a wavelength of 600 nm), with computer control and a detector that records radiation in the wavelength range 350 – 2000 nm (Fig. 4).

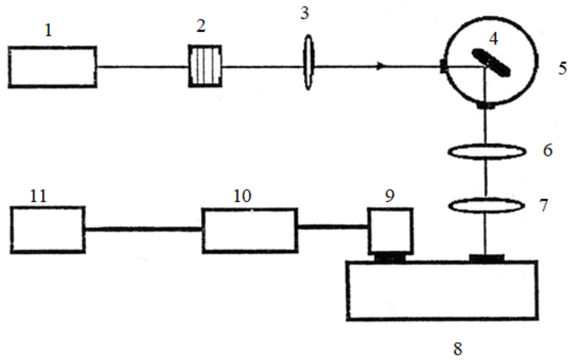

Figure 4. Scheme of the experimental setup for measuring photoluminescence of thin films of $Cd_{1-x}Mn_xSe$ (x=0.05) under the influence of laser radiation: 1- pulsed Nd:YAG laser, 2- light filters, 3, 6, 7 - lenses, 4- sample, 5- cryostat, 8-monochromator, 9-photoelectric current *amplifier, 10-storage oscilloscope, 11-computer system.*

The observed emission lines can be divided into three parts. Short-wave emission lines with maxima λ_1 = 868 nm (with a half-width of 3A°) and λ_2 = 888 nm refer to radiation associated with $Cd_{1-x}Mn_xSe$ (x = 0.05) and long-wave emission lines λ_3 = 933 nm (with a half-width of 4A°) (Fig.5).

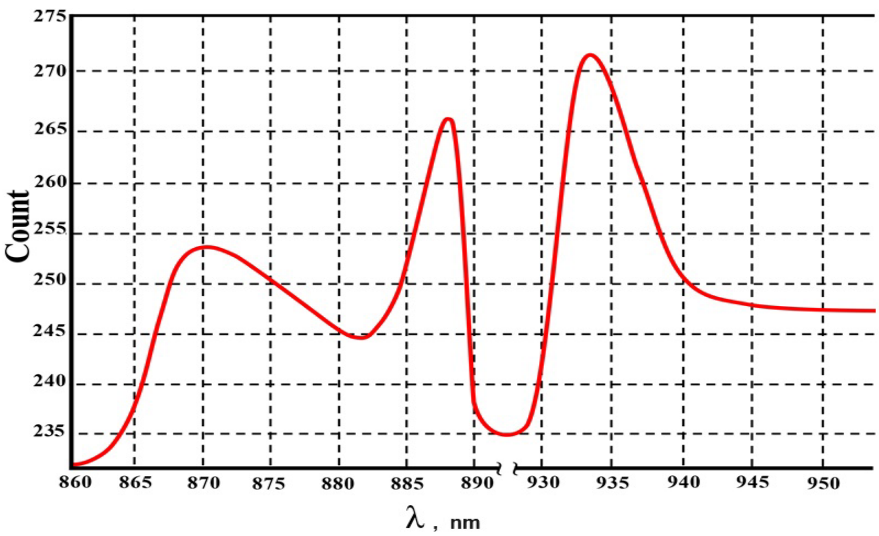

Figure 5. Luminescence spectra under the action of laser radiation in $Cd_{1-x}Mn_xSe$ (x=0.05) thin films at room temperature

In our opinion, the short-wavelength emission line corresponds to an optical transition in the region of the absorption band edge, since the band gap of $Cd_{1-x}Mn_xSe$ (x=0.05) is 1.7 eV [16-18]. Emission with a maximum λ_2 can be caused by an acceptor level located in the band gap of $Cd_{1-x}Mn_xSe$ (x=0.05) with activation energy E_a = 0.42 eV, or by a vacancy. As for the long-wavelength emission line, this is a fairly well-known line associated with the optical band-band transition and the annihilation of free excitons with a binding energy of - 15 meV.

Conclusion.

The studied semiconductors for photovoltaic cells is composed of SnO_2-coated glass and CdMnSe thin film. A study of the cells is made by examining the photoluminescence from the surface of the CdMnSe thin film with laser power and sample temperature for an as-grown cell, an air-annealed cell, and a cell that has undergone $CdCl_2$ treatment.

$Cd_{1-x}Mn_xSe$ (x=0.05) thin films were grown on a glass substrate. The lifetime of charge carriers under pulsed illumination was determined from the kinetic decay of the photocurrent. The study of relaxation curves of nonequilibrium photoconductivity under the influence of laser radiation confirmed the presence of two recombination channels - intrinsic and impurity. Photocurrent relaxation occurs through fast and slow recombination channels. The fast relaxation time τ = 13 μs associated with the intrinsic transition, and the slow relaxation time τ = 20 μs is due to impurity excitation.

The photoluminescence spectra of $Cd_{1-x}Mn_xSe$ (x=0.05) thin films were studied. The observed emission lines can be divided into three parts. Emission lines with maxima λ_1 = 868 nm, λ_2 = 888 nm and λ_3 = 933 nm, which are caused, respectively, by an optical transition in the region of the edge of the absorption band, an acceptor level located in the band gap and an optical zone-band transition and annihilation of free excitons.

Acknowledgement: The work was carried out with the financial support of the Science Fund of SOCAR (No. 22LR–EF/2024)

REFERENCES

[1] J.A.Luceño-Sánchez, A.M.Díez-Pascual, R.P. Capilla. *Materials for Photovoltaics: State of Art and Recent Developments.* International Journal of Molecular Sciences, 20, 976, 42 p., 2019

[2] M.P.Paranthaman, W.Wong-Ng, R.N.*Bhattacharya Semiconductor materials for solar photovoltaic cells.* Springer Series in Materials Science. 218, 2016,

[3] R.Souza da Silva, E.Soares de Freitas Neto, N.O.Dantas. *Optical, magnetic, and structural properties of semiconductor and semimagnetic nanocrystals.* Nanocrystals – Synthesis, Characterization, and Applications. p.62-80, 2012

[4] N.Badera, B.Godbole, S.B.Srivastava, P.N.Vishwakarma, L.S.S.Chandra, D.Jain, V.G.Sathe, V. Ganesan. *Photoconductivity in $Cd_{1-x}Mn_xS$ thin films prepared by spray pyrolysis.* Solar Energy Materials and Solar Cells. 92, p.1646–1651, 2008

[5] B.S.Munde, R.B.Mahewar, L.S.Ravangave. *Study of spectroscopic properties of $Cd_{0.6}Mn_{0.4}S$ chemical bath deposited thin film for solar cell applications.* International Journal of Research and Analytical Reviews, 5, 3, p.962-966, 2018,

[6] J.S.Dargad, L.P.Deshmukh. *$Cd_{1-x}Mn_xS$ dilute magnetic semiconductor: application in*

photoelectrochemical cells. Turk J Phys. 33, p.317 – 324, 2009

[7] A.E.Mali, A.S.Gaikwad, S.V.Borse, R.R. *Ahire Influence of* Mn^{2+} *magnetic ions on the properties of* $Cd_{1-x}Mn_xS$ *thin films synthesized by chemical bath deposition.* Journal of Nano- and Electronic Physics. 13,1, p.01004-5, 2021

[8] M.P.Gonullu, S. Kose. *On the Role of High Amounts of Mn Element in CdS Structure.* Metallurgical and Materials Transactions A. 48A, p.1321-1320, 2017

[9] A.N.Nwori, L.N.Ezenwaka, E.I.Otti, N.A.Okereke, N.LOkoli. *Study of the optical, electrical, structural, and morphological properties of electrodeposited lead manganese sulfide (PbMnS) thin-film semiconductors for possible device applications.* Journal of Modern Materials. 8,1, p.40-51, 2021

[10] J.J.Scragg, P.J.Dale, D.Colombara, L.M.Peter. *Thermodynamic aspects of the synthesis of thin-film materials for solar cells.* Chem Phys Chem. 13, p.3035 – 3046, 2012

[11] V.F.Gremenok, V.B.Zalessky, N.N.Mursakulov, M.S.Tivanov. *Thin-film solar cells based on* $Cu(\dot{I}n,Ga)(Se,S)_2$ *semiconductor materials with a chalcopyrite structure.* Baku, Elm, 252 p, 2013

[12] I.R. Nuriyev, M.A. Mehrabova, A.M. Nazarov, R.M. Sadigov, N.G. Hasanov. *On the growth, structure, and surface morphology of epitaxial CdTe films.* Semiconductors. 51, p.34-37, 2017, https://doi.org/10.1134/S1063782617010183

[13] M.A.Scarpulla, B.McCandless, A.B.Phillips, Y.Yan, M.J.Heben, C.Wolden, etc. *CdTe-based thin film photovoltaics: Recent advances, current challenges and future prospects.* Solar energy materials and solar cells. 255, 112289, 2023, https://doi.org/10.1016/j.solmat.2023.112289

[14] M.A.Mehrabova, A.O.Mekhrabov. *Effect of gamma irradiation on electrical and photoelectrical properties of* $Cd_{1-x}Mn_xTe$ *thin films.* Machine Science. 2, p.70-77, 2023, http://dx.doi.org/10.61413/GDKV8772

[15] I.R.Nuriyev, M.A.Mehrabova, A.M.Nazarov, N.H.Hasanov, R.M.Sadigov, S.S.Farzaliyev, N.V.Farajov. *Structure and Surface Morphology of* $Cd_{1-x}(Mn, Fe)_xSe$ *Epitaxial Films.* Journal of Surface Investigation: X-ray, Synchrotron and Neutron Techniques. 13, p.1083-1085, 2019, https://doi.org/10.1134/S1027451019060168

[16] Mehrabova M.A., Orujov H.S., Hasanov N.H., Kazimova A.I., Abdullayeva A.A. *Ab initio calculations of defects in CdMnSe semimagnetic semiconductors.* Mechanics of Solids, 55, 1, p.108–113, 2020, https://doi.org/10.3103/S0025654420010021

[17] J. Antoszewski, E.K.Pecold. *Fundamental optical properties of* $Cd_{1-x}Mn_xSe$ *single crystals. Solid State Communications.* 34, 9, p.733-735, 1980

[18] J.S. Dargad. *Preparation of* $Cd_{1-x}Mn_xSe$ *DMS Thin Films by CBD: Studies on Optical and Electrical Properties.* International Journal of Applied Research 1,10, p.926-932, 2015

Received: 15.12.2023
Accepted: 19.04.2024

MACHINE SCIENCE

ISSN: 2227-6912
E-ISSN: 2790-0479

web site: msj.aztu.edu.az; e-mail: msj@aztu.edu.az Tel: (+994 12) 538 94 12

SUBMISSION GUIDELINES

General requirements.
Article should not be earlier published in any edition, stated in the short form and edited. The scientific article maintenance should correspond to one of the following scientific directions: Designing of machines; Materials technology; Mechanics; Manufacturing engineering; Economy and management; Automatics and ICT; Technical information.

The documents applied to article.
The conclusion of the corresponding organization (chair, etc.); The expert opinion on expediency of the publication of the article; The covering letter; The Information on the authors (name, patronymic, surname, the exact address, place of work and position, scientific degree, area of scientific activity, contact phones, e-mail address ,etc.).

Preparation rules.
Format - A4; *Margins from each party* - 20 mm; *Program* - Microsoft Office Word; *Font* - Times New Roman, a font size - 12, an interval – 1,15.
The scientific article can be written only in English language, and it is represented in duplicate.
Article volume - 5 … 8 pages.

Sequence of compilation:
1. Article name - on the center;
2. Names and surnames of the authors - on the center;
3. Full addresses of a place of work of authors - on the center;
4. Co-ordinates of authors: e-mail address, phone numbers.
5. The abstract: not less than two-three offers, and no more than 100 words. In the summary: article summary, problem statement, and the information on the received results should be reflected.
6. Keywords: often used 3 ÷ 5 terms under the article.
7. The basic text.
8. The references.

The main text of article should be divided as follows:
For example: "*Introduction*", "*Problem statement*", "*Decision or test methods*", "*Results of the decision or tests and their estimation*".
In introduction: the description of the problem statement, the work purpose and etc.;
In the main part: formation of problem statements; research and methods of the decision, their advantage and difference from existing methods; examples confirming efficiency of the offered method of the decision and the results received.
In the conclusion: evaluation of the results.

Drawings. *Formats* - DOC, JPEG, TIFF and PDF (600 dpi). *The size* – min. 5 × 5, max. 10 × 15. *Arrangement* - ("In the text", in the center). Images of drawings should be accurately visible, and all symbols well are read.
Drawings, paintings, schedules and algorithms should correspond to standard requirements.

Tables are located in the text and are numbered, and the name of each table should be specified in the right top corner.

Formulas should be written down in format *Equation* in the separate line. It is not recommended to use special symbols in the text written on the same line in format *Equation*. Formulas should be written down in certain sequence and are numbered on the right.

The references should correspond to the text and sequence of article. It is recommended to refer to sources published in last 10 years.

The additional information. Edition has the right to spend necessary updating and reductions. Authors bear a scientific article maintenance responsibility. To the publication those articles which have received a positive response are represented only. If article is not published, the edition decision is possible to data of authors, the manuscript and disks do not come back.

MACHINE SCIENCE № 1, 2024

Editorial address:
AZ1073, Azerbaijan, Baku, H.Javid av., 25.
Telephone: (+994 12) 538 94 12

E-mail: msj@aztu.edu.az
Web site: http://msj.aztu.edu.az/

Format: 60×84 1/8.
Number of copies printed: 100.

Publisher: AzTU Publisher